Università degli Studi di Palermo

AREA RICERCA E TRASFERIMENTO TECNOLOGICO
SETTORE DOTTORATI E CONTRATTI PER LA RICERCA
U. O. DOTTORATI DI RICERCA

PhD Course Technologies and Science for Human Health
Department of Biological, Chemical and Pharmaceutical Sciences and Technologies (STEBICEF)

SSD BIO/18

Evaluation of the biodistribution and activity of new optimized readthrough molecules in Cystic fibrosis mouse model and other model systems

PhD Student:
LA DOTTORESSA
Dott.ssa Federica Corrao

IL COORDINATORE
Prof. Bruno Giuseppe Pignataro

IL TUTOR
Prof.ssa Laura Lentini

CO-TUTOR
Prof.ssa Maria Grazia Zizzo

CICLO XXXVI
2020/2023

Table of contents

ABSTRACT……...1

1. INTRODUCTION……..2

1.1 The advent of personalized medicine…… 2

1.2 Nonsense-related diseases (NRDs)…….... 3

1.2.1 The EJC-dependent and EJC-independent NMD…… 5

1.3 The translational readthrough mechanism…….…….... 8

1.4 Cystic Fibrosis (CF)……..11

1.4.1 Cystic Fibrosis (CF)……....11

1.4.2 Therapeutic approaches in CF……... 16

1.4.3 The suppression therapy…… 17

*1.4.4 Methods for the study of the CFTR activity in vitro and in vivo with readthrough molecules.*22

1.4.4.1 The Ussing chamber as a gold standard technique to evaluate CFTR function rescue…22

1.4.4.2 Mice models in CF and the importance of animal experimentation as preclinical systems for human health……...23

1.5 Immune Regulatory Disorders (PIRDs) associated with nonsense mutations…….…….……...25

1.5.1 Molecular description of LRBA gene and its involvement in PIRDs……...26

2. AIM OF THE PROJECT……30

3. MATERIALS AND METHODS……..32

3.1 Molecule solution preparation…….....32

3.2 *In vivo* study…… 32

3.2.1 Animals……... 32

3.2.2 Toxicity study: administration protocol and group constitution……..33

3.2.3 Organs collection protocol for histological analyses. ……34

3.2.4 Biodistribution study: administration protocol and group constitution……..35

3.2.5 Organs collection and preparation for HPLC-MS analyses……35

3.2.6 Generation and management of colony of CFTR mutant mice……36

3.2.7 PCR endpoint for DNA amplification and genotyping……37

3.2.8 Chronic treatment for drugs' efficacy study: molecule administration protocol and groups constitution to study the efficacy in vivo of NV848 molecule……..38

3.2.9 Immunohistochemical protocol for mutant mice tissue analyses……39

3.3 *In vitro* experiments……..39

3.3.1 Cells culture conditions……...39

3.3.2 Cell Proliferation assay……...40

3.3.3 Ussing chamber experiments……...40

3.4 Molecular analyses……...41

3.4.1. RNA extraction and Real-time RT PCR……..41
3.4.1.1 Protocol for RNA extraction……41
3.4.1.2 16HBE cell RNA extraction with Trizol……41
3.4.1.3 Real-time RT PCR method……41
3.4.2 Protein extraction and western blot analyses……43
3.4.2.1 Western blot set-up……...43
3.4.3 Immunofluorescence staining……..44
3.4.4 Next-Generation Sequencing (NGS) ……44
3.5 Statistic……45
4. RESULTS……46
Objective No.1: Evaluation of the safety and tolerability of NV molecules *in vivo* following acute single-dose administration, and biodistribution study of the NV848 molecule in C57BL/6 mouse model……46
4.1 Evaluating safety and tolerability of the three NV TRIDs in vivo after acute treatment……..46
a) Acute oral toxicity study: behavioural analysis……46
b) Acute toxicity study: body weight assessment……50
c) Acute toxicity study: macroscopic and histological examination of major organs……51
4.2 NV848 biodistribution in vivo……...57
Objective No.2: Establishment of a CFTR-G542X mutant mice colony and evaluation of NV848 readthrough activity *in vivo*……58
4.3 Generation and management of a CFTR mutant mice colony and genotyping of newborns……..58
4.4 Chronic administration for 15 days and evaluation of the CFTR protein expression.……59
4.4.1 Immunohistochemistry experiments for the evaluation of chronic treatment safety and CFTR protein rescue expression in vivo……..61
Objective No.3:
a) *In vitro* CFTR protein rescue evaluation by the Ussing Chamber technique in engineered 16HBE cells with the G542X and W1282X nonsense mutations……64
4.5 Study of the CFTR functionality in human bronchial epithelial cells through short-circuit current measurements. ……64
a) 16HBEge CFTR^{G542X} cells experiments……..64
b) 16HBEge CFTR^{W1282X} cells experiments……65
c) Real-time RT PCR on 16 HBEge CFTR^{G542X} and CFTR^{W1282X}……67
b) Assessing the ability of NV molecules to induce readthrough in a different genetic context *in vitro*, using primary human fibroblasts with the UGA-R1683X mutation in the *LRBA* gene.....68
4.6 Investigation of the effects and activity of NV848, NV914 and NV930 on primary human fibroblasts with the LRBA^{R1683XR1683X}mutation……...68
4.6.1 Evaluation of LRBA$^{R1683X/R1683X}$ primary fibroblasts after 24, 48, and 72 hours of NV compounds treatment……..68

4.6.2 Evaluation of LRBA protein expression, localization, and functionality rescue after 72 hours of NV molecules treatment.....69
5. DISCUSSION.....75
6. CONCLUSIONS.....79
7. SUPPLEMENTARY.....80
7.1 Histopathological analysis scores in mice undergoing the toxicity study.....80
7.2 NGS analyses for the evaluation of NV848 treatment safety towards the integrity of the mRNA sequence.....93
7.3 Ussing chamber curves on 16HBE CFTR^{G542X} and CFTR^{W1282X} cell lines.....93
7.3.1 Curves of the 16HBEge CFTR^{G542X}.....94
7.3.2 Curves of the 16HBEge CFTR^{W1282X}.....97
8. ACKNOWLEDGMENTS.....99
9. BIBLIOGRAPHY.....101

ABSTRACT

Nonsense mutations cause approximately 11% of inherited diseases, including Cystic fibrosis (CF), Duchenne Muscular Dystrophy (DMD), and some Primary Immune Regulatory Disorders (PIRD) can be mentioned.
Nonsense mutations, also known as stop mutations, result in the presence of a premature termination codon (PTC) in the mRNA sequence, leading to premature translation termination. The consequence is the production of a truncated and non-functional protein, which is degraded. Simultaneously, the nonsense-mediated pathway (NMD) is activated, eliminating the available mRNA pool for translation. Currently, there is no cure for this genetic defect, resulting in life-threatening pathologies, such as CF or PIRD.
CF is specifically caused by mutations in the gene encoding the Cystic Fibrosis Transmembrane Conductance Regulator (CFTR) protein. About 2500 different mutations are associated with CF with the most common being a three-base pair deletion causing the loss of phenylalanine at position 508 (ΔF508). Nonsense mutations in the CFTR gene represent approximately 10% of CF cases, resulting in the absence of functional protein and a more severe form of the disease.
Apart from symptomatic approaches to care for CF patients, a pharmaceutical strategy targeting the specific genetic defect has been pursued. Heterocyclic scaffolds play a crucial role in the personalized medicinal approach, as demonstrated by numerous studies in the CF field.
Similarly, PIRD is a heterogeneous group of immune diseases caused by 430 genes, among which *Lipopolysaccharides (LPS)-Responsive Beige-like Anchor (LRBA)* has been identified. The LRBA deficiency disease has been recently described, highlighting its multiple effects due to the ubiquitous localization of the LRBA protein, e.g., immune cells and endocytosis vesicles.
Concerning nonsense mutations, in the last years, the experimental approach proposed for these genetic alterations is the premature termination codon (PTC) translational readthrough (TR) by small molecules. These molecules promote the bypass of the PTC, allowing the production of a full-length protein.
The current proposal aims to study three new *Translational Readthrough-Inducing Drugs* (TRIDs) (NV848, NV914, and NV930) in a model system for CF and LRBA-PIRD.
The first part of the project was focused on CF and involved both *in vivo* and *in vitro* systems.
After evaluating the acute toxicity *in vivo* of the three NV molecules, attention was focused toward NV848, to study the biodistribution in a wild-type mouse model and the efficacy in a CF-nonsense murine model. Additionally, CF-nonsense-engineered cell lines (16HBEge) were used to assess if CFTR functionality was restored under NV848 treatment, utilizing the Ussing chamber technique.
The project's second part aimed at rescuing the LRBA protein in a specific nonsense mutation using the three NV TRIDs. The study specifically investigated the TRIDs' effectiveness on LRBA expression, and functionality in human primary fibroblasts carrying the stop mutation c.5047C>T (p. Arg1683*) after prolonged treatments with the TRIDs.

1 INTRODUCTION

1.1 The advent of personalized medicine.

The development and spreading of new technologies in molecular and clinical biology made possible the origin of the important and futuristic concept of personalized medicine.

This term indicates a new approach based on a deep knowledge of each patient, involving many aspects of the same, considering all the factors that can influence the way a patient can be treated at the best.

In this view, the first relevant innovation that contributed to defining personalized medicine is the emergence of the "omics sciences", such as genomics, proteomics, transcriptomics, and epigenomics. Due to this new vision, the consideration of inter-personal variability has risen among clinicians and researchers, and understanding the genetic and environmental background is very significant for therapy exigences (Goetz L. H., *et al*. 2018) (**Figure 1**).

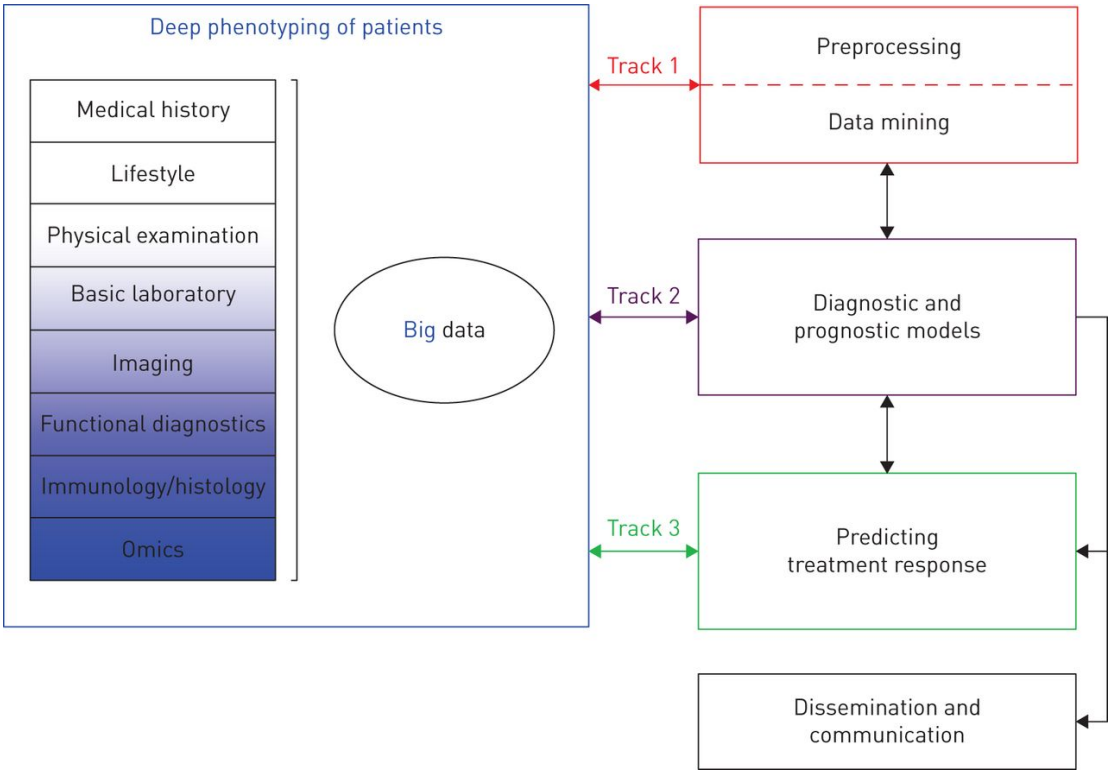

***Figure 1**. Schematic workflow of interdisciplinary and omics approaches for personalized medicine, for the design of the treatment based on the relation between genotype and phenotype (König, I. R., et al., 2017).*

For this reason, traditional medicine has recently been flanked by personalized medicine, creating the new concept of translational medicine, made up by the interplay between basic and clinical research.

In fact, for example, genotyping and next-generation sequencing have deeply helped in treating some types of cancers, or rare genetic diseases (Barry P. J., *et al.,* 2021).

In this scenario, designing specific treatments based on the genetic defect results in a promising approach. Moreover, in the field of rare genetic diseases, different pathologies share a similar genetic defect that could be dealt with the same way by an interdisciplinary approach.

1.2 Nonsense-related diseases (NRDs).

It has been estimated that about 11% of genetically inherited diseases are caused by nonsense mutations (Mort M., *et al*., 2008; Ghelfi M.D., *et al.*, 2023). Different pathologies are known to be interested by this alteration, even if the percentage of nonsense mutations for every specific disease is various. Some examples of nonsense genetic inherited diseases are the Fabry's disease, the Duchenne Muscular Dystrophy (DMD), the Choroideremia, the Lipopolysaccharide (LPS)-responsive and beige-like anchor (LRBA)-Primary Immune Regulatory Disorder (PIRD), and the Cystic Fibrosis (CF) (Schaefer E., *et al.*, 2005; Wilschanski M., 2012; Lopez-Herrera G., *et al.*, 2012; Bladen C., *et al.*, 2015; Imani S., *et al.*, 2018; Neri M., *et al*., 2020; Zhang M., *et al.*, 2021) (**Table 1**).

Disease	**% Nonsense mutations**
Fabry's disease	13% (Schaefer E., *et al.,* 2005)
Duchenne Muscular Dystrophy	14% (Neri M., *et al.*, 2020)
Choroideremia	39% (Imani S., *et al.*, 2018)
LRBA- Primary Immune Regulatory Disorders	< 1% (de Valles-Ibáñez G., *et al.*, 2018)
Cystic Fibrosis	10% and 20% in Italy (Elborn J. S., 2016; Campagna G., *et al*., 2022)

Table 1. *Percentage insurgence of nonsense mutations in different genetic disorders, considering rare and ultra-rare pathologies.*

Nonsense mutations cause the production of a premature termination codon (PTC) in the mRNA sequence, because one of the three natural stop codons, UGA, UAA, and UAG, is inserted in-frame, in place of a codon codifying for an amino acid. This causes the presence of a termination signal upstream of the natural termination codon (NTC), leading to the premature interruption in the translation process, during the polypeptide formation (Mort M., *et al.*, 2008; Clarke L.A., *et al.,* 2019; Potapova N. A., 2022) (**Figure 2**).

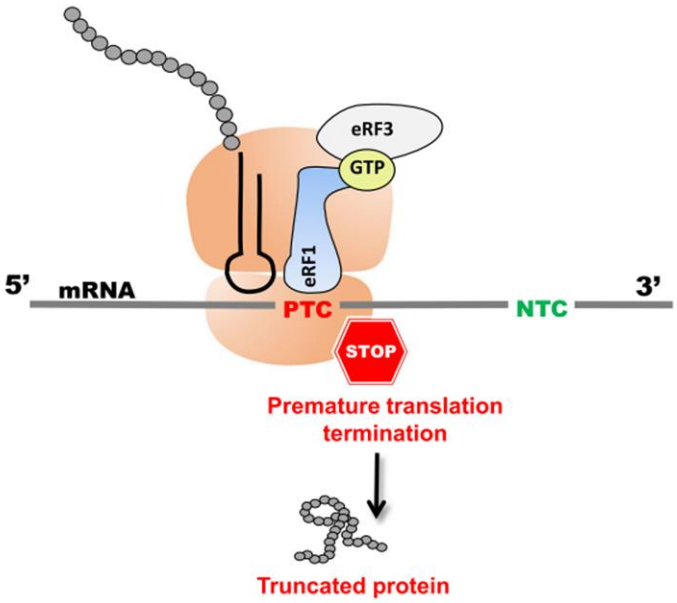

Figure 2. *Illustration of the translation interruption occurring when a nonsense mutation causes the presence of a PTC in the mRNA sequence. The termination complex (eRF1-eRF3) allows the recognition of the stop signal, causing the ribosome stalling at the PTC and the production of a truncated and nonfunctional protein, with the final release of mRNA from ribosome subunits and translation product degradation (Adapted from Dabrowski M., et al., 2018).*

The three termination codons, UGA, UAA, and UAG (namely, *opal, ochre,* and *amber*) are differently occurring as PTC in eucaryotes, respectively with a percentage of 51%, 31% and 18% (Benhabiles H., *et al.*, 2016).

Generally, the translation termination takes place when a stop codon (UGA, UAA, or UAG) occurs in the A site of the ribosome, causing the competition between the recruitment of the translation termination complex and near-cognate tRNAs (nc-tRNA), which could identify two of the three bases of the stop codons and allow the insertion of a codifying amino acid instead of the stop signal (Keeling K. M., *et al,* 2014; Palma M. and LeJeune F., 2020).

Particularly, in eucaryotes the Release Factor 1 (eRF1) is responsible for the identification of stop codons (Brown A., *et al*., 2015). Moreover, another factor is important to the definitive recognition of the stop codon, the Release Factor 3 (eRF3), a GTPase, which binds and is activated after the interaction with the poly-A binding protein (PABP). After GTP hydrolysis, eRF3 induces conformational changes in eRF1. This consents eRF1 to be positioned in the P site of the ribosome and allows the release of the nascent polypeptide together with ribosome 40S and 60S subunits disassembly (Keeling K. M., *et al.,* 2014; Hellen C.T.U., 2018) (**Figure 3**).

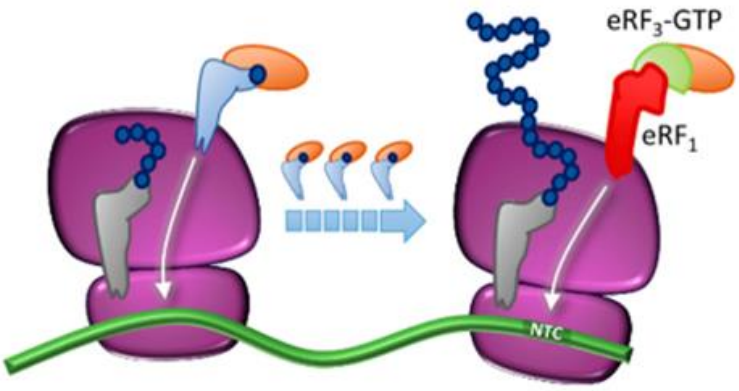

Figure 3. *Mechanism of natural translation termination, involving eRF1 and eRF3 factors, with the production of a full-length protein (Adapted from Lombardi S., et al., 2020).*

As described above, the presence of a stop codon causes the production of a truncated protein, also not functional and rapidly degraded, which results in the total absence of any protein product (Keeling K. M., *et al.,* 2014).

Another limit of the presence of a PTC in an mRNA is the surveillance pathway that recognizes and degrades the nonsense-mRNAs, known as nonsense-mediated mRNA decay (NMD).

NMD is one of the intracellular pathways responsible for maintaining cellular homeostasis, acting to eliminate aberrant mRNAs, but it is also involved in organism development, transcription, gene silencing, and DNA repair (Isken O. and Maquat L. E., 2007; Romão L., 2019).

When the nonsense-mRNAs are degraded by the NMD pathway, the consequence is the absence of the specific mRNA pool and, consequently, the lack of protein translation.

NMD is canonically divided into two typologies: the exon junction complex (EJC)-dependent and the EJC-independent.

1.2.1 The EJC-dependent and EJC-independent NMD.

After transcription and pre-mRNA formation, the splicing process is performed for the maturation of mRNA, and the multiprotein exon junction complex (EJC) is localized 20-24 nucleotides (nt) upstream of the splicing site, in the exon-exon junction (ex-ex j) (Le Hir H., *et al*.,2001; Lombardi S., *et al.,* 2020).

This is a signal for the recognition of incorrect mRNAs by NMD factors. When translation needs to start and ribosomes are assembled on mRNAs, several actors are nearby, such as those for the NMD pathway, because translation termination or mRNA degradation destinies depend on the dynamism of the ribosome itself.

Indeed, if the PTC is localized 30 nucleotides upstream of the open reading frame (ORF), as for NTCs, the ribosome proceeds rapidly, removing EJC, and avoiding NMD (Bongiorno R., *et al*., 2021). If the PTC is placed >50-55 nt upstream of the ex-ex j, this causes the stalling of the ribosome and impedes the discard of EJC, which acts as a platform for NMD proteins.

Particularly, the SURF protein complex is recruited at the blocked ribosome. SURF is composed of four main proteins: the Serine/threonine-protein kinase SMG1, a phosphatidylinositol 3-kinase (PI3K)-related protein kinase, Up-Frameshift Suppressor 1 (Upf1), an ATP-dependent RNA helicase, eRF1, and eRF3. Subsequently, when a PTC is recognized, the SURF complex binds to the mRNA-bound ribosome, and Up-Frameshift Suppressor 2 (Upf2) and 3 (Upf3) are then mobilized to form the DECID (DECay InDucing) complex, which permits the activation of Upf1 by SMG1 phosphorylation, thus allowing Upf1 to employ SMG6, an endonuclease, and the heterodimer SMG5 and SMG7. These last factors are necessary to induce mRNA decapping and deadenylation, mechanisms necessary to expose the mRNAs and proceed with their degradation. Also, Upf1 presence avoids the formation of other translation initiation complexes on the targeted mRNA. Lastly, Upf1 is dephosphorylated by protein phosphatase 2 (PP2A), DECID and SURF complexes are dismantled, and proteins are recycled for other NMD rounds (Isken O. and Maquat L. E., 2007; Popp M. W. and Maquat L. E., 2013; Kurosaki T., *et al.,* 2019; Lombardi S., *et al.,* 2020; Andjus S., *et al.,* 2021) (**Figure 4**).

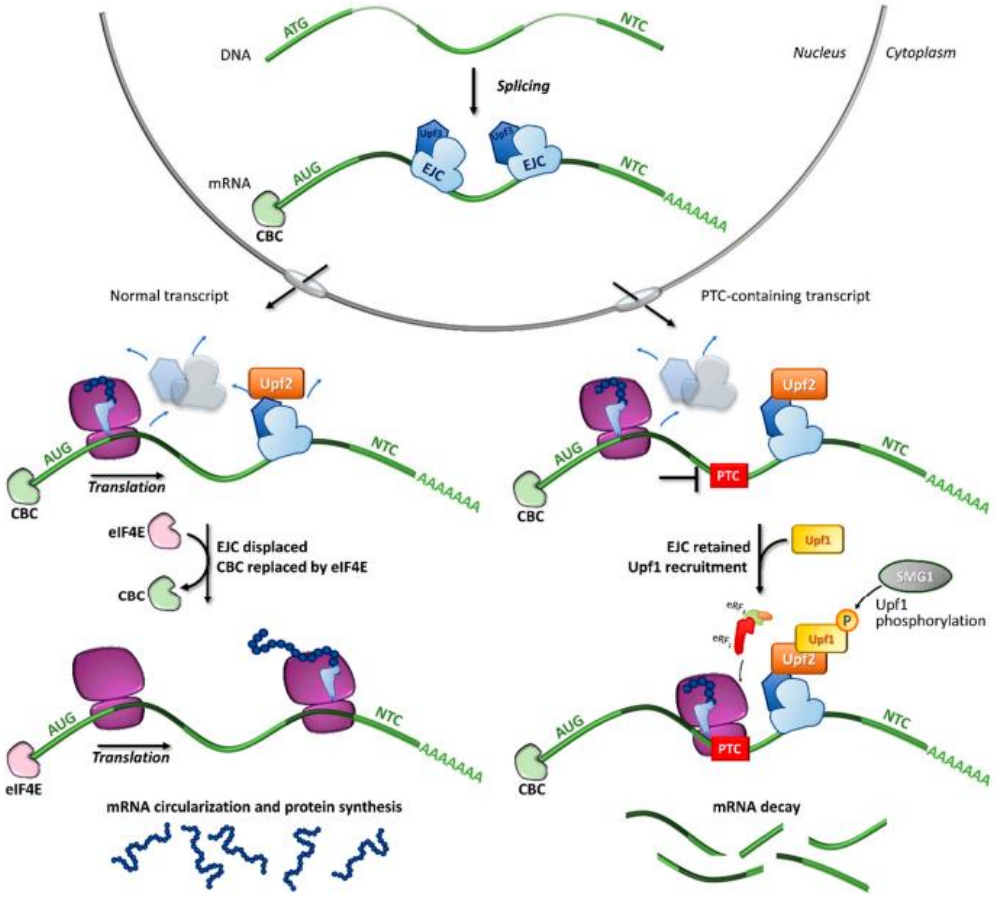

Figure 4. *Normal translation termination or EJC-dependent NMD activation after mRNA splicing (Lombardi S., et al., 2020).*

Notably, also the PABP is decisive in activating NMD, as recently explained in the new proposed model of the EJC-independent NMD, prior found in yeast and recently also in mammals (Kervestin S., *et al.,* 2004; Silva

A. L., *et al*., 2008; Lindeboom R. G., *et al*., 2016; Bongiorno R., *et al*., 2021). It is thought that mRNAs with extended 3'-UTR regions result free from EJC binding. Thus, if the stop codon is placed near the poly(A) tail, PABP-eRF3 assembly is ensured at the PTC, but, when PTC occurs far from 3'UTR, this interaction is failed, and this is the signal to elicit NMD (Bühler M., *et al*., 2006; Popp M. and Maquat L. E., 2013; Lombardi S., *et al.,* 2020). From this moment, SURF complex recruitment and all the steps described above are shared between the two NMD mechanisms (Metze S., *et al.,* 2013).

However, seeing that Upf1 is always recruited on mRNAs, the discrimination between PTC and NTC and of NMD substrates depends on the maintenance or the dissociation of Upf1 and its hydrolysis activity (Karousis E. D. and Mühlemann O. 2019; Andius S., *et al*., 2021) (**Figure 5**).

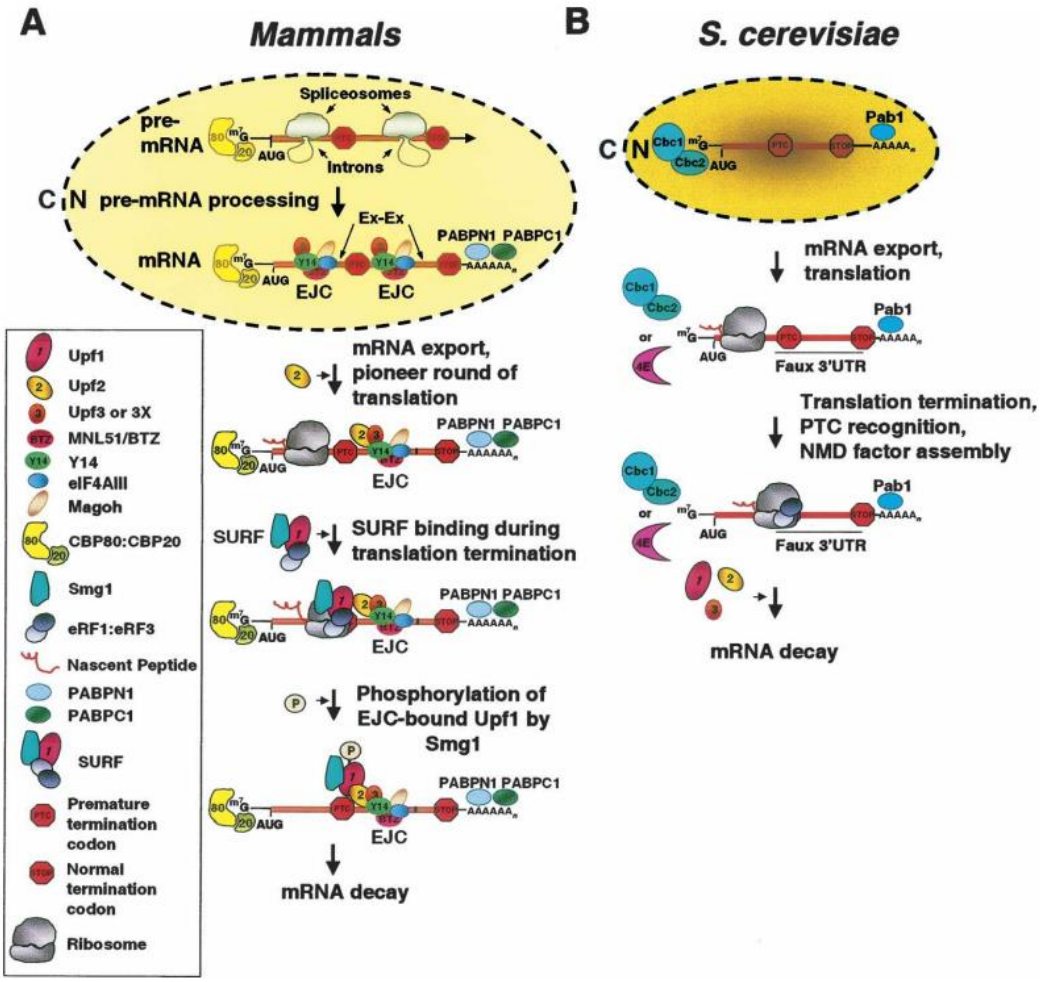

Figure 5*. The distinction between EJC-dependent and independent NMD, in mammals and yeast, respectively (Isken O. and Maquat L. E., 2007)*

Even so, it has been reported that there is a 5-25 % of altered mRNAs that can escape NMD, being successfully translated into truncated proteins or, if a correction mechanism occurs, in full-length and probably functional proteins (Isken O. and Maquat L. E., 2007; Lombardi S. *et al.,* 2020).

In the context of nonsense mutation rescue, an important strategy could be represented by the inhibition of the NMD pathway. Nowadays, there are several NMD inhibitor compounds discovered and synthetized to this scope, used in pre-clinical models, but the toxicity and the risks for human health need to be better understood for use in clinical experimentation (Spelier S., *et al.,* 2023).

To date, the main molecules that represent the most promising NMD inhibitors are caffeine, SMG1i, NMDI14 (or NMD-14), 5-azacytidine, and Amlexanox, having in common the ability to stabilize mRNA levels.

Caffeine was demonstrated to be able to suppress Upf1 phosphorylation and, consequently, inhibit SMG1 protein (Usuki F., *et al.,* 2004; Lentini L., *et al*., 2019).

In the same manner, SMG1i targets SMG1 protein and it was identified in 2012 by Gopalsamy and colleagues, presenting a pyrimidine-like structure (Gopalsamy A., *et al*., 2012).

NMDI14 was identified in 2014 to be well tolerated in different cell systems, and its action aims to impede SMG7-UPF1 interactions, interfering with NMD machinery (Martin L., *et al.,* 2014).

Surprisingly, 5-azacytidine, a natural analogue of cytidine, approved by the FDA as a drug for the treatment of myeloid leukaemia, was discovered to be an NMD inhibitor by screening in reporter cells. Its function is strictly correlated to its ability to induce MYC expression, one of the major actors involved in cell growth and proliferation (Wang D., *et al*., 2011; Bhuvanagiri M., *et al.,* 2014; Pawlicka K., *et al.,* 2020; Spelier S., *et al.*, 2023).

The last drug to be described is Amlexanox, which is an anti-inflammatory and anti-allergic drug, that in the last decade was also seen to be active in promoting both readthrough and NMD inhibition, with the reduction of Upf1 phosphorylation (Wang X., *et al.,* 2020).

Hence, NMD pathway inhibition could be a clever approach to allow, on one hand, the stabilization of PTC-mRNAs, and, on the other hand, to boost the readthrough activity of TRIDs synergistically.

1.3 The translational readthrough mechanism.

When a PTC occurs in the mRNA sequence, the NMD surveillance pathway degrades aberrant mRNAs, but as explained above, a percentage between 5% and 25% of PTC-mRNAs can escape NMD (Isken O. and Maquat L. E., 2007; Lombardi S. *et al.,* 2020).

In this event, aberrant mRNAs can undergo a translation process, with two possible consequences: **i)** the premature translation termination, with the production of a truncated protein, which is degraded; **ii)** the translation normally takes place, passing over the stop codon and producing a complete protein.

The stop codon bypass is due to the insertion of a nc-tRNA instead of the stop signal in the site of stop codon recognition, with a major binding energy than the release factors, allowing to continue the translation, rather than provoking its blockage (Palma M. and LeJeune F., 2021).

This last mechanism is called translational readthrough (TR) and it can be distinguished into three different types: **I) non-programmed TR**, which occurs in less than 0.1%, most efficiently in UAA stop codons; **II) programmed TR**: is generally involved in the production of elongated protein, frequently observed for the creation of protein isoforms (Sahoo S., *et al.*, 2022); **III) induced TR**: is performed by specific molecules that

promote a forced failure in the proofreading ribosome activity, to facilitate the production of full-length proteins in the pathological conditions due to PTC-harbouring mRNAs (Palma M and LeJeune F., 2021) (**Figure 6**).

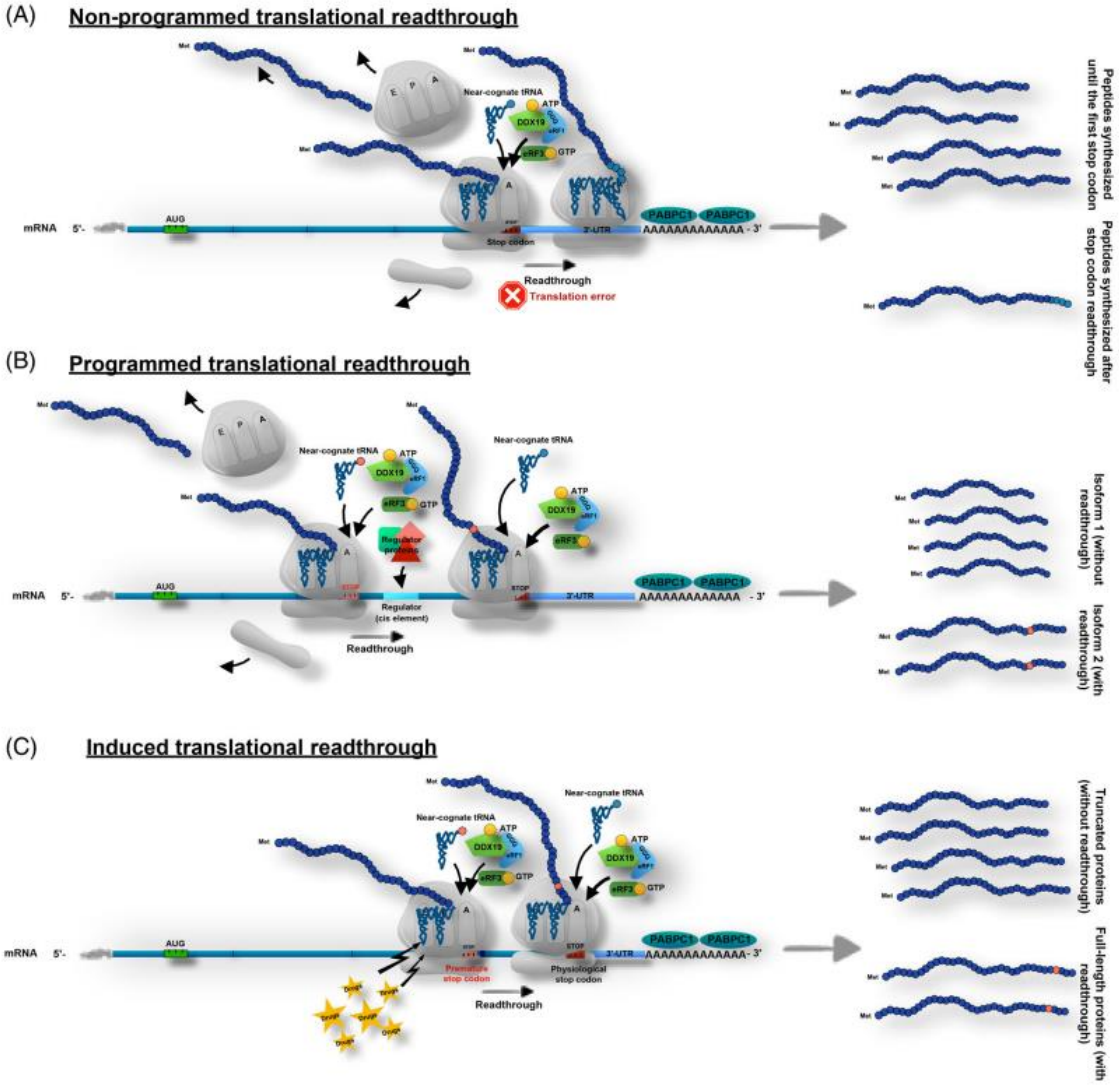

Figure 6. *Graphical description of the three types of translational readthrough: a) non-programmed, b) programmed; c) induced (Palma M. and LeJeune F., 2021).*

Moreover, UGA is found the most efficiently corrected. Specifically, it was also seen that UGA stop codon is most frequently corrected in arginine, cysteine, and tryptophan, while UAG and UAA in tyrosine, glutamine, and lysine (Bidou L., *et al.,* 2012; Roy B*., et al.,* 2016).

However, several factors influence the achievement and the results of TR, mainly the genetic context and the intracellular surveillance by the NMD.

The nucleotides surrounding the PTC, precisely the positions from -6 to +9 play an important role in TR.

Floquet and colleagues demonstrated that two principal determining factors influence the outcomes of the translation termination efficiency. Particularly, a cytosine (C) in position +4 and uracil (U) at -1 are correlated to a higher TR, indicating U-stop-C as a possible "consensus sequence" for the TR (Floquet C., *et al,* 2012).

At the same manner, an adenine (A) at -1 or -2 position can favour TR by mRNA structure distortion in the P site, playing a relevant role in the competition between eRF1 and nc-tRNA (Tork S., *et al*., 2004; Dabrowski M., *et al.,* 2015).

Finally, Wangen and Green have found that purine at the +1 position balances the equilibrium toward the termination of the translation, while a pyrimidine promotes the TR, as well as the two nucleotides downstream of the stop codon are crucial in the TR mechanism, affirming that A and U immediately nearby the stop codon facilitate the readthrough, oppositely the guanosine (G) and the C (Wangen J. R., and Green R., 2020; Palma M. and LeJeune F., 2020; Beryozkin A., *et al*., 2023) (**Figure 7**).

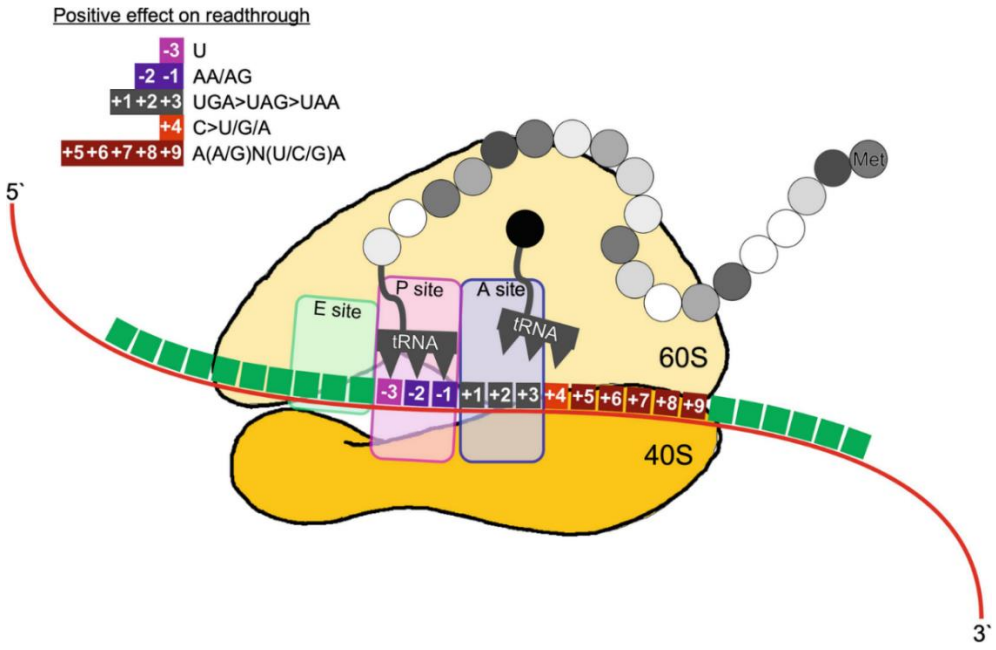

***Figure** 7. Genetic context actors that influence the readthrough mechanism (Beryozkin A., et al., 2023).*

Ultimately, Potapova reported that the position of the stop mutation in the mRNA is also worth, underlining that if PTCs are localized at the beginning of an ORF, near the AUG initiation codon, or at the end of the mRNA, near the poly-A tail, the mutation will not impact on the translation of the protein, because it is possibly removed or maintained, if not involving protein function (Potapova M. A., 2020).

Consequently, the lack of the protein, due to nonsense mutations is responsible for a severe phenotype; thus, the study of nonsense mutations is a challenge for researchers and clinicians. In addition, knowing the factors influencing TR could represent an instrument for genotype-specific patient treatment, that is at the base of the targeted therapy, in the view of the personalized medicinal approach.

The present project will focus attention on two main genetic diseases: Cystic fibrosis (CF) and Lipopolysaccharides (LPS)-Responsive Beige-like Anchor (LRBA) deficiency caused by nonsense mutations and the possibility of rescuing the expression of the related proteins by the use of molecules that possess readthrough activity (Pibiri I., *et al.,* 2015; Pibiri I., *et al.,* 2020).

1.4 Cystic Fibrosis (CF).

1.4.1 Cystic Fibrosis (CF).

CF is an autosomal recessive disease affecting 1:2,500 newborns in Europe and 1:3,500 in the USA, and, more recently, it has been reported that the worldwide number of people affected by CF is around 160,000, whose 35% still undiagnosed (Cystic Fibrosis Foundation Patient Registry. 2017. 2016 Annual Data Report. Bethesda, MD: Cystic Fibrosis Found) (**Figure 8**).

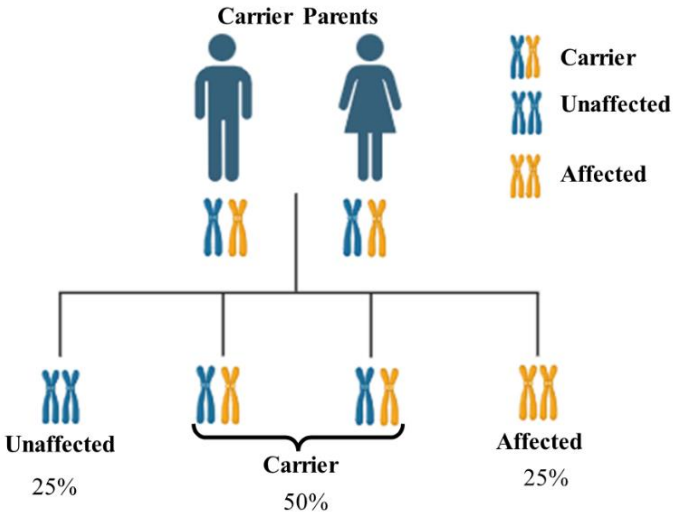

Figure 8. *Genetic hereditary pattern of autosomal recessive diseases.*

CF was described for the first time by Guido Fanconi and two years later (1938) by Dr. Dorothy H. Andersen (Andersen D. H., 1938). Then, in 1989, Riordan and collaborators characterized and identified the gene causing the pathology, the *Cystic fibrosis Transmembrane Conductance Regulator (CFTR)* gene (Clague S., 2014), also known as *ATP-binding cassette (ABC) subfamily C member 7 (ABCC7)*, because its membership to the *ABC* gene family.

CFTR gene is localized in the long arm of chromosome 7 (7q31.2) and it is constituted by 27 exons, codifying for a 1480-amino acids glycoprotein, localized into the bilayer of the plasma membranes of epithelial cells (Riordan J. R., *et al.,* 1989) (**Figure 9**).

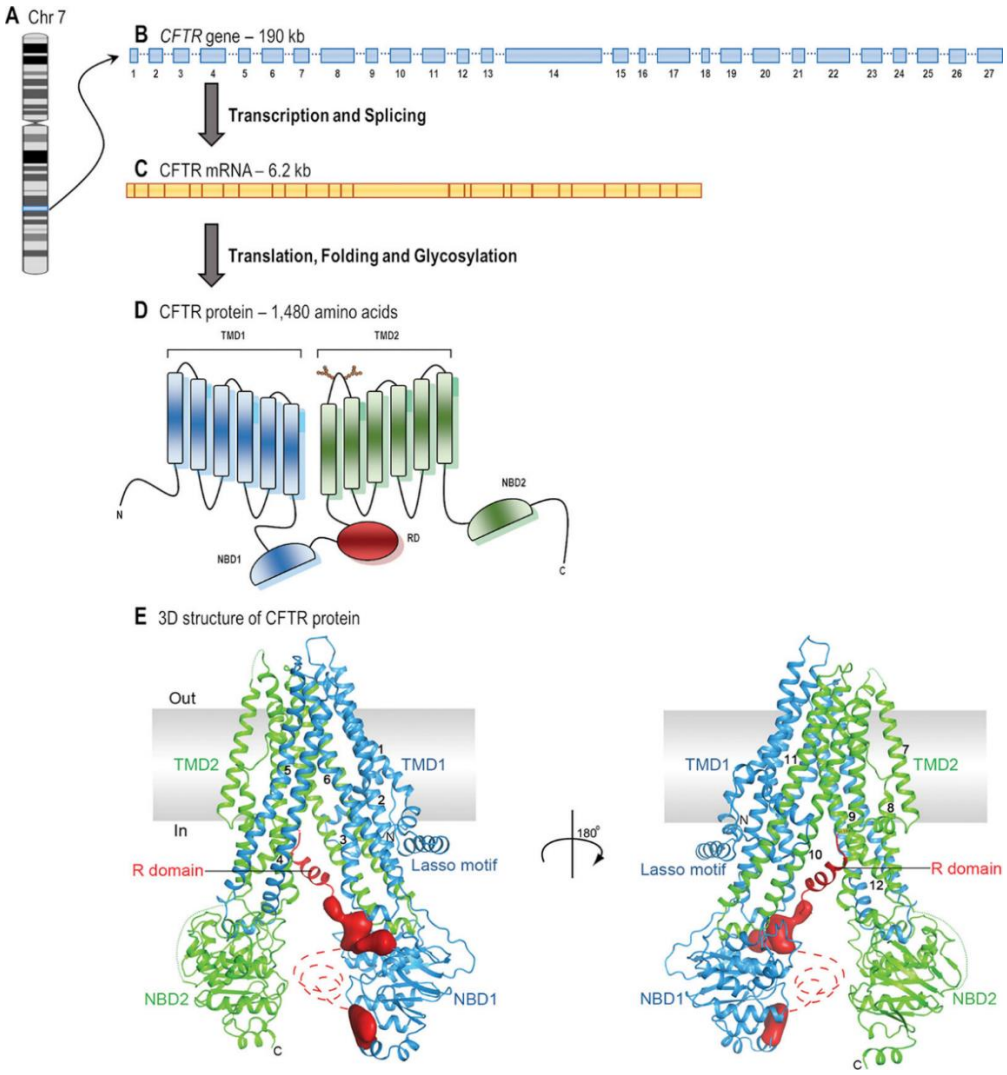

Figure 9. *CFTR gene (**A, B**), transcript (**C**), and 2D and 3D protein structures (**D, E**) (Adapted from Lopes-Paceco M., 2020).*

This protein is responsible for the ionic transport between the basal and the apical sides of cells, precisely involving chloride (Cl^-) and bicarbonate flux (HCO_3^-). Like the other ABC proteins, the structure is composed of three main domains: the transmembrane domain (TMD), the regulator (R), and the nucleotide-binding domain (NBD) (Dawson R. and Locker K., 2006; Liu F., *et al.,* 2017).

Precisely, the protein is constituted by two TMDs, counting 6 alpha helices each, which are linked to two NBDs on the intracellular side, in turn connected to the central R domain. The protein forms a channel mainly appointed to the transport of chloride, whose functionality is strictly regulated. Specifically, to obtain an open conformation, NBDs need to form a dimer through the ATP binding and be fully activated when the R domain is phosphorylated by Protein Kinase A or C (PKA) or (PKC) (Vergani P., *et al.,* 2005). Contemporary, PKA or PKC activation is realized by cAMP, so its production is necessary for the upstream CFTR activation (Della Sala A., *et al.,* 2021) (**Figure 10**).

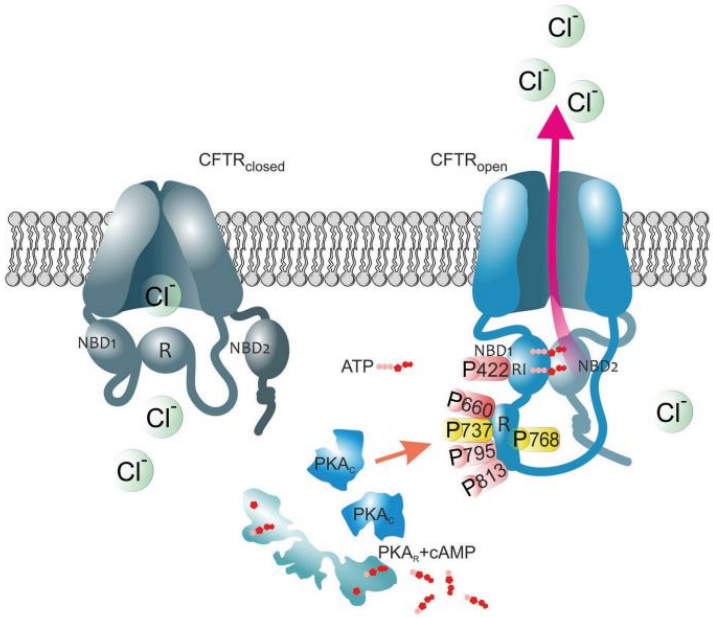

Figure 10. *Mechanism of activation that allows the open state conformation of CFTR protein under PKA/cAMP regulation and representation of the chloride transport through apical membranes following intracellular domains reorganization (Della Sala A., et al., 2021).*

The protein is localized in the apical membranes of epithelial cells of several organs, such as lungs, pancreas, liver, intestines, sweat glands, and vas deferens, underlying the relevant importance played by the channel protein in the physiological system and the multi-organs effects registered with CFTR impairment (Denning G. M., *et al.,* 1992; Wang Y., *et al.,* 2014; Lukasiak A. and Zajac M., 2021).

To date, over 2,500 mutations have been identified (CFTR1 database, http://www.genet.sickkids.on.ca), where about 75% of patients carry at least one allele with the most common defect, the CTT deletion between nucleotides 1521 and 1523, causing the phenylalanine deletion in position 508, while 10 % of people with CF harbour one nonsense mutation (Cystic Fibrosis Foundation Patient Registry. 2017. 2016 Annual Data Report. Bethesda, MD: Cystic Fibrosis Found). Considering the difficulties and the variability in describing all CFTR mutations, in 2014 De Boeck and Amaral proposed a simplified classification, based on the typology of the mutation, the possible therapeutic approaches, and the impact on life living (De Boeck K., and Amaral M. D., 2016).

In the below-described classification, the lowest number of the category corresponds to a major phenotype severity (**Figure 11-12**):

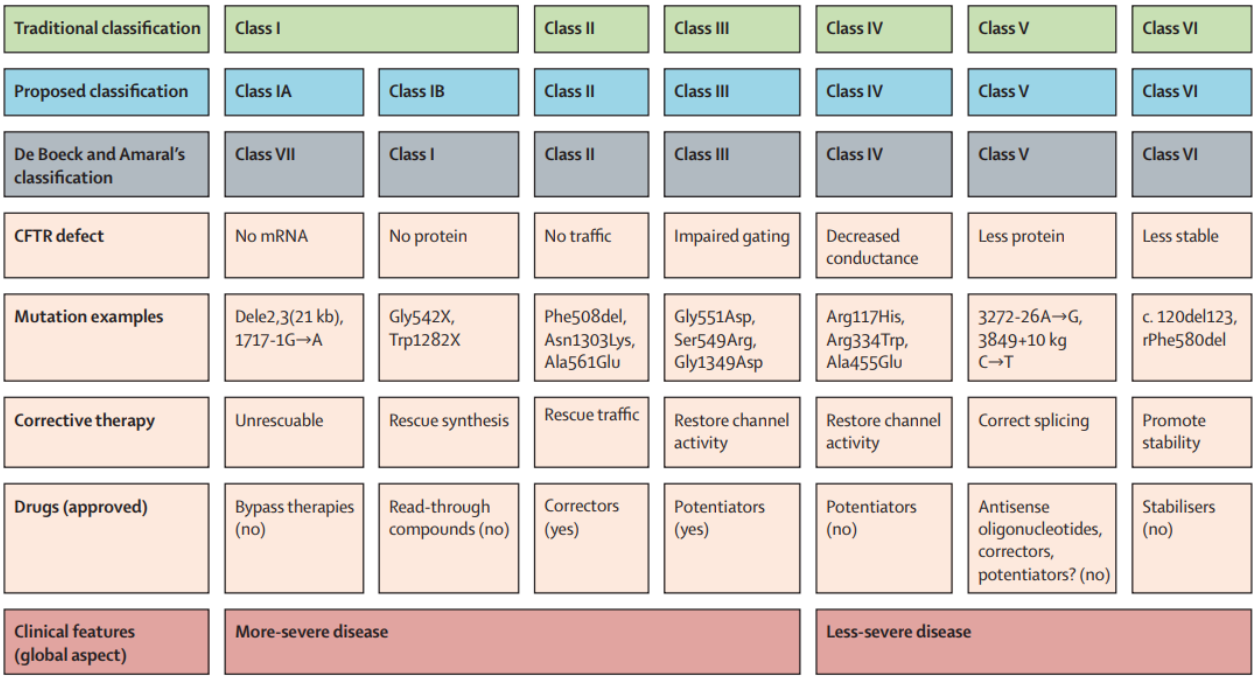

Figure 11. *Classification of CFTR mutations according to Marson and colleagues (Marson F. A. L., et al.*, 2016*).*

- **Class I** has recently been divided into two subclasses by Marson *et al.*: IA and IB (Marson F. A. L., *et al.*, 2016). **Class IA** includes the mutation known as "un-rescuable", often due to the presence of a splicing mutation or severe deletions. An important and mostly detected mutation in Europe is a 21kb deletion, consisting of deletion from intron 1 to 3 (dele2,3), bringing to the production of a PTC and associated with a severe phenotype, characterised by a serious pancreatic insufficiency (Marson F.A. L. *et al.,* 2016; Pranke I. *et al.*, 2019). Then, **class IB** is characterized by nonsense mutations, leading to the elimination of the mRNA, by the NMD pathway (De Boeck, K., and Amaral, M. D., 2016), and/or the production of a truncated non-functional protein, rapidly degraded. The most diffused nonsense mutations are the G542X, W1282X, R1162X, and R553X. The actual percentage of CF patients harbouring this type of alteration is calculated to be between 10% and 50 %, depending on the homozygosity or heterozygosity (Elborn J. S., 2016). Besides, all class I alterations are also known as "orphan" mutations because of the lack of specific treatments.
- **Class II**: this is the most known group because the most common CFTR mutation is listed here, that is the three base-pairs deletion of the codon codifying for Phenylalanine in position 508 (F508del). Also, missense mutations belong to this class and the consequence is the production of misfolded proteins, bringing to the total absence of ions traffic. Due to the impairment in protein post-translational modifications and its subsequent degradation ubiquitin-proteasome dependent, proteins are not functional and, even if they reach the correct localization in the plasma membrane, the open-close state of the channel is defective, so ions flux is compromised. The main representative mutation F508del involves 75% of CF patients, but

Asn1303Lys and Ala561Glu are counted in class II, too (Marson F.A. L. *et al.,* 2016; Dechecchi M. C., *et al.,* 2018)

- **Class III**: in general, NBD mutations are found in this category. These lead to defective regulation of gating and open-closed conformation, with a consequent loss opening state of the channel. The most diffused mutation is G551D with a frequency of 2-4% of cases (Pranke I., *et al.,* 2019).
- **Class IV**: it is characterized by missense mutations with alterations in TMDs, causing ionic conductance issues. So, the protein reaches the localization into the plasma membrane, but only a residual Cl^- secretion is registered. R117H is one of the most representative variations of this class (Fanen P., *et al.,* 2014; Pranke I., *et al.,* 2019).
- **Class V**: splicing mutations involve acceptors and donor splice-sites, causing the complete or partial exclusion of an exon, in the case of exon skipping, or the insertion of an intron in the mRNA sequence. The most common mutation of this category is the exon 10 skipping due to the presence of a polymorphism consisting in the polypyrimidines tract upstream of the acceptor site. If the number of thymine is comprised between 7 and 9, correct splicing will take place at 90%, while a lower number is associated with an impairment in the splicing process, giving rise to mostly aberrant mRNAs and only 10-40% normal (Chu C. S. *et al.,* 1993; Fanen P., *et al.,* 2014).
- **Class VI**: it is constituted by all the mutations that cause a rapid turnover of the CFTR protein so that the protein is produced but its function is notably reduced (Pranke I. *et al.,* 2019). One of the most representative mutations is c.120del23, identified in two Portuguese CF patients in 2009 (Ramalho A. S. *et al.,* 2009). Precisely, the deletion causes the abolition of the natural start codon, producing an N-terminal truncated protein, reducing its stability and, consequently, ions' conductance.

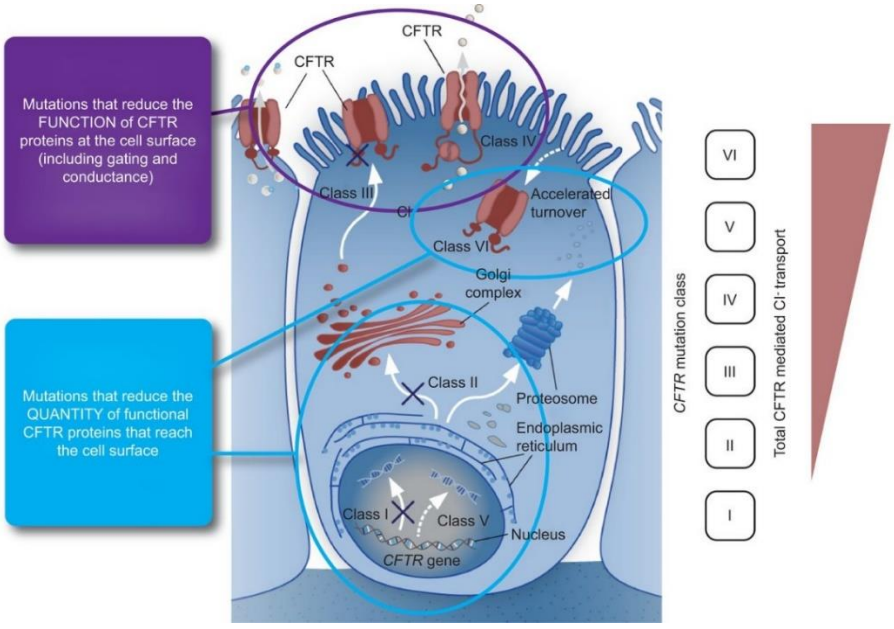

Figure 12. *Graphical and detailed representation of the different classes of CFTR mutations and their relationship with the derived severity of the phenotype (Derich N., 20123).*

In general, a worldwide percentage of incidence is attributable to each class or specific aberration, precisely, 75% to F508del, 10% to nonsense, 15% to missense, frameshift, splicing, insertions/deletions (Bobadilla J.L., *et al.,* 2002; Tsui L.C., *et al.,*2013; Pranke I. *et al.,* 2019).

1.4.2 Therapeutic approaches in CF.

CF involves various organs, such as the lungs, pancreas, liver, glands, testis, intestines, heart, and immune system, the reason why the common therapy for all patients is the targeted treatment against symptoms (**Figure 13**).

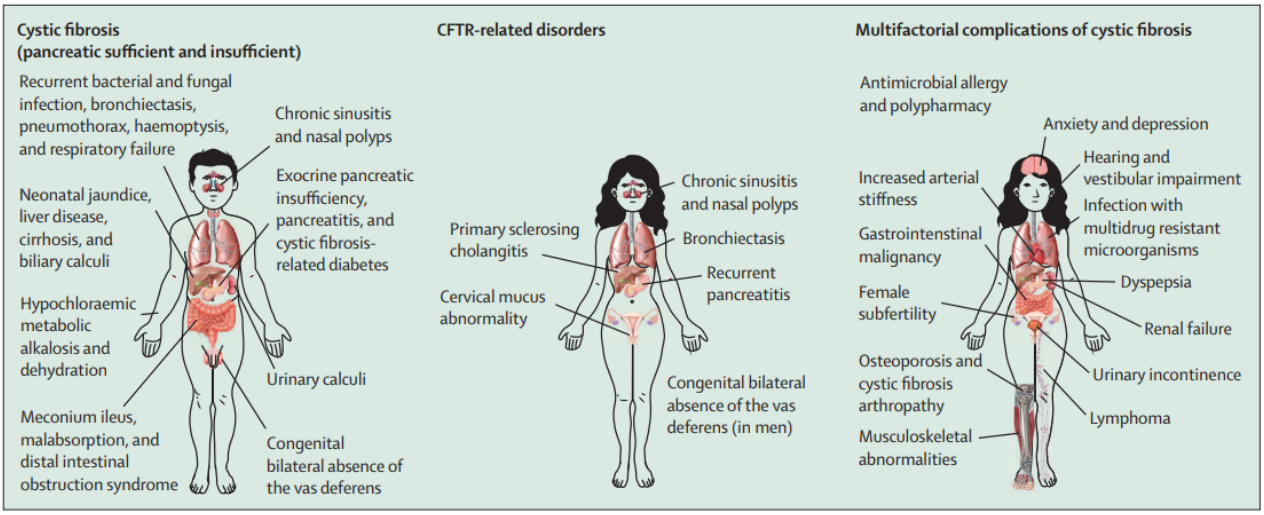

***Figure 13**. Clinical symptoms of CF and CF-related disorders, underlining the multi-organ impact of the disease (Shteinberg M., et al., 2021).*

Particularly, since the first description of the disease, the most diffused and useful therapeutic approach was based on various treatments, aimed at treating the symptomatology. The different cures are provided for implementing pancreatic enzymes, to help nutrient absorption and avoid intestinal dysfunctions and malnutrition; the airway clearance therapy associated with pulmonary physiotherapy, as well as antibiotics to avoid the diffusion of bacterial infections, often rising in the thick layer of mucus in lungs (Elborn J. S., 2013) (**Figure 14**). These clinical manifestations make clear how the defect in CFTR protein is life-threatening for patients and the numerous precautions that need to be taken in daily life.

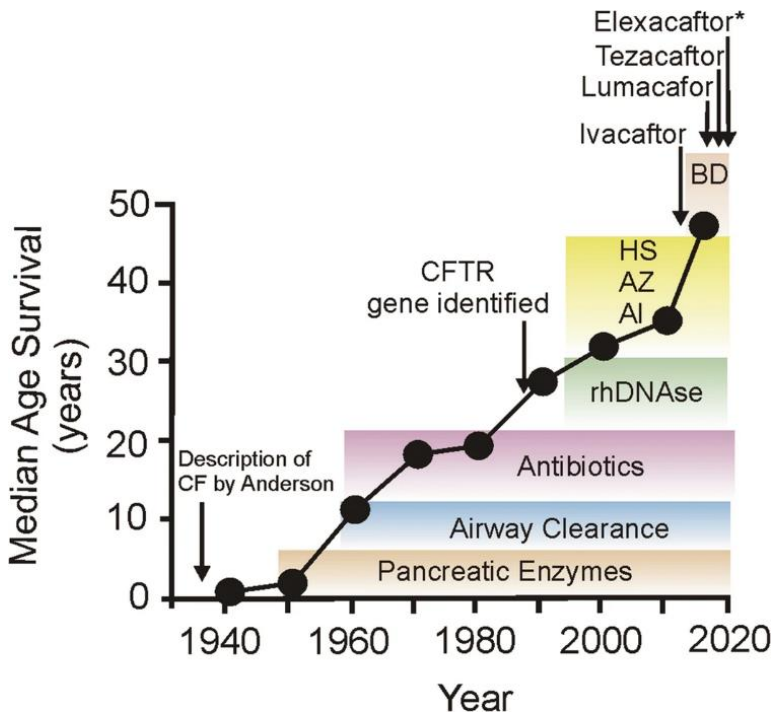

Figure 14. *Graphical representation of research and clinical advances in treating CF patients since the discovery of the disease (Bradbury N.A., 2020).*

By 2012, the main pharmaceutical revolution took place with the discovery and the subsequent approval of molecules, called potentiators and correctors, produced by Vertex Pharmaceutical. The first drugs act to potentiate CFTR open-state and, subsequently, chloride transport; besides, the second ones improve the folding of misfolded protein derived from missense mutations, among which the F508del and G551D are the most representative, allowing it to reach the proper localization and perform its activity in apical membranes (Yu H., *et al*., 2012; Pranke I., *et al.,* 2019). First, Ivacaftor (Kalydeco®), then the combination of Lumacaftor and Ivacaftor (Orkambi®), followed by the double therapy of Tezacaftor and Ivacaftor (Symkevi®), until the most recent triple combination of Tezacaftor, Ivacaftor, and Elexacaftor (Kaftrio®), have completely changed lifestyle and expectancy in patients with CF, but not for all, because, even if mostly 85-90% of patients can be treated with Vertex compounds, the remaining about 10-15% of nonsense, splicing and ultrarare mutations are still untreatable, so named "orphans" of cure (King J.A., *et al*., 2022; Jia S., and Taylor-Cousar J. L. 2023).

1.4.3 The suppression therapy.

In the last decades, several strategies have been proposed to overcome the genetic defects due to nonsense mutations, and some strategies are now developed by pharmaceutical companies and gone into clinical trials. Among the possible approaches to correct the basic defect, we can name three main categories: **i) genetic editing**, which consists almost in the use of the CRISPR/Cas technology to promote both mRNA and DNA correction (Ledford H. and Callaway E., 2020; Melfi R., *et al.,* 2020); **ii) suppressor t-RNAs**, that are modified tRNAs that recognize a stop codon but introduce an amino acid instead of the stop signal (Albers S., *et al.*,

2023); **iii) readthrough compound,** aimed to act during the translation process (Nagel-Wolfrum K., *et al.,* 2016).

A promising approach consists of the use of small molecules that show translational readthrough (TR) activity, indeed named *Translational Readthrough-Inducing Drugs* (TRIDs) (Pranke I, *et al.,* 2019).

As explained before (see section 1.4), TRIDs should work by inducing a mistranslation by the ribosome and recruiting near-cognate tRNAs codifying for an amino acid instead of the stop codon signal. So, a full-length protein is generated. The induced TR takes advantage of the small pool of NMD-escaping mRNAs (Palma M. and LeJeune F., 2021).

Several molecules and drugs have been tested and developed in this panorama as TRIDs.

In particular, the first category of molecules discovered to have this activity was a group of aminoglycoside antibiotics, such as Gentamicin and Geneticin (G418). Generally, they act by altering the A-site conformation of the ribosome, which consents to the misreading and to complete the translation, even in the presence of the stop codon (Krause K. M., *et al*., 2016) (**Figure 15**).

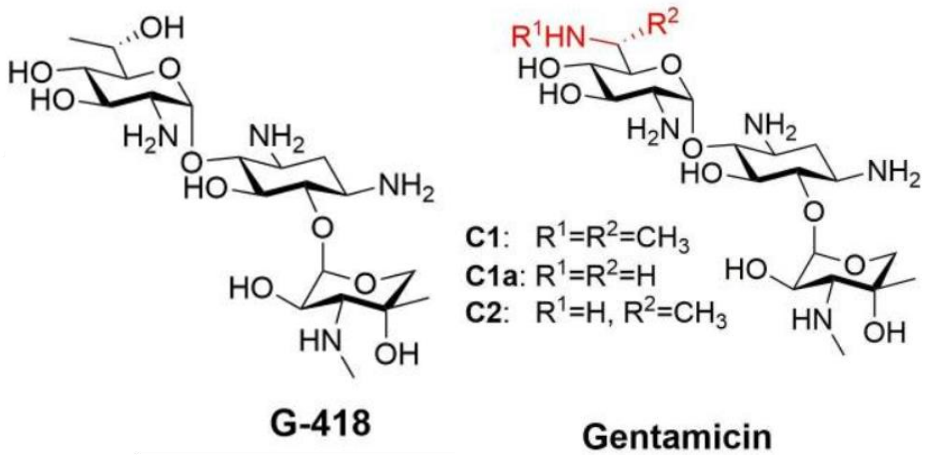

Figure 15*. Chemical structure of Geneticin (G418) (left) and Gentamicin (Jospe-Kaufman M., et al., 2020).*

Moreover, despite the TR activity, the prolonged treatment resulted to be cytotoxic, and oto- and nephrotoxicity were mainly evidenced (Martins-Dias P and Romão L., 2021). In this context, recent studies were focused on finding strategies to decrease toxicity, with antioxidants or other TR molecules, to lower the effective dosage, to be used in synergy (Manuvakhova M., *et al.,* 2000; Krause K. M., *et al*., 2016; Jospe-Kaufman M., et al., 2020; Wohlgemuth I., *et al*., 2021; Le T. A., *et al.,* 2023; Li S., *et al.,* 2023).

In 2007, a new promising drug, presenting an oxadiazole core, was discovered by high-throughput screening (HTS) and developed by PTC therapeutics under the trade name of Traslarna™, also known as Ataluren (or PTC124) (Welch E., *et al*., 2007) (**Figure 16**). After having shown very interesting data *in vitro* and in animal models (Du M., *et al.,* 2008; Kayali R., *et al*., 2012; Pibiri I., *et al.,* 2015), this drug underwent clinical trials for CF and DMD, and it has also completed clinical trials for Dravet Syndrome, and Aniridia (NCT02647359, NCT02647359), while pre-clinical studies have been carried on Choroideremia and Mucopolysaccharidosis I-Hurler (MPS I-H) (Torriano S., *et al.,* 2018; Wang D., *et al.,* 2022).

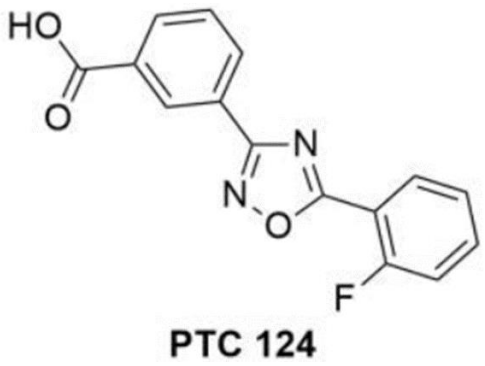

***Figure 16**. Structure of the 3- [5-(2-Fluorophenyl)-1,2,4-oxadiazol-3-yl] benzoic acid, also named Ataluren (or PTC124) (Traslarna™, PTC Therapeutics) (Campofelice A., et al., 2019).*

Precisely, for CF, phase II (NCT00237380) safety and efficacy trial gave positive results, but phase III trial outcomes did not reach the expected endpoints (NCT00803205), so, following conflicting results, clinical experimentation for CF was interrupted (Kerem E., *et al.,* 2014; Zainal Abidin N., *et al.,* 2017).

However, a second phase III trial (NCT02139306) was prompted, suggested by a possible interference between aminoglycosides and Ataluren (PTC124) in the patients' cohort, still confirming the previously observed results (Konstan M.W., *et al.,* 2020).

Nonetheless, in 2014 (Ryan N.J., 2014), the European Medicines Agency (EMA), seeing the positive results of DMD trials, approved the use and market of Ataluren (PTC124) for DMD, confirming the authorization in 2016, renewed until the 15th of September 2023, when EMA diffused a communication of non-renewal for Ataluren (PTC124) in DMD due to a negative benefit-risk balance for patients (https://www.ema.europa.eu/en/news/ema-recommends-non-renewal-authorisation-duchenne-muscular-dystrophy-medicine-translarna).

In this scenario, an improved synthetic aminoglycoside-derived molecule, named ELX-02 (former NB124), was discovered and entered phase I and II clinical trials, after having shown positive results *in vitro* in CF and Cystinosis (Brasell E.J., *et al.,* 2019; Crawford D. K., *et al.,* 2020; Crawford D. K., *et al.,* 2021; Chen J., *et al*., 2023) (**Figure 17**).

In addition, a recent study highlighted that the U-UGA-C stop codon is an advantageous context for ELX-02 activity (Pranke I., *et al.,* 2023)

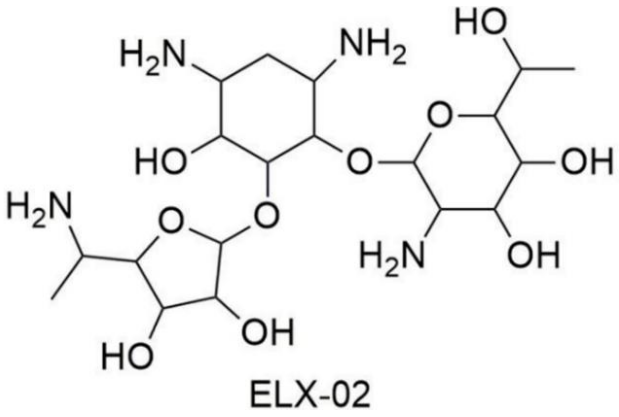

Figure 17*. Structure of ELX-02 (NB124) (Campofelice A., et al., 2019).*

Then, the safety, pharmacokinetics, and tolerability of ELX-02 were positively evaluated in three different phase I trials (NCT03292302, NCT03776539, NCT03309605), underlining the absence of the toxicity normally evidenced with antibiotics aminoglycosides. Thus, phase II trials for CF were conducted (NCT04126473, NCT04135495, NCT04069260), but, contrary to very promising preliminary results, it failed phase II (*Eloxx Pharmaceuticals reports September 14, 2022*).

Contemporary with the study of ELX-02, another molecule was identified and investigated in the possibility of performing the readthrough. The 2,6-Diaminopurine (DAP) was shown to act specifically on the UGA stop codon, with major efficacy than the other two PTCs, individuating the possible mechanism of action, explained by the inhibition of the enzyme FtsJ RNA 2'-O-Methyltransferase 1 (FTSJ1), a tRNA methyltransferase specific for the modification of $tRNA^{Trp}$. Interestingly, a study of pharmacokinetics and TR efficacy *in vivo* showed promising results (Trzaska C., *et al*., 2020; Leroy C., *et al.*, 2023) (**Figure 18**).

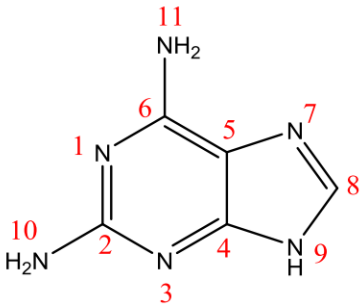

Figure 18. *Chemical structure of the 2,6-Diaminopurine (DAP) (Trzaska C., et al., 2020).*

In this panorama, three new optimized leads, Ataluren (PTC124)-derivatives, have been recently discovered by HTS by the research group of professors Lentini and Pibiri at the University of Palermo. The three oxadiazole-core compounds, named NV848, NV914, and NV930 (hereafter NVs) have been patented (Italian Patent No 102017000134511, European Patent No. 3713934, US Patent No 11,203,578) and validated in

several in *vitro* models of nonsense mutation related diseases (Tutone M., *et al.,* 2020; Pibiri I., *et al.,* 2020; Bezzerri V., *et al.,* 2022) (**Figure 19**).

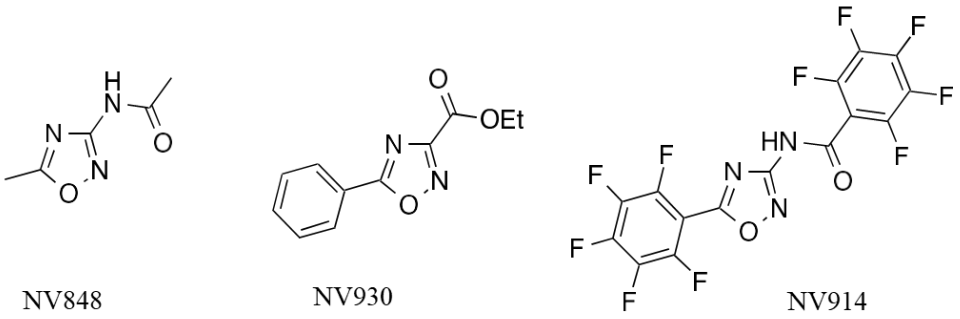

Figure 19. *In this scheme are shown the chemical structure of the three oxadiazole molecules NV848, NV914, and NV930 (Carollo P. S., et al., 2023).*

In addition, as for DAP, also NVs were shown to influence the activity of FTSJ1, suggesting this enzyme as a possible target explaining the probable molecules' mechanism of action (Carollo P. S., *et al.,* 2023). Seeing that these three molecules could represent potential treatment drugs against nonsense mutations, *in vivo* model studies are required, reason why safety *in vivo* has been also assessed during the development of this project (Corrao F., *et al.,* 2022).

However, TRIDs alone can surely help to bypass the defect, but multiple and contemporary intracellular targets involved in translational machinery and mRNA processing are needed, particularly NMD inhibitors, to enrich available PTC-harbouring mRNA to be targeted by TRIDs (Spelier S., *et al*., 2023; Osum S. H., *et al.*, 2023; Wagner R. N., *et al.,* 2023) (**Figure 20**).

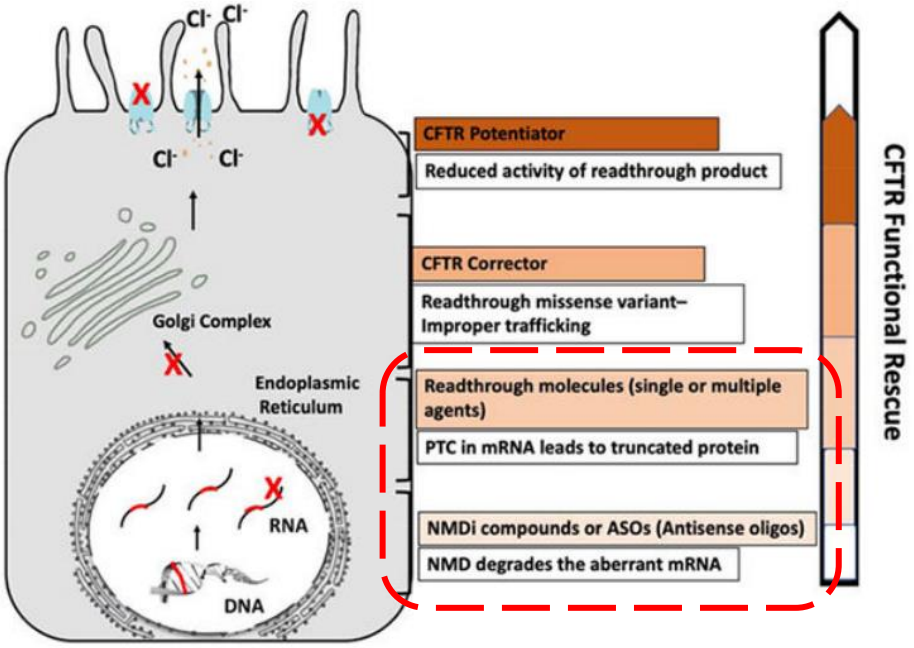

Figure 20. *Scheme representing all the therapeutic approaches to treat CFTR different mutations, with a specific focus on the treatments for nonsense mutations (Adapted by Sharma J., et al., 2020).*

1.4.4 Methods for the study of the CFTR activity in vitro and in vivo with readthrough molecules.

1.4.4.1. The Ussing chamber as a gold standard technique to evaluate CFTR function rescue.

One standardized method to study the CFTR function *ex vivo* is the Ussing Chamber technique (De Jonge H.R., *et al*., 2004; Ramalho A.S., *et al.*, 2022).
This technique allows to evaluate the transepithelial electrical measurement, thus ions transport, from basal to apical sides of an epithelium. The ions transfer is registered by imposing a voltage clamp on tissues or monolayer cells, which reveals any changes in electrical current, due to ions movement. So, the system registers a short-current circuit (Isc) expressed in µA/cm^2 unit (Li H., *et al.,* 2004; Thomson A., *et al.,* 2019) (**Figure 21**).

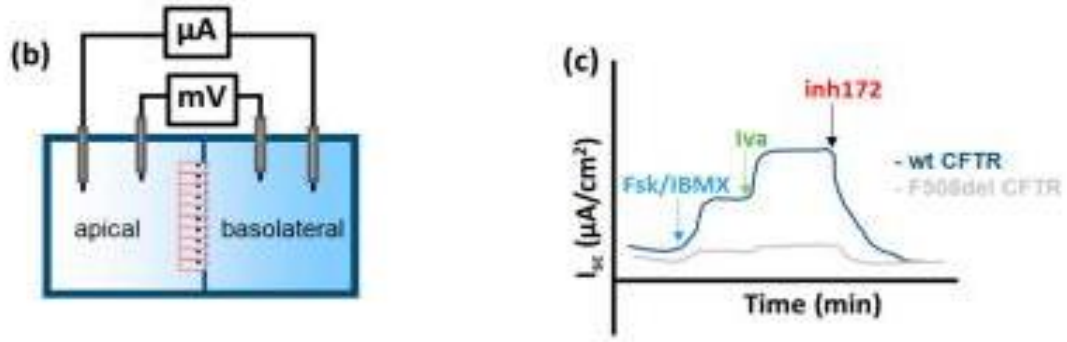

Figure 21. *Schematical representation of the Ussing Chamber technique and Isc measurement (Adapted from Ramalho A.S., et al., 2022).*

This methodology has been adapted to study CFTR protein recovery in different *in vitro* or *ex vivo* models and it found application in different systems, mainly in patients'-derived nasal or bronchial cells.
However, the peculiar feature is to develop a 2D culture, independently from the chosen model.
Focusing on the patient's cells, these are harvested from the people, then kept in culture to grow and, subsequently, to differentiate on apposite inserts provided with a specific membrane, that allows the development of the basal and the apical sides in the conditionally reprogrammed cells (Golec A., *et al*., 2022).
It has been shown that airway epithelium is constituted by several types of cells deputed to specific functions:

- basal cells represent the progenitors and are necessary in case of impairment or injury in the epithelium;
- brush cells, important for drug metabolism;
- goblet cells, also named secretory, involved in mucus secretion;
- ciliated cells, which represent around 50% of the cells in airway epithelia, are responsible for mucus elimination, but also for trans-differentiation and repair;
- ionocytes, which express a lot of ion channels, contributing to mucus viscosity (Crystal R. G., *et al*., 2008; Yaghi A., and Dolovich M. B., 2016; Montoro D., *et al*., 2018; Davis J. D., and Wypych T. P. 2021) (**Figure 22**).

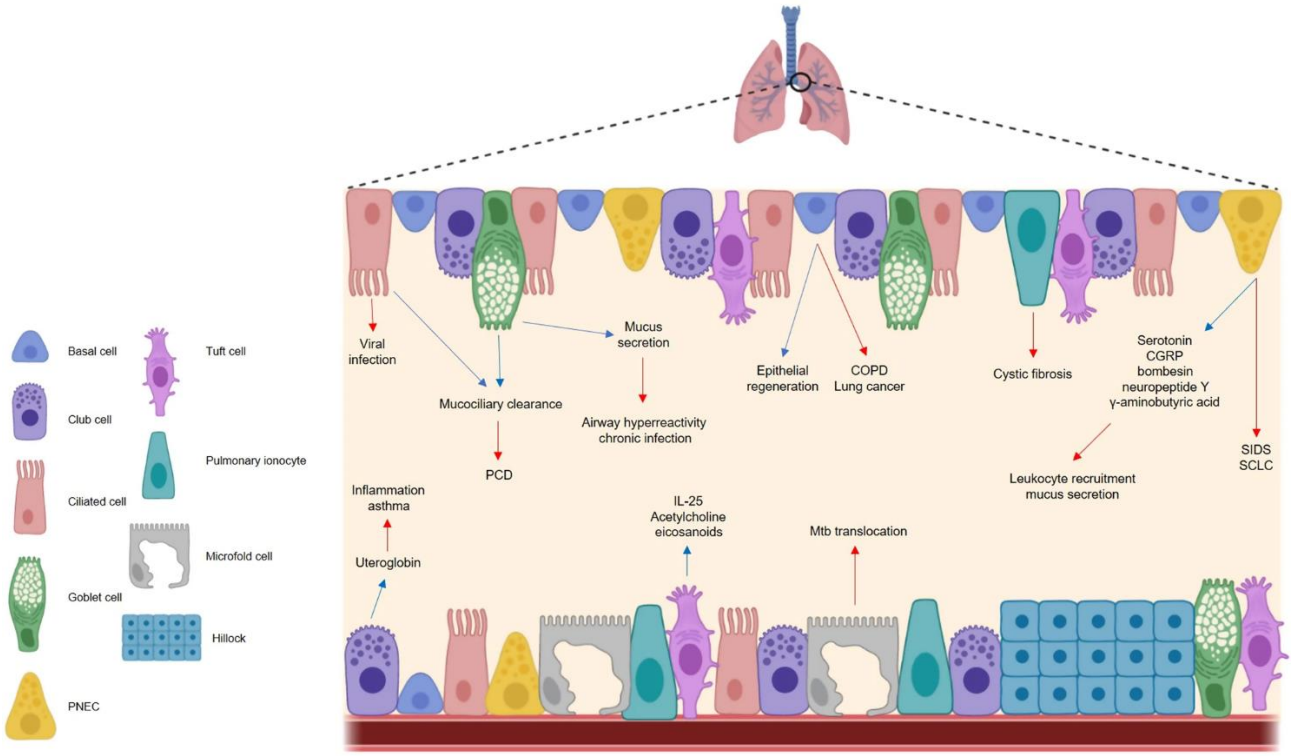

Figure 22. *The scheme shows the cell types found in airway epithelia. In this representation, specific features of each cell are also indicated, like the morphology, together with the pathway where each cell type is involved, or the factors secreted or characterizing every cell (Davis J. D., and Wypych T. P. 2021).*

Considering that the cells expressing the most CFTR protein were identified in the ionocytes, the ciliated, and the secretory cells, "reprogramming" and inducing cell differentiation from patients' derived samples is the most suitable strategy to study CFTR expression and function restoration under specific treatment (Montoro D., *et al.,* 2018; Okuda K., *et al*., 2021).

A possible application of the Ussing Chamber could be the evaluation of the rescue of CFTR protein function after readthrough compound treatment, indeed a recovery in chloride current can indicate the efficacy of these molecules.

In the more and more diffused vision of personalized medicine, tailored to everyone, this could also allow the evaluation of how the genotype-phenotype correlation could influence the response to treatment. (Park J. K., *et al*., 2020).

1.4.4.2. Mice models in CF and the importance of animal experimentation as preclinical systems for human health.

Even if *in vitro* and *ex vivo* assays consent to rapidly testing drugs' safety or examining the efficacy of some treatment, *in vivo* experimentation remains a relevant resource for researchers.

Historically, animal models contributed significantly to the advancement of biomedical research, to understand pathological and biological processes. Based on the principle of comparative medicine, animal models are an

instrument able to replicate human physiological and pathological processes. Considering the hypothesis and objective of each project and the anatomical, functional, and genetic similarities to humans, the researcher can select the right animal model (Ericsson A. C., *et al.,* 2013).

Although non-animal methods, such as cell or tissue/organ culture, and computational models may help to predict clinical outcomes and reduce animal use (Freires I. A., *et al.,* 2023), animals remain the best model for the study of disease in patients (Garattini S. and Grignaschi G., 2017).

However, ethical committees strictly regulate animal experimentation to ensure animal fitness, wealth, and well-being. For this purpose, before performing any kind of procedure on animal models, authorization is needed, and several rules are required to be respected. One of the most important is the 3R principle (Replace, Reduce, Refine), established by Russell and Burch in 1959 (Russell W.M.S. and Burch R.L., 1959; Hubrecht R. C., and Carter E., 2019), aimed to avoid improper use of animals in research projects, to protect them from harmful, stressful, and not necessary procedures. Subsequently, every experiment must be justified, authorized, and ruled.

Taking into account the importance of *in vivo* models for biomedical research and drug development, and considering the ethical concerns, various committees were created in the last decades, and more and more guidelines were drawn up, like the ARRIVE principles (Percie du Sert N., *et al.,* 2020). In addition, several guidelines were established for the use of animals for drug testing and discovery, after *in vitro* preliminary results achievement. In particular, the *in vivo* step is required to establish safety, pharmacokinetics, bioavailability, biodistribution, and effectiveness (Robinson N. B., *et al.,* 2019). For these purposes, the Organism for Economic Co-operation and Development (OECD) (https://www.oecd.org/chemicalsafety/testing/oecdguidelinesforthetestingofchemicals.htm), or the Globally Harmonized System of Classification and Labeling of Chemicals (GHS) (https://unece.org/transport/standards/transport/dangerous-goods/ghs-rev9-2021) drafted specific and detailed protocols.

Particularly, mice represent the most convenient model for the study of some pathologies, because they can produce an elevated number of newborns in less time and mating, besides the relatively low costs, the easiness of managing them, the fewer ethical concerns, and the existing protocol based on mouse model.

In the case of rare genetic diseases such as CF, different mouse models were created, since mouse CFTR has an identity of 78 % with the human gene (McCarron A., *et al*., 2021).

The similarity in all mice models is the lack of pulmonary symptoms, that are among the most important in humans, while they are mainly affected in the gastrointestinal tract, suffering from intestinal obstruction, like CF patients (Colledge W. H., *et al.,* 1992; Borowitz D., and Gelfond D., 2013; Tobias J., *et al.,* 2022).

Besides, other phenotypes were observed in CF mouse models, involving infertility, and diminished survival, because death usually occurs between the 5th and the 20th day of birth, and reduced growth (Hodges C. A., *et al.,* 2008).

Concerning the absence of lung manifestations in mice, this is justified by various reasons. The first important aspect is that mice are grown and raised in a germ-controlled environment, protecting them from contracting lethal, severe, and contagious infections. Then, compensation by calcium-dependent chloride channels (CaCC)

was observed, together with a low expression of β-epithelial sodium channel (ENaC). All these factors contribute to avoiding the formation of hyperdense and thick mucus layers in mice lungs (Wilke M., *et al*., 2011).

Nevertheless, animal models remain an important tool for preclinical CF study, and, in general, in human diseases investigations.

In this study, to evaluate the ability of the three NV compounds to promote the readthrough *in vivo* a specific CF mouse model with a nonsense mutation in the endogenous CFTR gene was chosen. Specifically, more recently, in 2018 the research group of Professor Craig A. Hodge, in Ohio, created by CRISPR/Cas9 technology the first mouse model with a nonsense mutation, the G542X mutation in the endogenous CFTR gene in all organs (McHugh D.R., *et al*., 2018).

1.5 Primary Immune Regulatory Disorders (PIRD) associated with nonsense mutations.

The second part of this PhD project focused on rescuing the expression of the LRBA (Lipopolysaccharide (LPS)-responsive and beige-like anchor) protein using TRIDs. The gene that encodes this protein is found to be mutated in Primary Immunodeficiency Regulatory Disorders (PIRDs), with nonsense mutations being one of the identified types of mutations. PIRDs comprise 430 different diseases, whose 65 have been described in the past two years (Tangye S. G., *et al.,* 2020) (**Figure 23**).

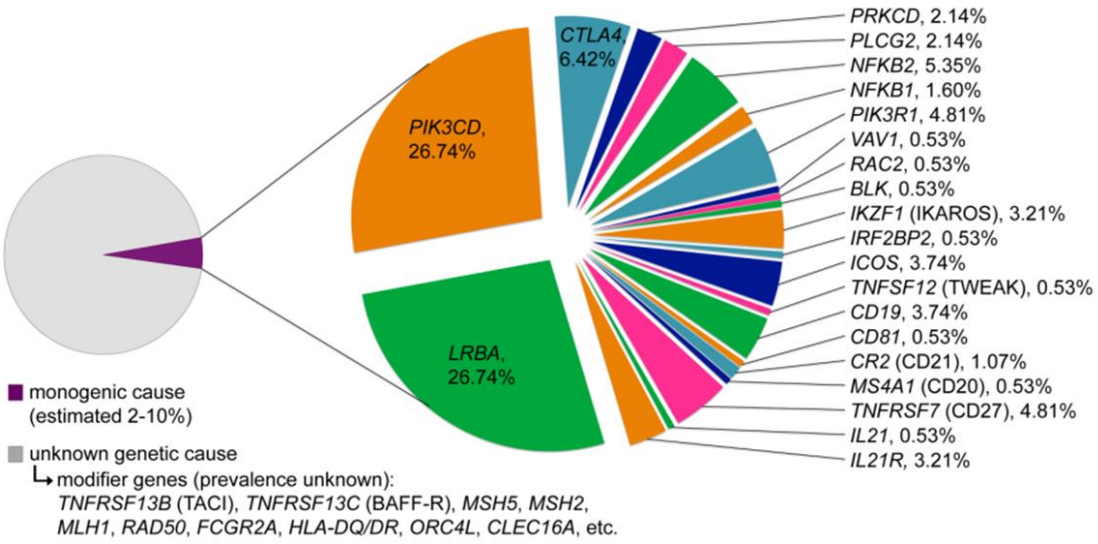

Figure 23. *Association of genes involved in PIRDs genesis and percentage of cases reported in the literature (Bogaert D. J., et al., 2016).*

The common characteristic is immune dysregulation due to gene loss-or-gain of function, depending on the inheritance, dominant or recessive, bringing various symptoms and phenotypical consequences (Kolukısa B. and Barış S., 2020). The symptomatology is varied too, but it also depends on the gene of interest.

In general, people living with PIRD suffer from common clinical symptoms, namely, autoimmunity and immune impairment, inflammation, allergy, frequent infections, lymphocytic infiltration, hypo- or agammaglobulinemia, thrombocytopenic purpura, anaemia, bowel diseases, hepatosplenomegaly, and predisposition to develop malignancies (Picard C., *et al.,* 2015; Gámez-Díaz L., *et al.*, 2016; Martínez-Jaramillo C., *et al*., 2019; Meyts I., *et al.,* 2021).

1.5.1 Molecular description of LRBA gene and its involvement in PIRDs.

The *LRBA* gene was identified and characterized for the first time in 2001 by Wang and collaborators (Wang J-W., *et al.,* 2001), and its dysregulation was associated with cancer cell growth in 2004 (Wang J-W., *et al.,* 2004). Besides, the first association of *LRBA* with immune system misfunction was affirmed by Lopez-Herrera in 2012 (Lopez-Herrera G., *et al.,* 2012).

It is localized on chromosome 4 (4q31.3), counts 58 exons, and codifies for 2683 amino acids, forming a 319 kDa protein. The protein is responsive to lipopolysaccharide stimulation and is expressed in various tissues, with a major concentration in the brain, endocrine system, gastrointestinal tract, liver, pancreas, reproductive systems, and, mainly in lymphoid tissues and bone marrow (https://www.proteinatlas.org/) (Martinez-Jaramillo C. and Truijllo-Vargas C. M., 2018).

The protein is classified as one of the 9 members of the BEACH (Beige and Chediak-Higashi)-WD40 domain-containing protein. Among the other 9 members, the most important and common are the BEACH, WD, PH, and ConA-like domains.

The BEACH and the WD domains are located at the C-terminus of the protein; the first is made of ~280 amino acids and forms an unusual structure with a hydrophobic core, while the second is 40-amino acids repeats of tryptophan and aspartic acid, forming a beta-helix structure. Both domains are typical of proteins involved in vesicle trafficking, receptor signalling, protein interaction, autophagy, apoptosis, as well as cell cycle control.

Pleckstrin Homology (PH) domain, always preceding the BEACH-WD40 region, counts 100 amino acids and is necessary for the association of the protein to phospholipids and other proteins, explaining its involvement in membrane and cytoskeleton rearrangement and vesicular trafficking, besides signal transduction.

Lastly, the ConA-like domain, containing lectins, is responsible for binding carbohydrates, justifying its role in protein and vesicle trafficking, a common feature with the previous domains (Cullinane A.R., *et al*., 2015; Alkhairy O.K., *et al.*, 2016) (**Figure 24**).

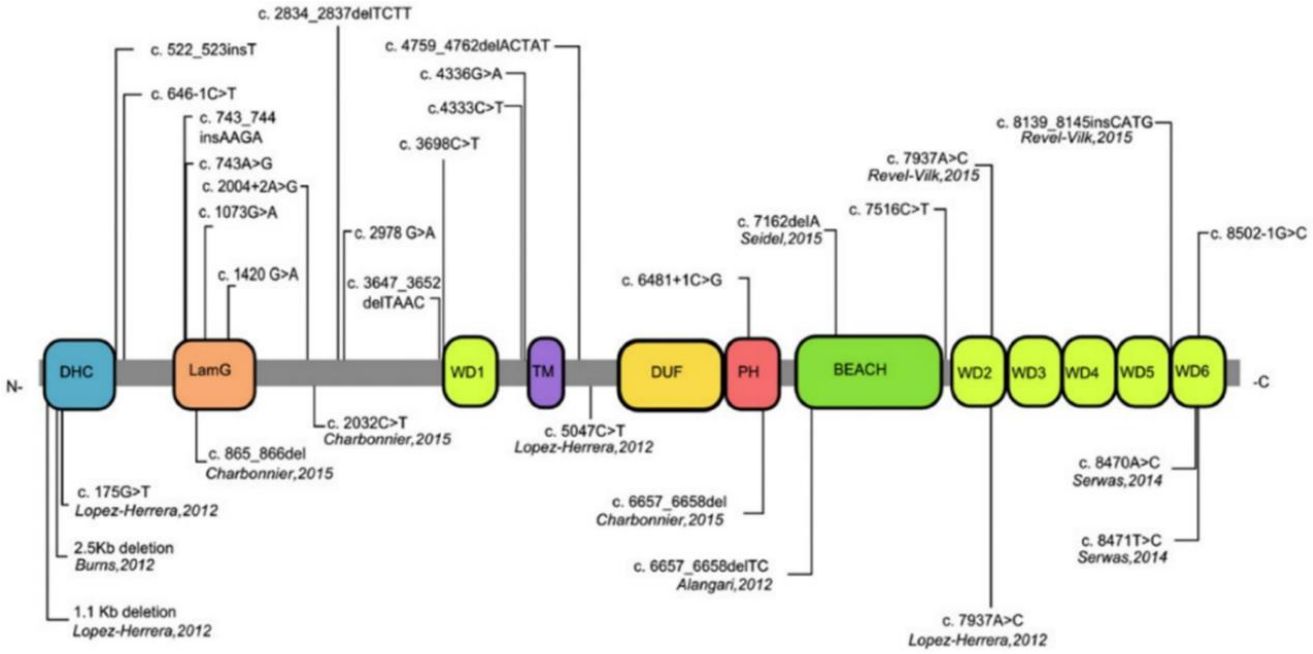

Figure 24. *Graphical representation of LRBA protein with functional domains and the majority of identified mutations in LRBA gene (Gámez-Díaz L., et al., 2016).*

More recently, LRBA has been indicated as an A-kinase anchoring protein (AKAP), because the protein presents two sites for RI and RII PKA subunits binding, so LRBA can link to cyclic PKA and form a complex, necessary for intracellular signal transduction. Indeed, it has been demonstrated that, particularly in T and B lymphocytes, LRBA binds PKA, and any dysregulation in this process could cause immunodeficiency, because of the lymphocytes' lack of signal transduction in pathways involved in immune response activation and function. The function of the AKAP-LRBA complex in T and B cells is linked to proliferation, survival, and immunoglobulin secretion, whose lack leads to Common Variable Immunodeficiency (CVID) onset (Moreno-Corona N.C., *et al.,* 2020; Pérez-Pérez D., *et al*., 2023).

LRBA is mostly expressed in the endomembrane systems and its function as AKAP, as well as and its implication in vesicle trafficking and signal transduction is evident considering the turn-over of three other proteins: the Cytotoxic T-Lymphocyte Antigen 4 (CTLA-4), expressed in T lymphocytes, and two important receptors, the Epidermal Growth Factor Receptor (EGFR), and the death receptor Fas.

These three proteins are associated with different pathways: CTLA-4 is a receptor responsible for immune checkpoint activity, whose expression attenuates the activation of the immune system, switching off the response; EGFR is activated under EGF binding and tyrosine residues phosphorylation by PKC, to favour transcription of genes related to proliferation and cell survival; Fas, after Fas Ligand (FasL) association, is implied in apoptosis triggering, following Fas internalization (Avraham R, and Yarden Y., 2011; Martinez-Jaramillo, C., and Truijllo-Vargas, C. M., 2018; Sobhani N., *et al.,* 2021).

Thus, LRBA is correlated to the internalization, trafficking, and recycling of the above-mentioned receptors. Particularly, the involvement in CTLA-4 performance is better understood, while for EGFR and Fas, lots of information and knowledge are still missing. CTLA-4 function is strictly regulated to allow a controlled

immune response activity so that CTLA-4 internalization and recycling are necessary. Recently, Janman and collaborators have demonstrated that CTLA-4 recycling is managed by LRBA and Ras-related in brain (Rab) 11, through vesicle trafficking, and that Rab11 colocalizes with CTLA-4. So, LRBA impairment could cause CTLA-4 and immune dysregulation (Janman D., *et al.,* 2021) (**Figure 25**).

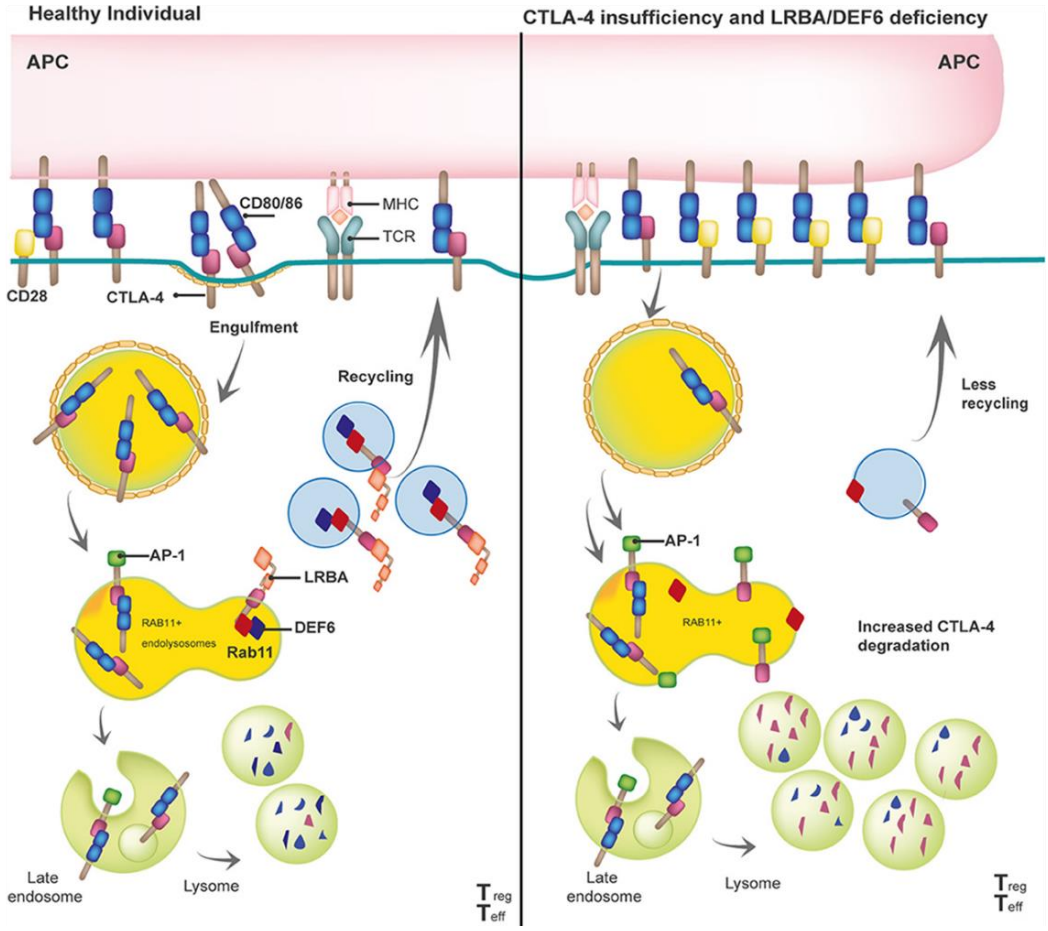

Figure 25. *Schematic overview of the LRBA protein mechanism in regulating cellular trafficking of CTLA-4 in T lymphocytes in health (left) and pathological condition, with LRBA deficiency (right) (Gámez-Díaz L. and Seidel M.G., 2021).*

In the same manner, EGFR trafficking is mediated by vesicles with the participation of LRBA, Rab, and Clathrin, but the role of the trafficking remains unclear. This is because in some publications EGFR regulation is associated with cancer cell growth and, more recently, it has been shown that LRBA dysregulation evidence also a tendency to develop some form of cancer (Wang J-W., *et al*., 2004; Ceresa B. P., 2006; Tomas A., *et al.,* 2014). However, EGFR internalization is a useful process for both EGFR recycling and the maintenance of signalling, together with its degradation (Sigismund S., *et al.,* 2008; Sigismund S., *et al.,* 2018; Murphrey M. B., *et al.,* 2022) (**Figure 26**).

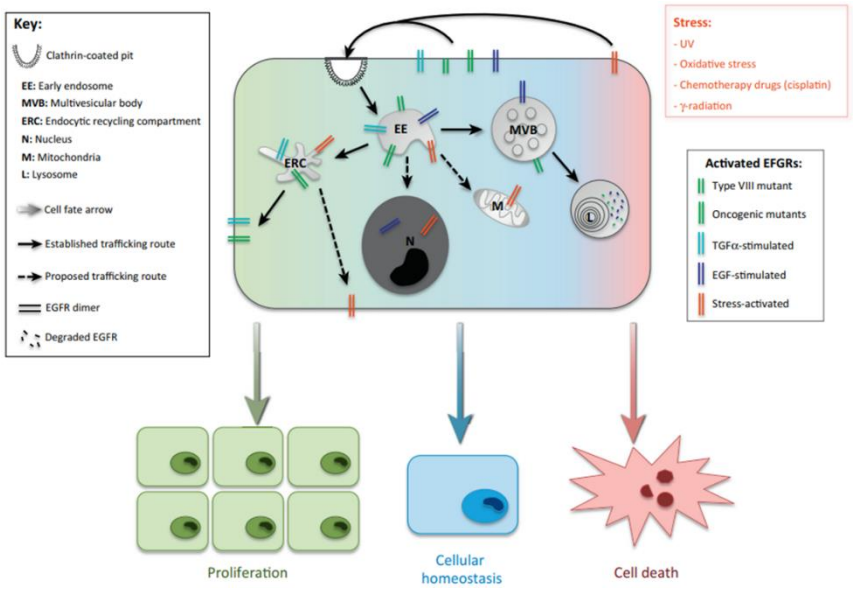

Figure 26. *EGFR endosomal vesicle trafficking and regulation with the related outcomes and pathway activated after EGFR expression or inhibition (Tomas A., et al., 2014).*

Considering the significant impact that rare and ultra-rare diseases associated with nonsense mutations have on human health, one of the most widely discussed topics in the scientific community is the search for potential treatments for these conditions. With the concurrent advancement of technology and the emergence of omics techniques, the collaboration between biomedical researchers and clinicians has led to the establishment of foundations and international partnerships dedicated to discovering potential remedies for the underlying issues in nonsense mutations.

Furthermore, the notion that a patient's genotype can influence not only their phenotype but also the outcomes of treatment has popularized the concept of targeted therapy as a means of developing individualized and tailored cures. Within this research field, the three NV molecules have found their place.

Therefore, this Ph.D. project aimed to assess safety, biodistribution, and efficacy experiments on these compounds *in vivo*, with a special focus on the NV848, in addition to using various *in vitro* systems that replicate patient characteristics.

These steps are essential for progress and serve as a prerequisite for preclinical studies.

2 AIM OF THE PROJECT

Nonsense mutations cause life-threatening diseases, affecting approximately 11% of inherited pathologies (Mort M., *et al*., 2008; Ghelfi M.D., *et al.,* 2023). Currently, there is no cure, even though the last two decades have seen the emergence of technologies and strategies aimed at finding a possible treatment for nonsense mutation defects.

So far, the lack of a specific treatment represents still a challenge for the scientific community. Anyway, among the developing strategies for fighting nonsense mutations, suppression therapy by *Translational Readthrough-Inducing Drugs* (TRIDs) seems one of the most promising and adaptable to various genetic contexts (Martins-Dias, P., and Romão, L., 2021). However, despite a series of studies conducted in recent years, there is still no effective molecule against this type of genetic alteration.

In this scenario, three optimized TRIDs (NV848, NV914, and NV930) were previously synthesized and studied *in vitro* by the research group of Professors Pibiri and Lentini at the University of Palermo (Pibiri I., *et al.,* 2015*;* Pibiri I., *et al.,* 2018).

In this thesis, different aspects were investigated to better characterize the efficacy of these molecules.

The first aim was to further investigate the ability of NV TRIDs to promote readthrough in advanced nonsense model systems in an *in vivo* murine model.

For this reason, the first step was aimed at establishing the safety and tolerability of the NV molecules in C57BL/6 mouse models.

This evaluation of the toxicity in wild-type (WT) model allows us to identify the safety profile of each compound before testing the molecules on the nonsense mutated model for CF. For this aim, specific international guidelines, in particular, the OECD No.420 guidelines were applied in this study, choosing an acute-single dose administration protocol (OECD, 1992).

Then, a further preliminary and necessary step was to determine the biodistribution of NV TRIDs. Particularly, for the following studies *in vivo* the attention was focused on one of the TRIDs, the NV848, that we consider our lead compound.

In this context, the focus was on the biodistribution of NV848 in the principal organs, particularly on the organs affected in CF, and in those important for drug metabolism: plasma, pancreas, lungs, intestines, brain, and kidney.

The second aim of the project was to assess the efficacy of NV848 in promoting the readthrough of a PTC produced by the G542X mutation in the CFTR gene, using a murine model recently generated by Hodge et al. (McHugh D. R., *et al*., 2018). For this purpose, a homozygous CFTR $^{G542X/G542X}$ colony was established through the mating of heterozygous mice C57BL/6 CFTR $^{WT/G542X}$. A chronic oral treatment was then administered for 15 days, to assess CFTR protein rescue through molecular analyses on lungs.

In addition, a study of the restoration of CFTR channel functionality in a cellular model was conducted at the Institut Necked Enfants Malades (INEM), in Paris (France). In this particular case, 16 HBE cells, characterized by G542X and W1282X CFTR mutations were utilized in Ussing chamber experiments.

Furthermore, as NV molecules were tested *in vitro* for CF, and Schwachman-Diamond (SD) syndrome, we also explored whether another genetic context involving a nonsense mutation in a different gene could be also responsive to NV treatment (Pibiri I., *et al.* 2020; Bezzerri V., *et al.,* 2022).

Therefore, primary fibroblasts with $LRBA^{R1683X/R1683X}$ genotype were employed to assess the ability of all three NV molecules in rescuing mRNA and protein expression and localization, given that LRBA is one of the causative genes for PIRDs (Lopez-Herrera G*., et al.,* 2012).

3 MATERIALS AND METHODS

3.1 Molecule solution preparation.

NV molecules have been synthesized as reported by Pibiri and colleagues (Pibiri I., *et al*., 2020).
For the toxicity study, NV848 was dissolved in distilled water, then sonicated in continuum at 13% power for 2 min, with Branson Digital Sonifier (Marshall Scientific, Hampton, NH, USA). Ataluren (PTC124), NV914, and NV930 were dissolved in DMSO (Sigma-Aldrich Merck, Darmstadt, Germany) stock solution and further diluted in olive oil (~75%). The maximum DMSO in the final solution was 25% for NV914 and NV930 and about 40% for PTC124.
Considering the different solubilities in water or organic solvent (DMSO), stock solutions for NV molecules were prepared.
Each mouse dosage was calculated according to the body weight, and a maximum volume of 250 µl was administered to each subject.
For the biodistribution and the efficacy studies, all three molecules have been prepared in stock solution in DMSO and resuspended in distilled H_2O or olive oil, for NV848 or NV914 and NV930, respectively, according to their solubility characteristics.
Lastly, for the *in vitro* study, molecules were prepared in stock solutions of 100 mM in DMSO and used at 12µM.

3.2 *In vivo* study.

3.2.1 Animals.

Adult wild-type (WT) C57BL/6 mice were purchased from ENVIGO Srl (San Pietro al Natisone UD, Italy). both sexes were used to examine any possible difference in response to the test molecules, due to gender.
C57BL/6 CFTR $^{G542X/G542X}$ mice were gently gifted by Professor C. Hodges (Case Western Reserve University, Cleveland-USA). Animals were housed in temperature-controlled rooms with 22–25 ◦C, 50–60% humidity, and with a 12 h light/darkness cycle. They were fed with standard pellet chow and water, ad libitum, until the beginning of the protocol.
The experimental protocol was performed in conformity with the Italian D.Lgs 26/2014. All procedures and care were approved by the University of Palermo Animal Care and Use Ethics Committee and by the authorization of the Italian Ministry of Health (Authorization n.1235/2020; Authorization n° 2/2022-PR) and following the national and EU Directive 2010/63/EU for the handling and use of experimental animals.

3.2.2 Toxicity study: administration protocol and group constitution.

30 adult mice of the C57BL/6 strain (6–8 weeks old, weight 18.0 ± 4.0 g) were used in this study. The acute toxicity study was performed, following the criteria determined by the Organization for Economic and Co-operation Development (OECD) established in 1992 (OECD, 1992) and the ARRIVE guidelines (Percie du Sert N., *et al.,* 2020).

According to OECD guideline No. 420, animals were administered with a fixed-single acute dose of each substance, and the possible occurrence of toxic effects was observed for the first four hours constantly, and once for the following four hours. Then the body weight variations, related to changes in food intake, all visual observations of mortality, various changes in physical appearance, or behaviour, and any injury or illness were observed once daily for 14 days.

As indicated in the OECD No.420, to determine the dose for the main study, a pilot study was performed on one subject. evaluating the effect of a single administration via oral gavage at a single dose of 2000 mg/Kg. For this purpose, we based the choice on the outcomes (A, B, or C) indicated in annex 3 of the guidelines (**Figure 27**), so we proceeded with the same or a lower dosage of 300 mg/Kg.

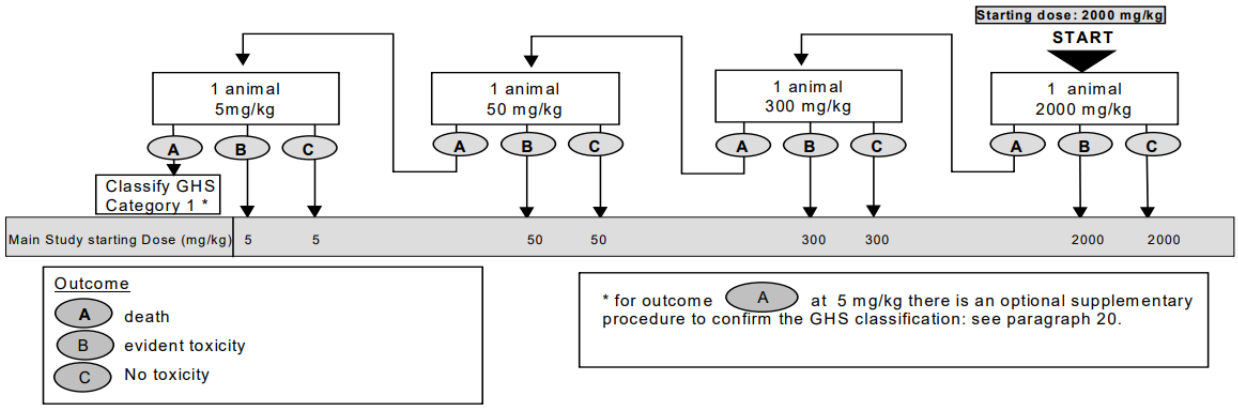

Figure 27. *Scheme of annex 3 of OECD no.420, showing the protocol for the main study of a fixed-single acute dose administration procedure.*

All animals received oral gavage with an appropriate plastic feeding needle, as indicated in the standard protocol (Turner P. V., *et al.,* 2011). The effects of NV molecules were compared to the effects of Ataluren (PTC124) used as a positive control.

15 male and 15 female mice (6 weeks aged, weighing around 20 g), were randomly assigned into six groups:

(I) negative control group (N = 3 per group) receiving 250 µl of vehicle (water);

(II) negative control group (N = 3 per group) receiving 250 µl of vehicle (a solution of 40% DMSO (dimethyl sulfoxide) and 60% olive oil);

(III) positive control (3 mice of each sex; N = 6 per group) receiving 250 µl of Ataluren (PTC124) (2000 mg/Kg);

(IV) test group 1 (3 mice of each sex; N = 6 per group), receiving 250 µl of NV848 (300 mg/Kg);

(V) test group 2 (3 mice of each sex; N = 6 per group), receiving 250 µl of NV914 (2000 mg/Kg);

(VI) test group 3 (3 mice of each sex; N = 6 per group), receiving 250 µl of NV930 (300 mg/Kg) (**Figure 28**).

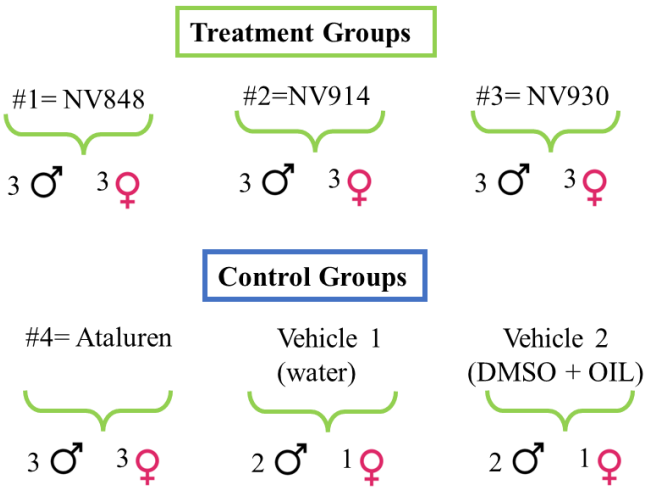

Figure 28. *Schematic representation of group constitution for toxicity study. Treatment and Ataluren (PTC124) (positive control) groups were constituted by 3 males and 3 females, while negative controls (vehicles), were composed by 2 males and 1 female each.*

The sample size was determined by G Power analysis (Charan J. and Kantharia N. D., 2013). Animals were fasted 3-4 hours before and one and a half-hour after the administration.
All the solutions were prepared on the same day of the experiment (see paragraph 2.1).

3.2.3 Organs' collection protocol for histological analyses.

On the 15th day, all animals were anesthetized with 2% isoflurane and then euthanized through cervical dislocation Blood samples were collected by cardiac puncture into EDTA-containing tubes. The organs, namely the brain, heart, lung, liver, pancreas, spleen, small and large intestine, kidney, lymph node, ovary, testis, and bone marrow were carefully excised and weighed. These organs were preserved in a fixation medium of 10% buffered formalin for 24 h. Successively, samples were vigorously washed with abundant water and preserved in 70% ethanol before paraffin fixation.
After tissue sample fixation, four-micrometre-thick tissue sections were deparaffinized and rehydrated. Then, slides were stained to perform histopathological analyses with haematoxylin and eosin (H&E). All the sections were analysed using Zeiss Axio Scope A1 optical microscope (Zeiss, Germany) and images were taken using an Axiocam 503 Color digital camera with the ZEN2 imaging software (Zeiss Germany).
The possible histological change was scored using a semi-quantitative scoring system, including many variables for each organ (Corrao F. *et al*., 2022). To each variable or sign of toxicity or macroscopic changes,

a precise score was assigned, based on the degree of severity (0, absent; 1, mild; 2, moderate; 3 severe) and the extent (1, focal; 2, multifocal; 3, diffuse) (see **Supplementary** section).

3.2.4 Biodistribution study: administration protocol and group constitution.

For this objective, 75 C57BL/6 male mice (4 weeks aged, weighing 18.0 ± 4.0 g) were used. Animals were randomly assigned into 5 groups: two control groups (receiving once vehicles, namely distilled H_2O, or DMSO and olive oil) and one treatment group for NV848 molecule.
In each group animals were then randomly assigned to 5 subgroups (n=5 mice/ each) corresponding to different time-points 1) T0, 2) T 45', 3) T 60'(1h), 4) T 120'(2h), 5) T 1440'(24h) (**Figure 29**).

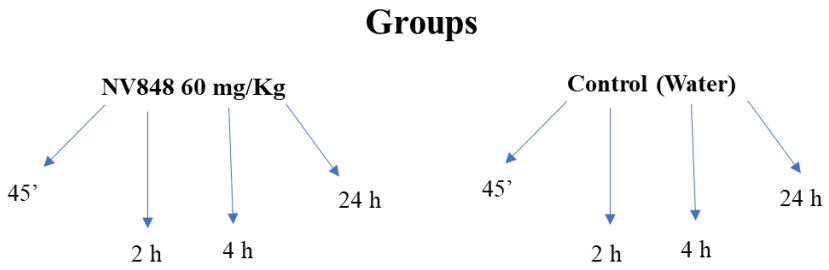

Figure 29. *Schematic representation of the division and the constitution of the different groups of treatment and control for biodistribution protocol development.*

The dosage of 60 mg/Kg was chosen in agreement with the paper of Du M. and collaborators (Du M., *et al.,* 2008), due to the similarity in chemical structure between Ataluren (PTC124) and NVs.
Molecules or vehicles were administered once at the beginning of the study (T0) by oral gavage and mice were euthanized under isoflurane anaesthesia by cervical dislocation at the fixed time points; organ collection was performed for each mouse, then samples were immediately cryopreserved in liquid nitrogen and quickly stored at – 80°C.
Blood samples collected by intracardiac puncture were preserved in EDTA-containing tubes and then centrifuged at 3000 rpm for 10 minutes, to separate plasma stored at -20°C.
The following step planned the drawing up of a protocol for molecule extraction from organs. To this aim, a precedent protocol found in the literature (Kayali R. et al., 2012) was used with few modifications.

3.2.5 Organs' collection and preparation for HPLC-MS analyses.

Cryopreserved organs were used for the following step of molecule extraction from tissues and chemical analyses.
In detail, organs were homogenized, using the Omni TH Tissue Homogenizer (Kennesaw GA, USA), in a 10 ml tube with 200 µl of 0,9% NaCl solution. Successively, 600 µl of iced acetonitrile was added and samples

vortexed for 2 minutes. Later, tubes were put in a refrigerated (4°C) centrifuge (Thermo Scientific™, Sorvall™ RC 6 Plus Centrifuge) for 10 minutes at 14000 rpm, to separate the supernatant from the pellet, which was discarded, contrary to the supernatant that was preserved at -20°C. Then, samples were freeze-dried using a refrigerated lyophilizer (CoolSafe, SCANVAC, Labogene, Allerød, Denmark) that works at -100°C and at vacuum conditions. The product lyophilized was stored at -20°C. The following step consisted of sample restoration and High-Performance Liquid Chromatography (HPLC) (HPLC Agilent 1250 infinity, Agilent Technologies 6540 UHD accurate mass Q-TOF LC/MS) analysis.

To restore lyophilized products, a 3:1 mixture of acetonitrile (ACN) CHROMASOLV™ LC-MS (Honeywell, U.S.) and high pure water CHROMASOLV™ LC-MS (Honeywell, U.S.) was prepared and stored at 4°C, prior to use. 100 µl of this solution was added to each sample and then, they were vortexed for 5 minutes. Samples were centrifuged at 14000 rpm for 10 minutes at 4°C (Thermo Scientific™, Sorvall™ RC 6 Plus Centrifuge) and the supernatant was collected for the HPLC analysis.

Before HPLC analyses, tests were done by preparing a calibration curve, made up of a constant aliquot of an untreated sample added to solutions of different known concentrations of analytes, used to make the calibration curve self. Each analysis was performed in triplicates, for the calibration curve, and duplicates, for the experimental samples.

Moreover, to calculate the efficiency of the extraction method, a recovery test was also performed for all the tissues analysed.

In the recovery test, a standard solution of the molecule at the concentration of 1mM was added to an untreated sample, and the extraction protocol was then performed. In the meantime, a standard solution of 1mM of the chosen molecule was added to an untreated sample. All the tests were performed in triplicates.

3.2.6 Generation and management of colony of CFTR mutant mice.

$CFTR^{G542X/G542X}$ homozygous mice were produced by breeding heterozygous ($CFTR^{WT/G542X}$; Cleveland, USA; McHugh D. R., *et al.,* 2018); wild-type (WT) mice were used as controls (**Figure 30**).

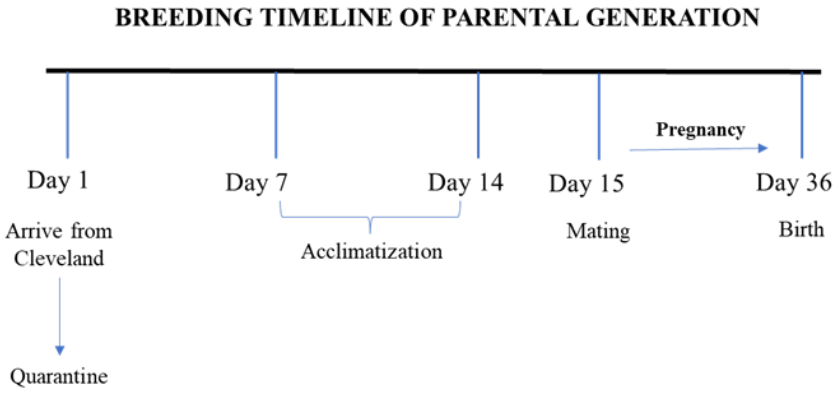

***Figure 30**. Schematic timeline of parental heterozygous mice breeding and mating to obtain $CFTR^{G542X/G542X}$ colony, since parental mice arrival.*

At 3 weeks (21 days) Tissue was obtained by ear biopsies from newborn mice and DNA extraction (PureLink™ Genomic DNA Mini Kit (Invitrogen™, Thermo Fisher Scientific, U.S.), following the manufacturer's instructions) was performed for genotyping by PCR analysis.

Briefly, lysis of tissue samples was performed overnight (O.N.) using a mix of digestion buffer and proteinase K, at 55°C and 300 rpm shaking. The day after, supernatants were collected, and samples were centrifuged, followed by RNAse A addition. Then, Genomic Lysis/Binding Buffer was added to samples, with the same volume of absolute DNase-RNase-free ethanol (96-100%). DNA binding step was carried on by chromatography affinity columns, with two washing with specific washing buffers. For the last step, the elution, columns were put in new clean and sterile Eppendorf 1,5 ml tubes. 50 µl DNase-RNase free water was added on each membrane and incubated for 5 minutes at R.T. To elute DNAs, centrifugation at maximum speed for 1 minute was carried out.

After the DNA quantification with NanoDrop™ 2000 (Thermo Scientific™, U.S.), DNA quality was evaluated also by 1% agarose gel (UltraPure™ Agarose, Invitrogen™, Thermo Fisher Scientific, U.S.) run, prepared with 1X TAE (Tris-Acetate-EDTA) homemade buffer.

3.2.7 PCR endpoint for DNA amplification and genotyping.

To characterize mice offspring genotypes, specific designed primers were used, based on the protocol made up by McHugh et al. (McHugh D. R., *et al.,* 2018). Primers were designed to recognize the two allele variants of CFTR WT and CFTR G542X. The expected amplification product counts 319 base pairs (bp). Reverse primer is the same for both alleles, while forward primers differ only in the last two nucleotides of 3' terminus (evidenced in bold red).

Specifically, primers' sequences are shown below (**Table 3**):

Name	***Nucleotide Sequence***	***Type of primer***	***Allele identified***
P 1	5' – ACA AGA CAA CAC AGT TCT **CT** – 3'	Forward	CFTR G542X
P 2	5' – TCC ATG CAC CAT AAC AAC AAG T – 3'	Reverse	CFTR (general)
P 3	5' – ACA AGA CAA CAC AGT TCT **TG** – 3'	Forward	CFTR WT

Table 3. *Nucleotide sequence of primers utilized for the discrimination of G542X or WT allele in CFTR DNA.*

For the PCR the REDTaq DNA Polymerase (Sigma-Aldrich, USA) was used following manufacturers' instructions.

Two different reaction mixes were prepared, one for each allele.

Mixes were constituted as follows:

- REDTaq 12,5 µl

- Primer Forward (P1 or P3) 1 µM 1,25 µl
- Primer R (P2) 1 µM 1,25 µl
- DNA 2 µl
- H2O 8 µl

Samples were put in the thermocycler (2720 Thermal Cycler, Applied Biosystems) and a specific thermal set-up was used, illustrated below, and repeated for 40 cycles (**Figure 31**).

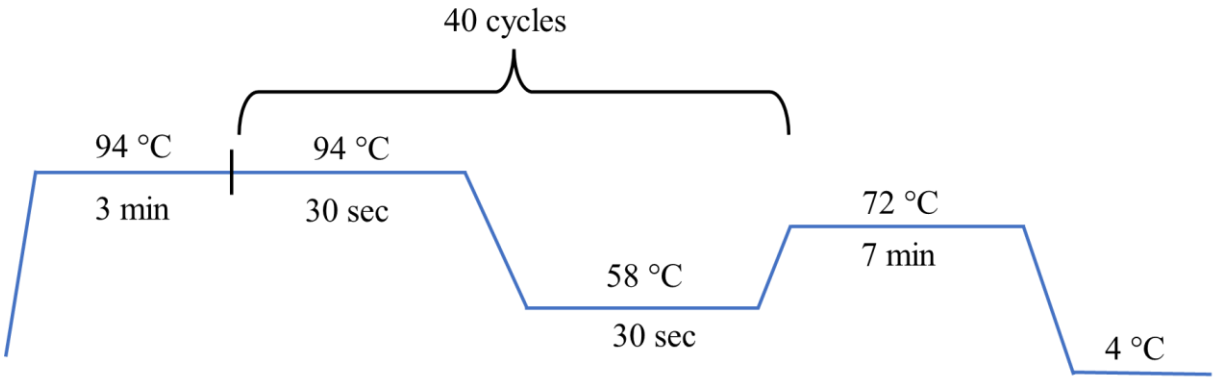

***Figure 31**. Thermal profile used to perform PCR reaction to detect mice genotypes.*

The samples were analysed on 1% agarose gel in 1X TBE buffer.

3.2.8 Chronic treatment for drugs' efficacy study: molecule administration protocol and groups constitution to study the efficacy in vivo of the NV848 molecule.

WT CFTR$^{+/+}$, heterozygous CFTR$^{+/G542X}$, and homozygous CFTR$^{G542X/G542X}$ mice were divided into treatment (NV848) and negative control groups (5 mice/each group receiving the drug or the vehicles) (**Figure 32**).

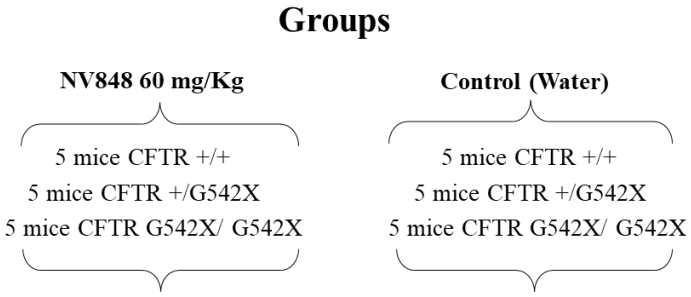

***Figure 32**. Schematic division of subjects into treatment with NV848 and negative controls with the vehicle.*

NV848 was prepared daily (paragraph 2.1), at the fixed dosage of 60 mg/Kg.

Mice for each group received intragastric administration of vehicle or NV848 (60 mg/kg) starting at the 21st postnatal day once daily for 15 days. At day 15 the animals were sacrificed, and the organs collected weighed, and stored at -80 °C for immunohistochemistry, Western blot, and Real-time RT PCR assays, to assess CFTR protein and gene expression in target organs.

3.2.9 Immunohistochemical protocol for mutant mice tissue analyses.

Immunohistochemical evaluation was performed on the lungs of treated and untreated mice, both mutant and WT. Samples were fixed in formalin (10% [vol/vol]), then embedded in paraffin (FFPE), and cut into 3µm sections. Two different proteins were evaluated: Thyroid Transcription Factor 1 (TTF1), as an experimental epithelial control marker, and CFTR, the target. Briefly, to verify tissue sections' immunohistochemical reactivity and responsiveness, sample slides were incubated with antibody anti-TTF1 (SP141, Roche Ventana). Then, other slides were incubated with the antibody anti-CFTR (SAB4501942, Sigma-Aldrich, Merck, Darmstadt, Germany).
The buffer ULTRA Cell Conditioning solution (ULTRA CC1, Roche Ventana 950-224) was used for 64 minutes at 95°C for antigen unmasking. The primary antibodies anti-TTF1 (Roche Ventana 749-4756) (ready to use) and the anti-CFTR 1:200 were incubated for 36 minutes at 37° C, while the revelation system used implied the *ultra*View Universal HRP Multimer Detection Kit (Roche Ventana, 760-500) and UltraBenchmark (Roche Ventana) instrument, according to the manufacturer's instructions.

3.3 *In vitro* experiments.

3.3.1 Cells culture conditions.

16HBE cells:
After thawing, 16HBEge CFTR^{W1282X} and CFTR^{G542X} cells were plated in T25 flasks (Corning, U.S.) until reached 80% confluency, when they were split in T75 flasks (Corning, U.S.) to expand. Culture medium was constituted by MEM (Minimum Essential Medium Eagle, Gibco™, Thermo Fisher Scientific, U.S.) 1X (Invitrogen™, Thermo Fisher Scientific, U.S.), enriched with 10% Foetal Bovine Serum (FBS) (Invitrogen™, Thermo Fisher Scientific, U.S.), 1 % penicillin and streptomycin (P+S) (Invitrogen™, Thermo Fisher Scientific, U.S.), and 1 % glutamine (Invitrogen™, Thermo Fisher Scientific, U.S.).

Fibroblasts LRBA$^{R1683X/R1683X}$:
Cells harvested by the patient's biopsy were plated in T25 flasks (Corning, U.S.), were cultivated with culture medium MEM 1X (Minimum Essential Medium Eagle, Gibco™, Thermo Fisher Scientific, U.S.), implemented with 2% Ultroser G (Fisher Scientific, Thermo Fisher Scientific, U.S.), 1% non-essential amino acids (Gibco™, Thermo Fisher Scientific, U.S.), and 1% glutamine (Invitrogen™, Thermo Fisher Scientific, U.S.). In all cell cultures, media were changed every 48 hours.

3.3.2 Cell Proliferation assay.

Cell proliferation in fibroblasts LRBA$^{R1683X/R1683X}$ was assessed after 24, 48, and 72-hour chronic treatment. 50,000 cells were seeded in duplicate in 12 multiwell plates (Corning, U.S.). The experiment was repeated in triplicate.

NV848, NV914, NV930, and Ataluren (PTC124) were prepared in a DMSO stock solution of 1 mM and used at 12 μM, for the treatment, while G418 was used at 430 μM. Untreated cells were used as a negative control. Cells were counted at the indicated time points using the Burker chamber.

3.3.3 Ussing chamber experiments.

100.000 cells were seeded onto porous inserts (0,33 cm^2, Transwell Permeable Supports, 6.5 mm Inserts, 24 well plates, 0.4 mm Polyester Membrane, Corning, U.S.) previously coated with fibronectin (see above) and maintained in culture in the liquid-liquid interface (liq-liq) until the differentiation in forming an epithelium, for 7 days. For experiments, 48-hour chronic treatments were performed, adding compounds in both basal and apical sides.

Specifically, for each condition, two inserts were prepared, with the following treatments:

- DMSO (vehicle), as negative control;
- NMD inhibitor SMG1(hereafter NMDi, 5 μM) and VX modulators: VX-445 (3μM) and VX-661 (3μM) (MedChemExpress, MCE), in chronic, as experimental control;
- G418 (100 μM) as positive control;
- G418 (100 μM) + NMDi (5 μM) and VX modulators (see above);
- NV848 (1 mM);
- NV848 (1 mM) + NMDi (5 μM) and VX modulators (see above).

The short-circuit-current (Isc) was measured under voltage clamp conditions using EVC4000 Precision V/I Clamp (World Precision Instruments). A chloride (Cl^-) gradient across the two sides of epithelium (apical and basal) was generated by using two different Ringer solutions: the apical was composed of 145 mM Na-Gluconate, 10 mM HEPES, 10 mM D-Glucose, 3.3 mM K2HPO4, 1.2 mM CaCl2, 1.2 mM MgCl2, while the basal differed because of the 145 mM NaCl instead of NA-Gluconate. Inserts were assembled in Ussing chambers (Physiologic Instruments, San Diego, CA, USA). Experiments were carried on at 37°C, and epithelia were bubbled with a pCO2= 5% and a pO2 = 95%.

During the recording, to specifically activate and inhibit the CFTR channel, the following drugs were added, after Isc baseline stabilization, in order: on the apical side, Amiloride (100 μM; into apical and basal parts, Forskolin (10 μM) and 3-isobutyl-1-methylxanthine (IBMX 100 μM); VX-770 (10μM); CFTR inhibitor CFTRinh172 (10 μM); ATP (100 μM) CFTRinh172, VX-770, and ATP were put only in the apical side.

The summary response to Forskolin/IBMX and VX-770 was used as an index of the CFTR function.

Current registration and analysis were made with LabChart8Reader (ADInstrument, Dunedine, New Zealand).

3.4 Molecular analyses.

3.4.1 RNA extraction and Real-time RT PCR.

3.4.1.1 Protocol for RNA extraction.

Mice: 20-25 mg of tissues were weighted for RNA extraction.
Cells: 600.000 fibroblasts LRBA $^{R1683X/R1683X}$ were used to performe RNA extraction, using RNeasy Mini Kit (Qiagen, Germany) following manufacturer's instructions.
Briefly, a mix of RLT buffer and β-Mercaptoethanol was added to each sample for mechanical homogenization. Then, 1 volume of 70% DNase-RNase-free ethanol was mixed into samples, which were transferred to the RNaeasy spin column and centrifuged. A first washing step was followed by in-column DNAse treatment, and then previously reconstituted Buffer RPE was added twice. Samples were washed twice and centrifuged. A further centrifuge was performed to eliminate any residual reagent. Lastly, RNA was collected from spin columns with 30 µl of DNase-RNase-free water elution, by centrifugation.
RNA was quantified by spectrophotometric assay, using NanoDrop™ 2000 (Thermo Scientific™, Invitrogen, U.S.).

3.4.1.2 16HBE cell RNA extraction with Trizol.

16HBE cell inserts derived from Ussing chamber experiments were used to extract RNA.
To this aim, 100 µl Trizol (Minimum Essential Medium Eagle, Gibco™, Thermo Fisher Scientific, U.S.) was added to each insert, left incubating for 2 minutes, and then cells scraped and collected. 200 µl Chloroforme/ml Trizol was added to each sample, vortexed, and incubated for 10 minutes on ice. A centrifuge was performed, and the aqueous phase was collected, to add 1 volume of isopropanol, mix, and preserve a -20°C O.N. The day after, tubes were placed at -80°C for 60 minutes, then left to defrost and centrifuged. The pellet was preserved, washed with ethanol, and centrifuged. Then, again the pellet was kept and left drying. Elution of pellet was made with DNase-RNase free water.
RNA was quantified by spectrophotometric assay, using NanoDrop™ 2000 (Thermo Scientific™, Invitrogen, U.S.).

3.4.1.3 Real-time RT PCR method.

Reverse transcription
1 µg of total RNA extracted was retrotranscribed in cDNA using the High-Capacity cDNA Reverse Transcription Kit (Thermo Fisher Scientific, U.S.) using manufacturer's instructions.
For each sample, a reaction mix was prepared as follows:

- 2 µl Buffer RT;

- 2 µl Random Primers;
- 1 µl dNTP;
- 1 µl Reverse Transcriptase;
- RNAse-free water to reach 20 µl of the final volume.

cDNA was then used to perform qPCR with the following steps.

Real-time RT PCR

The following primer sequences were used for mouse and cell gene expression (**Table 4**):

Gene		***Nucleotide Sequence***	
CFTR mouse	FORWARD	5' – CTACATGGAACACATACCTTCG - 3'	*Divangahi M., et al., 2009*
CFTR mouse	REVERSE	5' – GGTGATAATCACTGCATAGC – 3'	*Divangahi M., et al., 2009*
ACTIN mouse	FORWARD	5' –ACCGTCAAAAGATGACCCAGA- 3'	*Designed with Primer Express software (Applied Biosystems)*
ACTIN mouse	REVERSE	5' – GAGGCATACAGGGACAGCACA – 3'	*Designed with Primer Express software (Applied Biosystems)*
LRBA	FORWARD	5' – TCCGAGCCCTCAATGTGTTC - 3'	*Designed with Primer-BLAST (NIH)*
LRBA	REVERSE	5' – CATGGCAGAACCTCTGGGAG – 3'	*Designed with Primer-BLAST (NIH)*
GAPDH	FORWARD	5' – CTCATGACCACAGTCCATGCC- 3'	*Designed with Primer Express software (Applied Biosystems)*
GAPDH	REVERSE	5' – GCCATCCACAGTCTTCTGGGT – 3'	*Designed with Primer Express software (Applied Biosystems)*
CFTR human	FORWARD	5' – GGACAGTTGTTGGCGGTTGC – 3'	*van Meegen M. A., et al., 2011*
CFTR human	REVERSE	5' – CTTGGAGATGTCCTCTTCTAG – 3'	*van Meegen M. A., et al., 2011*
B-2M (microglobulin)	FORWARD	5' – GAGGCTATCCAGCGTACTCCA – 3'	*Ma B., et al., 2019*
B-2M (microglobulin)	REVERSE	5' – CGGCAGGCATACTCATCTTTT – 3'	*Ma B., et al., 2019*

Table 4. *Recapitulation of the primers used for Real-time RT PCR to calculate relative gene expression for CFTR and LRBA genes.*

Actin, β-2M, and GAPDH were used as housekeeping genes for *CFTR mouse, CFTR human,* and *LRBA* relative gene expression evaluation, respectively.

A reaction mix was prepared for each couple of primers, specific for the gene of interest and the related housekeeping, here in detail indicated for each sample:

a. SYBR MIX (Life Technologies, Thermo Fisher Scientific, U.S.) 12,5 µl;

b. Primers (Forward + Reverse 2 µM) 5 µl;
c. *H2O* DNase/RNase-free 5,5 µl;
d. cDNA 2 µl.

Each sample was loaded in triplicate with a final volume of 25 µl each. The plate was centrifuged at 2500 rpm for 5 minutes prior to the experiment started. Real-time RT PCR machine (7300 Real-Time PCR System, Applied Biosystem) and the 7300 System Software were used to perform the analysis.

3.4.2 Protein extraction and Western blot analyses.

For protein extraction, a lysis solution of RIPA (Pierce™ RIPA Buffer, Thermo Scientific™) and 1% protease inhibitor (Halt™ Protease and Phosphatase Inhibitor Cocktail, Thermo Scientific™) was used.
For tissues, about 40 mg of tissues were used. Samples were homogenized mechanically with lysis solution (100 µl for every 10 mg of tissue) and then incubated for one and half hours in ice at 4°C.
For protein extraction from LRBA$^{R1683X/R1683X}$ 250.000 cells were seeded in a T25 flask per each treatment condition (Untreated, PTC124, NV848, NV914, NV930, all molecules at 12 µM), and trypsinized with 0,25% trypsin (Thermo Fisher Scientific, U.S.) after 72 hours of chronic treatment; then, the pellet containing about 1 million of cells was used to extract proteins, as described above.
Subsequently, samples were centrifuged at 12000 rpm for 20 minutes at 4°C. After that, the supernatant containing proteins was collected and 2 µl was used for the quantification by Bradford colorimetric assay.

3.4.2.1 Western blot set-up.

30 µg of proteins were analysed in 3-8% SDS-PAGE gel at 150 V 100 mA for 1 hour.
Proteins were transferred to PVDF (polyvinylidene fluoride or polyvinylidene difluoride) membrane (Invitrogen™, Thermo Fisher Scientific, U.S.) by blotting O.N. at 4°C at 12V 50 mA. Blocking was performed at R.T. for 1h with 5% non-fat milk with TBS-TWEEN 1X (Pierce TBS-Tween 20X, Invitrogen™, Thermo Fisher Scientific, U.S.).
Membranes were incubated O.N. at 4° with primary antibodies anti-CFTR (#PA1-935, Invitrogen™, Thermo Fisher Scientific, U.S.) 1:1000, anti-LRBA (A304-478A, Bethyl Laboratories Inc., Texas, U.S.) 1:1000, and anti- β-tubulin (Sigma-Aldrich, USA) 1:5000. Membranes were washed three times with TBS-TWEEN 1X, and then incubated with HRP (Horseradish peroxidase)-conjugated secondary antibodies, anti-rabbit (Promega, U.S, 1:3000) or anti-mouse (Invitrogen™, Thermo Fisher Scientific, U.S., 1:5000), respectively.
After three washing with TBS-TWEEN 1X, West Femto (SuperSignal™ West Femto Maximum Sensitivity Substrate, Thermoscientific) reagent was used for the band detection by Chemidoc XRS (BioRad) and Quantity One software (BioRad). Protein bands were quantified with ImageJ software (NIH).

3.4.3 Immunofluorescence staining.

50.000 LRBA$^{R1683/R1683X}$ fibroblasts were seeded in coverslip in 12-well plates. Cells were treated chronically for 72 hours, and per each condition (paragraph 2.4.2), a duplicate was performed. Cells were fixed with methanol stored at -20°C and washed three times with PBS 1X without calcium and magnesium (Ca^{2+} - Mg^{2+}). A different step with EGFR IF consists of membrane permeabilization and staining. Precisely, prior to blocking, Triton-X100 0,01% was incubated for 10 minutes at R.T. Following washing, to visualize membranes, wheat-germ agglutinin (WGA)- Alexa594-conjugated antibody (Invitrogen™, Thermo Fisher Scientific, U.S.) 1:1000 was incubated 10 minutes at R.T., so cells washed.
Then, blocking was performed with 0,1% BSA for 1 h at R.T. Subsequently, cells were incubated O.N. at 4°C with anti-LRBA (A304-478A, Bethyl Laboratories Inc., Texas, U.S.) or anti-EGFR (sc-57092, Santa Cruz Biotechnology, U.S.) 1:100 primary antibodies. After washing, secondary anti-rabbit Alexa647-conjugated antibody (Thermo Fisher Scientific, U.S.) 1:500, or secondary anti-mouse Alexa488-conjugated antibody were incubated for 1 h at R.T. After washing, coverslips were mounted on slides with DAPI staining and sealed.
Cells were visualized by fluorescence microscope (AxioVision, Zeiss) at 63X magnification, and images were analysed using ImageJ software (NIH).

3.4.4 Next-Generation Sequencing (NGS).

Total mRNA extracted from LRBA $^{R1683X/R1683X}$ fibroblasts were retrotranscribed (paragraph 2.4.1.b). Then, cDNA was amplified with specific primers designed with Primer Blast (NIH) (indicated as "LRBA stop") that anneal in the region flanking the c.5073 C>T (R1683X), present in exon 30 of the gene, to enrich the pool of specific amplified product before sequencing, giving a 350 bp product.
The amplified products then underwent a further PCR reaction with specific primers (indicated as "LRBA NGS") for NGS analyses, particularly harbouring an adaptor sequence for the Illumina sequencing, in detail (**Table 5**):

Gene		***Nucleotide Sequence***
LRBA stop	FORWARD	5' – TTTAGAAGTCAATAAGTCTCCG – 3'
LRBA stop	REVERSE	5'- CTGAGGCTTGGGCTGAATC – 3'
LRBA NGS	FORWARD	5'- TCGTCGGCAGCGTCAGATGTGTATAAGAGACAGTTTAGAAGTCAATAA GTCTCCG – 3'
LRBA NGS	REVERSE	5'- GTCTCGTGGGCTCGGAGATGTGTATAAGAGACAGCTGAGGCTTGGGCT GAATC – 3'

Table 5. *Table reporting the nucleotide sequences of primers to amplify the LRBA mRNA region flanking the c.5047 C>T mutation (R1683X) is indicated as "LRBA stop", while those for NGS analyses are named LRBA NGS, in which the underlined nucleotides indicate the adaptor sequence specific for the Illumina NGS.*

3.5 Statistics.

Data have been indicated as mean± SEM and statistical analyses were carried by Prism ver. 5.0 (GraphPad Software, Inc., La Jolla, CA, USA).

4 RESULTS

Objective No.1: Evaluation of the safety and tolerability of NV molecules *in vivo* following acute single-dose administration, and biodistribution study of the NV848 molecule in C57BL/6 mouse model.

4.1 Evaluating safety and tolerability of the three NV TRIDs in vivo after acute treatment.

NV TRIDs are molecules synthesized and developed with the aim of performing the readthrough of the premature stop codons caused by nonsense mutations. They have previously been extensively tested and studied *in vitro*, using different engineered and primary cells of CF and SD syndrome. Moreover, one of the potential intracellular targets has been suggested, and its specificity has been demonstrated (Pibiri I., *et al.,* 2020; Bezzerri V., *et al.,* 2022; Carollo P. S., *et al.,* 2023; Perriera R., *et al*., 2023). In the field of drug discovery, a crucial step is the preclinical research using animal models to evaluate the performance of any compound *in vivo.* In our case, the safety, tolerability, and biodistribution of NV molecules were assessed in WT C57BL/6 mice before testing the activity of NV molecules in the nonsense mouse model for CF.

a) Acute oral toxicity study: behavioural analysis.

Acute oral toxicity of NV molecules was assessed *in vivo* using a fixed-dose procedure in accordance with OECD No.420 criteria, with authorization by the Animal Care and Use Ethics Committee of the University of Palermo and by the Italian Ministry of Health n.1235/2020. Oral administration was selected as the route of treatment, to simulate the potential oral intake of the drug.
Before starting the main study, a pilot sighting study was conducted, with one animal for each tested drug, in order to determine the tolerated dosage (**Figure 33**).

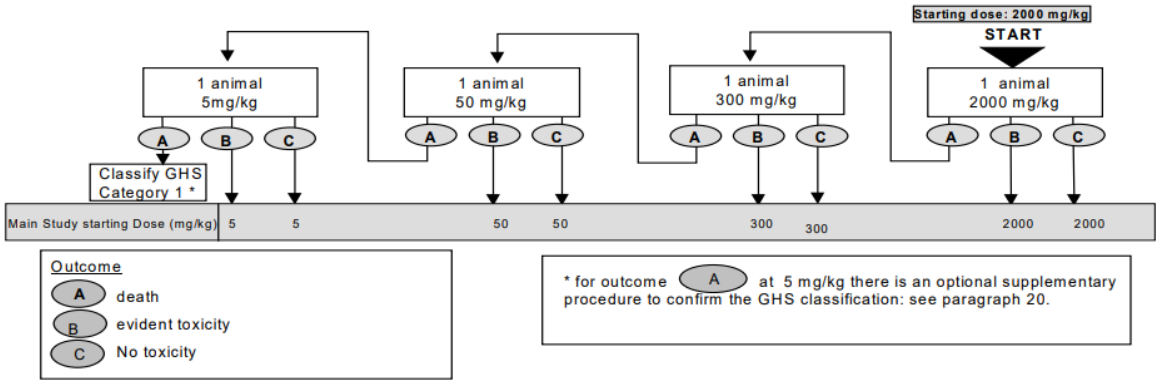

Figure 33. *A schematic representation of Annex 2 of OECD No.420, illustrating the workflow of the sighting study (OECD No. 420, 1992).*

All the NV molecules were initially administered each to one animal at a dose of 2000 mg/Kg, following the procedure in Annex 2. In case of death, a lower dosage was administered.

The preliminary study revealed that NV914 was tolerated at 2000 mg/Kg, while NV848 and NV930 resulted in lethality at 2000 mg/Kg but were tolerated at 300 mg/Kg.

Once the maximum tolerated dosage for each molecule had been determined, the main study was conducted in accordance with the guidelines outlined in Annex 3 (**Figure 27**). For the main study, animals were randomly assigned to different groups.

Male and female C57BL/6 mice (6 - 8 weeks old, mean weight 18±4 gr) were orally administered with the tested molecules and observed over a 15-day period.

Although no lethality was observed in all treated mice, in all groups behavioural signs associated with potential toxicity were observed. However, these symptoms were temporary and resolved within 4 hours post-administration, for NV848, and within 3 hours for the mice treated with NV914, NV930, and Ataluren (PTC124).

The following manifestations were taken into consideration: hyperactivity, hypoactivity, abdominal pain, itching and scratching, changes in skin appearance, ruffled fur, tremors, convulsions, changes in eyes, changes in mucus membranes, salivation, lethargy, diarrhoea, coma, death.

The specific symptoms observed for each treatment are detailed below.

In the group of animals treated with NV848 at 300 mg/Kg, hypoactivity, convulsion, abdominal pain, and tremors were observed in 3 of 6 mice (**Table 6**).

NV848 300 mg/kg										
	30 min		**1h**		**2h**		**3h**		**4h**	
PARAMETERS	**M**	**F**	**M**	**F**	**M**	**F**	**M**	**F**	**M**	**F**
Hyperactivity		X		X		X				
Hypoactivity	X		X		X		X	X	X	X
Abdominal Pain			X		X	X	X	X	X	X
Itching and scratching										
Changes in skin										
Ruffled Fur										
Tremors			X			X				
Convulsions			X		X	X	X	X		
Changes in eyes										
Changes in mucus membranes										
Salivation										
Lethargy										
Diarrhoea										
Coma										

Death										

Table 6. *The table outlines all the effects observed following the administration of a single 300 mg/Kg dose of NV848 (Corrao F., et al., 2022).*

In the group of mice treated with NV914 at a dosage of 2000 mg/Kg, hypoactivity (5 of 6 mice), hyperactivity and abdominal pain (4 of 6 mice), and itching and scratching (2 of 6 mice) (**Table 7**) were observed. Alternating episodes of hyperactivity and hypoactivity were noticed at different time intervals during the observation period, with hyperactivity typically preceding hypoactivity, in mice that exhibited both symptoms.

NV914 2000 mg/kg										
	30 min		**1h**		**2h**		**3h**		**4h**	
PARAMETERS	**M**	**F**	**M**	**F**	**M**	**F**	**M**	**F**	**M**	**F**
Hyperactivity			X	X		X				
Hypoactivity		X			X		X	X		
Abdominal Pain		X	X	X		X				
Itching and scratching		X		X		X		X		
Changes in skin										
Ruffled Fur										
Tremors										
Convulsions				X		X		X		
Changes in eyes										
Changes in mucus membranes										
Salivation										
Lethargy										
Diarrhoea										
Coma										
Death										

Table 7. *The table outlines all the effects observed following the administration of a single 2000 mg/Kg dose of NV914 (Corrao F., et al., 2022).*

In the group of animals receiving 300 mg/Kg of NV930 the following manifestations were observed: abdominal pain (3 of 6 mice), tremors and convulsions (5 of 6 animals), and only one exhibited hyperactivity. Like NV914 treated mice, also NV930 caused itching and scratching but in 4 cases (**Table 8**).

NV930 300 mg/kg										
	30 min		1h		2h		3h		4h	
PARAMETERS	**M**	**F**	**M**	**F**	**M**	**F**	**M**	**F**	**M**	**F**
Hyperactivity	X	X	X	X	X					
Hypoactivity										
Abdominal Pain		X	X	X		X		X		
Itching and scratching		X		X	X	X	X	X		
Changes in skin										
Ruffled Fur										
Tremors										
Convulsions		X	X	X	X	X	X	X		
Changes in eyes										
Changes in mucus membranes										
Salivation										
Lethargy										
Diarrhoea										
Coma										
Death										

Table 8. *The table outlines all the effects observed following the administration of a single 300 mg/Kg dose of NV930 (Corrao F., et al., 2022).*

The groups of animals treated with the vehicle or with Ataluren (PTC124) constituted negative and positive control respectively.

Ataluren (PTC124) administered at 2000 mg/Kg resulted in hypoactivity in 3 of 6 mice, abdominal pain in 4 of 6 mice, and in 1 of 6 mice tremors, convulsions, and hyperactivity (**Table 9**). No fatalities were observed following Ataluren (PTC124) treatment.

Ataluren (PTC124) 2000 mg/kg										
	30 min		1h		2h		3h		4h	
PARAMETERS	**M**	**F**	**M**	**F**	**M**	**F**	**M**	**F**	**M**	**F**
Hyperactivity				X		X				
Hypoactivity	X		X		X					
Abdominal Pain	X	X	X	X	X	X	X	X		
Itching and scratching	X		X							
Changes in skin										

Ruffled Fur										
Tremors										
Convulsions				X		X				
Changes in eyes										
Changes in mucus membranes										
Salivation										
Lethargy										
Diarrhoea										
Coma										
Death										

Table 9. *The table outlines all the effects observed following the administration of a single 2000 mg/Kg dose of Ataluren (PTC124) (Corrao F., et al., 2022).*

Finally, the vehicles did not induce any change in behaviour or clinical manifestation in the animals during the 15-day period of observation.

Based on these results, in accordance with OECD guidelines and the Globally Harmonized System (GHS), NV848 and NV930 can be classified in category 4, which is associated with a low health risk, while NV914 can also be classified in category 5, indicating a low threat to health (GHS, United Nations, 2013; Corrao F., *et al.,* 2022).

Consequently, it can be concluded that the three NV TRIDs exhibited similar toxicity signs as the control molecule (Ataluren-PTC124) and can be classified as low-risk substances for health (GHS, United Nations, 2013) (Corrao F., *et al.,* 2022).

b) *Acute toxicity study: body weight assessment.*

The evaluation of body weight over the 15-day observation period revealed no significant differences in weight variations among animals treated with NV848, NV914, NV930, or Ataluren (PTC124) when compared to the control groups (**Figures 34-A and 34-B**).

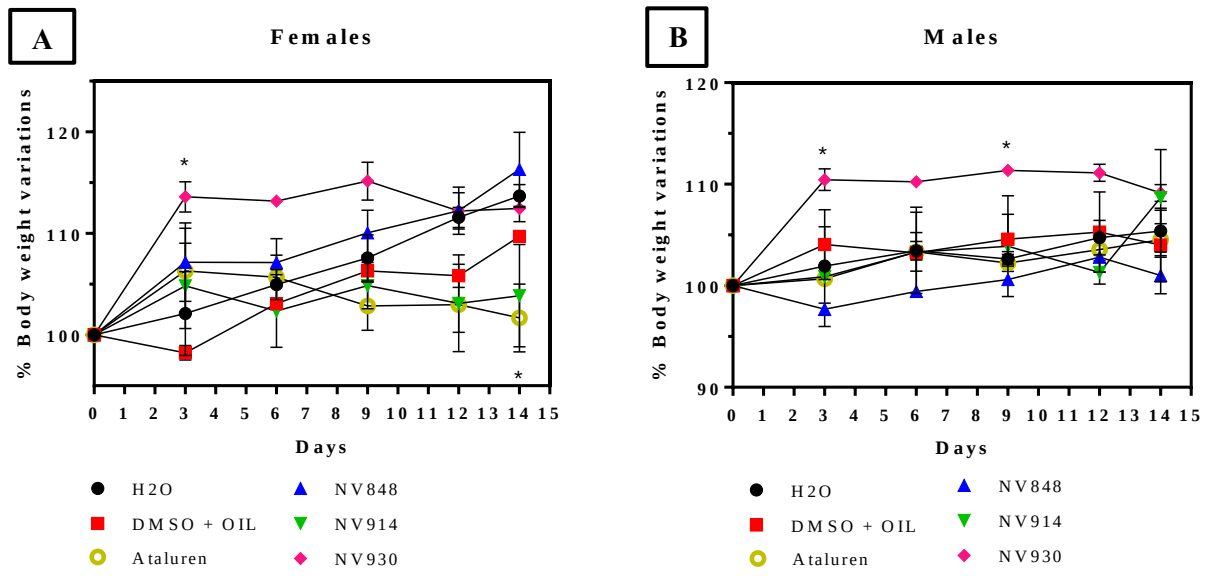

***Figure 34**. Graphs show the percentage of body weight of female (**A**) and male (**B**) subjects. Data are indicated as mean ± SEM. P<0,0001 (*) was calculated by Two-way ANOVA test (Corrao F., et al, 2022).*

Nonetheless, a slight and temporary increase in the mean of body weight values was observed on the third day in females, and on the third and the ninth day in males treated with NV930 when compared to the control group (vehicle) (* = p< 0.0001). Furthermore, a small but significant decrease was recorded in females treated with Ataluren (PTC124) on the 14th day, compared to the control group (* = p< 0.0001) (Corrao F., *et al*, 2022).
In addition, water and food intake were monitored, but no differences were evidenced during all experimentation.

c) *Acute toxicity study: macroscopic and histological examination of major organs.*

At the conclusion of the study, a macroscopic observation of lungs, heart, liver, pancreas, small and large intestines, kidney, spleen, brain, ovary or testis, and bone marrow was conducted, revealing no abnormalites or changes related to the treatments.
Additionally, a histological analysis was performed and a score for morphological alterations was assigned prior to the analyses. A score of 0 was assigned when there was a total absence of any alteration, while 1 indicated mild importance, and 2 was associated with high significance (**Supplementary, Tables S1 -12**).
In general, the analyses comparing treated groups (NV848, NV914, and NV930) (**Figures 35 – 37**) and the control groups (Ataluren-PTC124, water/DMSO+olive oil) (**Figures 38 – 40**) revealed no significant alterations in tissue morphology.

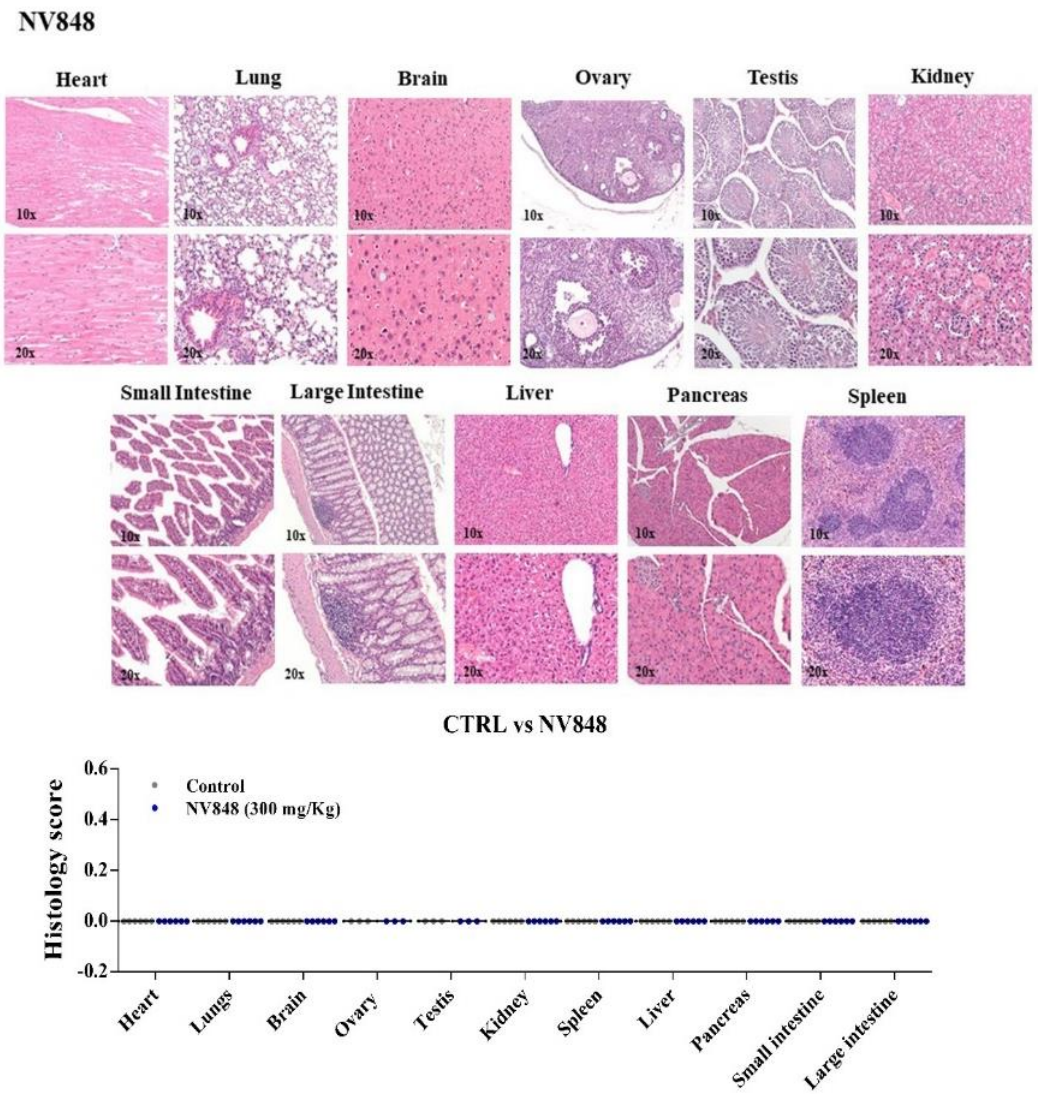

Figure 35. *A representative panel of histopathological evaluation on tissues derived from NV848-treated mice is displayed. In the lower part, a graph showing the exact histopathological scores for each subject is reported (score = 0) (Corrao F., et al, 2022).*

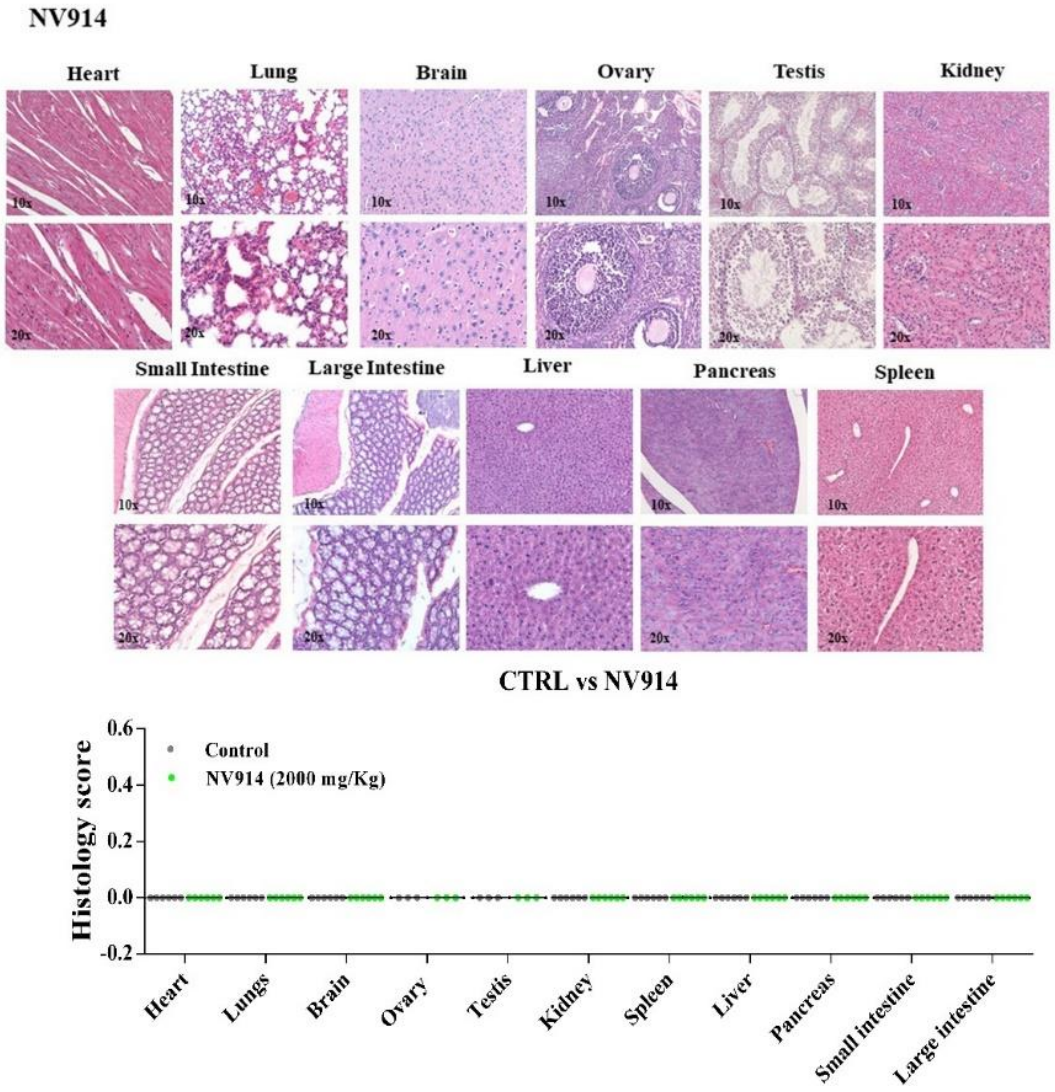

Figure 36. *A representative panel of histopathological evaluation on tissues derived from NV914-treated mice is displayed. In the lower part, a graph showing the exact histopathological scores for each subject is reported (score = 0) (Corrao F., et al, 2022).*

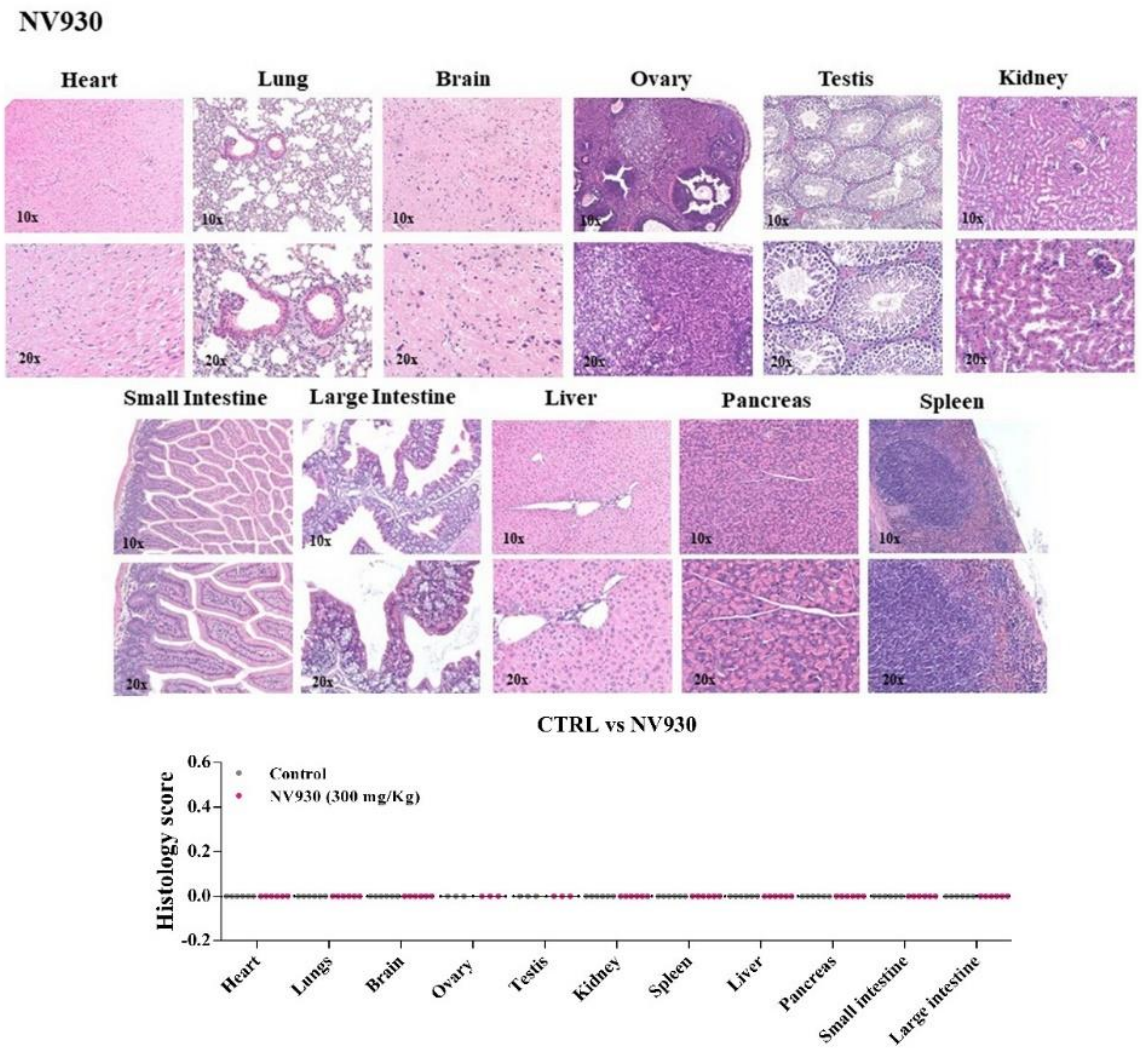

Figure 37. *A representative panel of histopathological evaluation on tissues derived from NV930-treated mice is displayed. In the lower part, a graph showing the exact histopathological scores for each subject is reported (score = 0) (Corrao F., et al, 2022).*

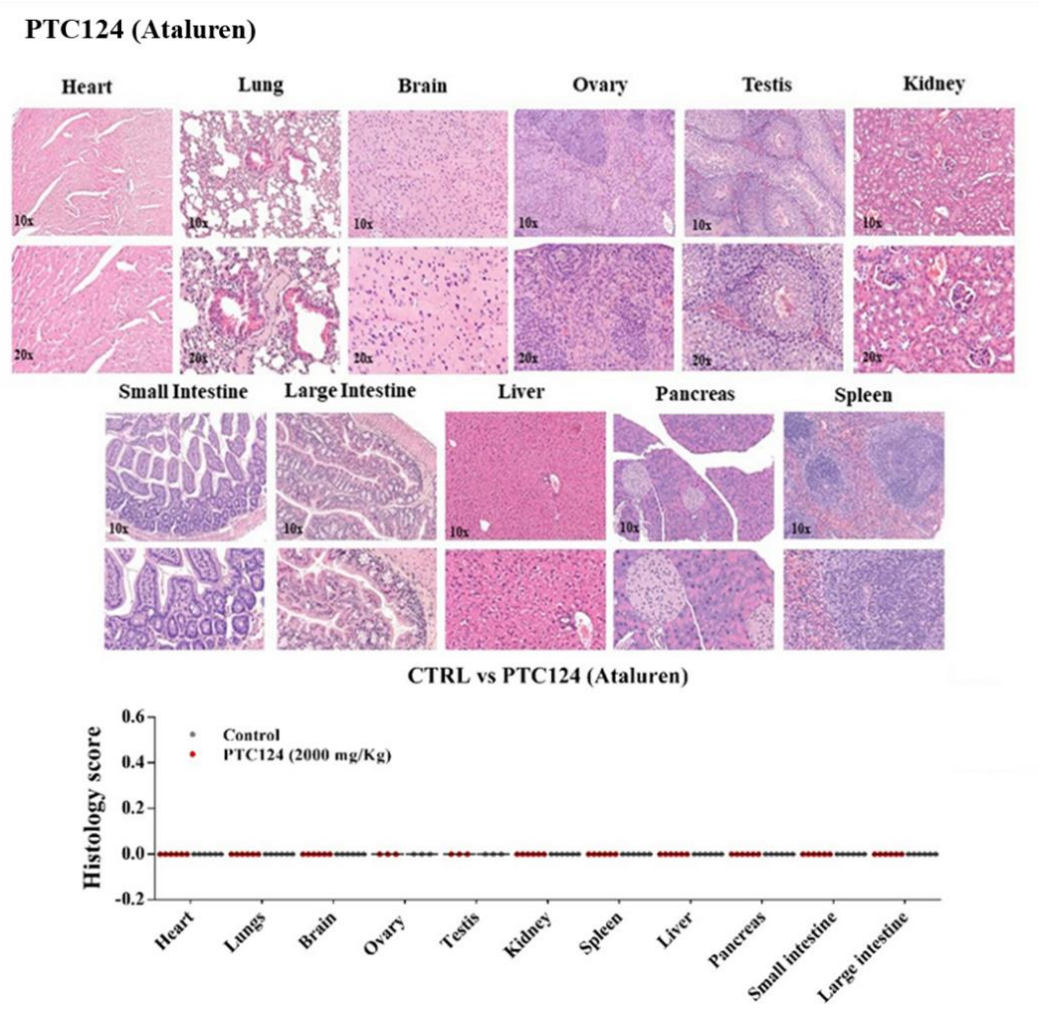

Figure 38. *A representative panel of histopathological evaluation on tissues derived from Ataluren (PTC124)-treated mice is displayed. In the lower part, a graph showing the exact histopathological scores for each subject is reported (score = 0) (Corrao F., et al, 2022).*

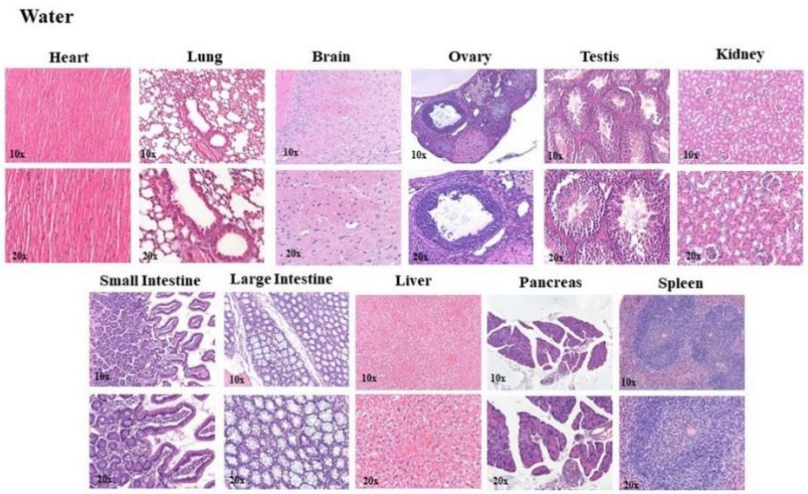

Figure 39*. A representative panel of of histopathological evaluation on tissues derived from water-administered mice is displayed (Corrao F., et al, 2022).*

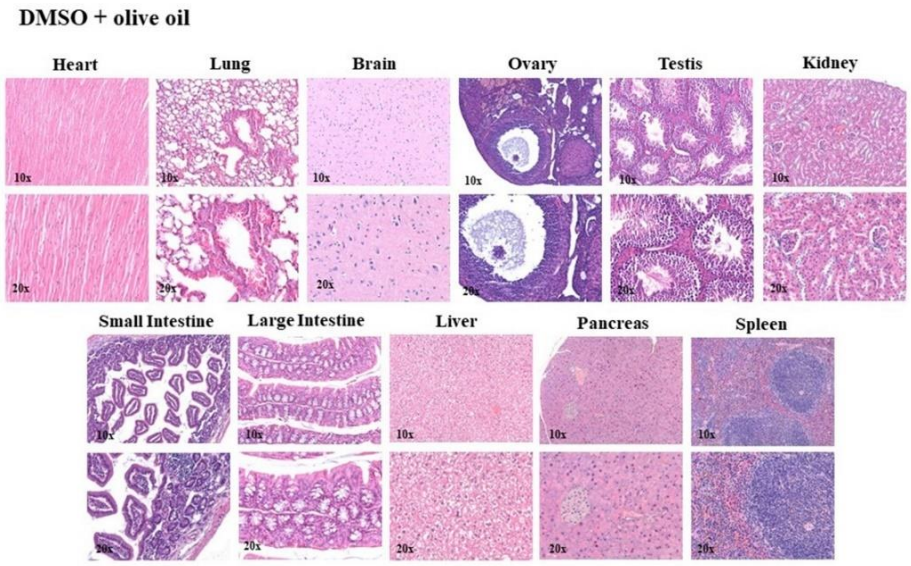

***Figure 40**. A representative panel of of histopathological evaluation on tissues derived from DMSO+olive oil-administered mice is displayed (Corrao F., et al, 2022).*

However, only in two mice treated with 2000 mg/Kg of Ataluren (PTC124), and in two animals from the 2000 mg/Kg NV914 treatment group, a slight tendency toward maturation perturbation of neutrophils (score 1) was observed, along with a mild expansion of the erythroid lineage (**Figures 41**).

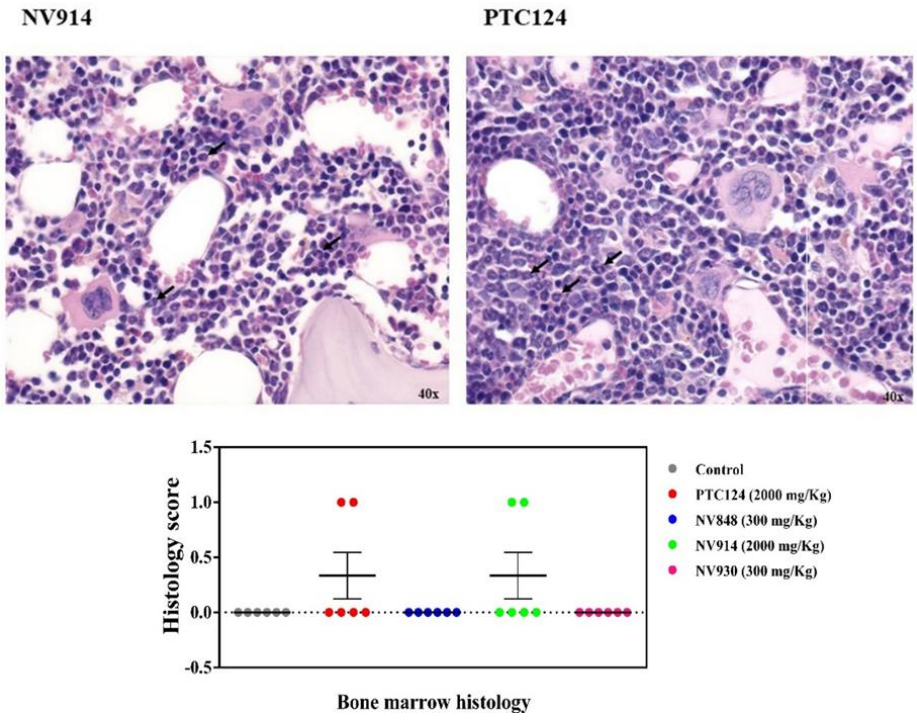

***Figure 41.** This panel provides a detailed bone marrow histopathological examination of samples from mice treated with NV914 and Ataluren (PTC124). The black arrows indicate a slight expansion of the erythroid lineage. As shown in the graph, this event was observed in only two samples of each treatment (score =1) (Corrao F., et al, 2022).*

Specifically, the following features were noted: nuclear hypo-segmentation, reduced cytoplasmic granularity, and neutrophilic anisocytosis (Corrao F., *et al*., 2022).

Based on this evidence, all treatments can be considered safe and free from any tissue damage or morphological abnormalities.

4.2 NV848 biodistribution in vivo.

The second objective was to investigate the *in vivo* distribution of NV848, by assessing its concentration in target tissues (plasma, lungs, pancreas, intestine, brain, and kidney), at different time points after the administration of 60 mg/Kg NV848 to the mice.

Molecules were extracted from the collected organs and the supernatants were analysed by High-Performance Liquid Chromatography (HPLC), to evaluate the distribution *in vivo* of the NV molecules.

In detail, after 45 minutes, the highest concentration of NV848 was found in plasma reaching 26 µg/mL (**Figure 42- A**). In the lungs, it was 0.17 µg/mL (**Figure 42- B**), in the pancreas 0.13 µg/mL (**Figure 42- C**), in the intestine 2.45 µg/mL (**Figure 42- D**), in the brain 3.4 µg/mL (**Figure 42- E**), and in the kidney 0.25 µg/mL (**Figure 42- F**). Moreover, the detection of the molecule significantly decreased at 2 hours in plasma, lungs, and kidneys, while it was still well detectable in the brain, intestine, and pancreas.

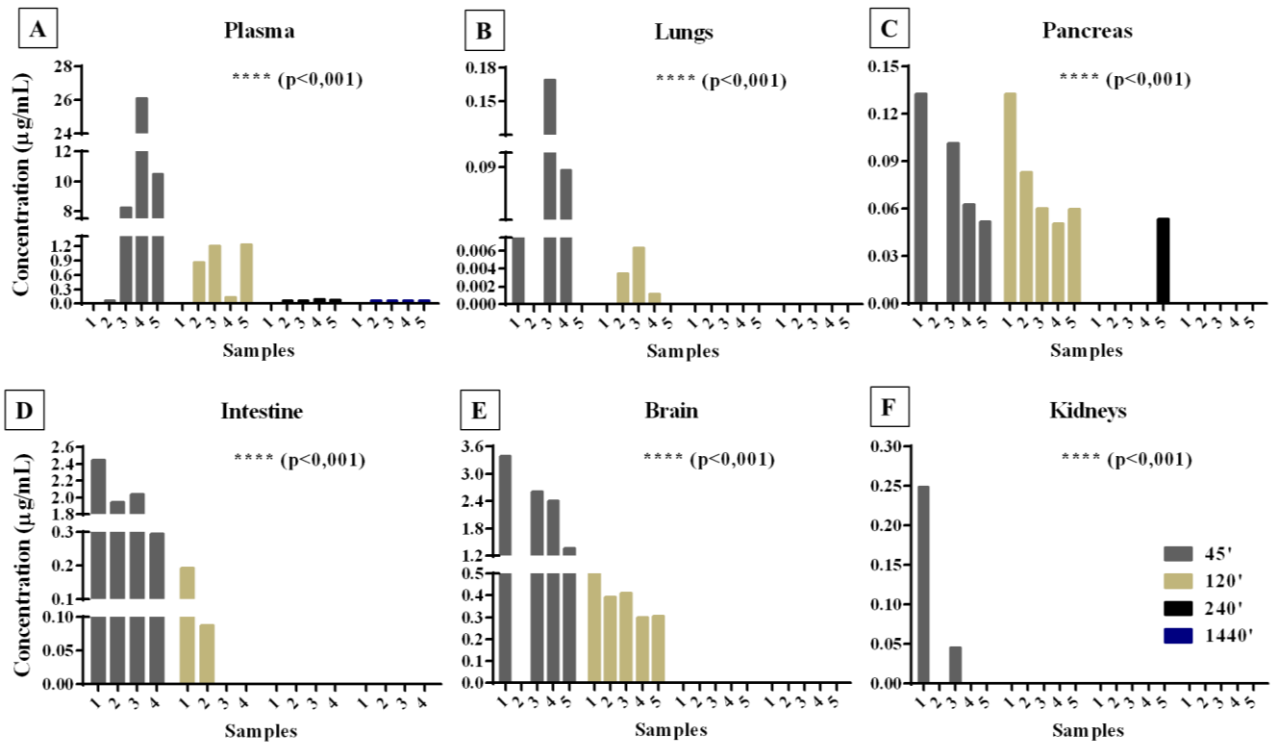

Figure 42*. The graphs show data of NV848 concentration (µg/mL) in plasma (**A**), lungs (**B**), pancreas (**C**), intestine (**D**), brain (**E**), and kidney (**F**) samples. A recovery test was performed for each organ, yielding recoveries of 27%, 14%, 55%, 15%, 48%, and 30% respectively (plasma, lungs, pancreas, intestine, brain, kidney). p<0.0001 (*) was calculated using a Two-way ANOVA test, performed using GraphPAD Prism 6.0.*

The data are collectively presented in the graph in **Figure 43**. The results indicate that the NV848 reached its highest concentration in the plasma (**Figure 42-A**), as expected, and that the concentration gradually decreased in the brain, intestine, kidney, lungs, and pancreas, respectively, in proportion to the increasing time points. Additionally, the 45 minutes and 120 minutes time points were detectable in most cases, whereas the other two time points analysed (240 minutes, and 1440 minutes) remained undetectable, except for the pancreas.

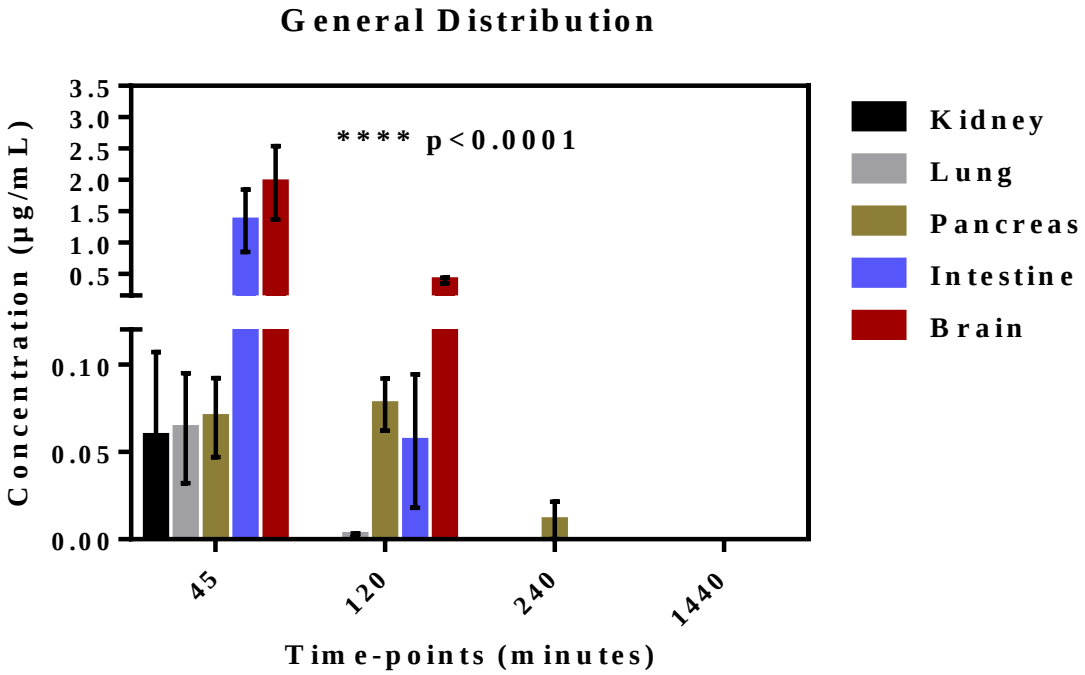

Figure 43. *The graph displays the aggregated data, represented as mean ± SEM of the values indicated in figures 42 A-F. p<0.0001 (*) was calculated using a Two-way ANOVA test, performed with GraphPAD Prism 6.0.*

Objective No.2: Establishment of a CFTR-G542X mutant mice colony and evaluation of NV848 readthrough activity *in vivo*.

4.3 Generation and management of a CFTR mutant mice colony and genotyping of newborns.

Following the confirmation of the safety of the three NV TRIDs and the biodistribution of NV848 at a dose of 60mg/Kg, the next step was to assess the efficacy of NV848 *in vivo*. To begin, a mutant CFTR-G542X mice colony was established, by breeding heterozygous females and male mice $CFTR^{WT/G542X.}$

After a gestation period of approximately 20 days of pregnancy, delivery occurred, and genotyping was conducted on the 21st day after birth using specific primers designed for the two different alleles. Throughout the course of this project, a total of 42 subjects were obtained and genotyped as shown in **Figure 44** through two illustrative panels.

It was observed that primers designed for the CFTR G542X allele amplified a non-specific product in DNA samples from WT subjects, (with a size of approximately 100-200 base pairs) in the absence of a specific target. In G542X homozygous subjects, the primers correctly amplified a 319 bp PCR product.

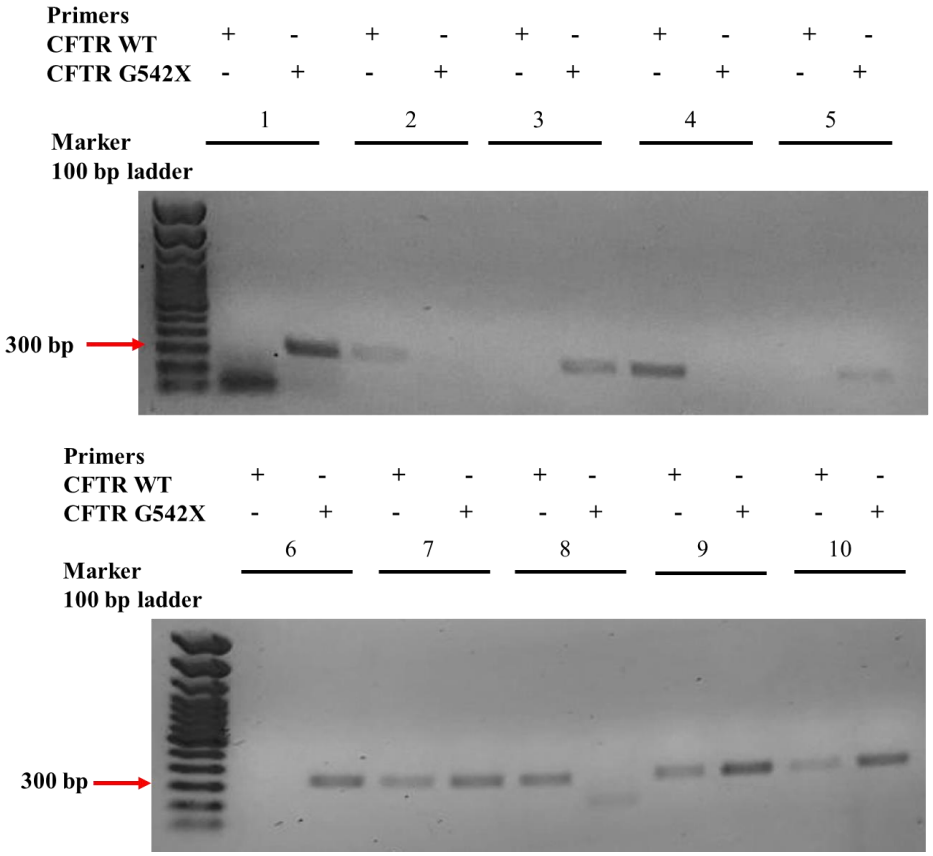

Figure 44. *These images display representative results of PCR performed on DNAs extracted from mice ear biopsy. PCR products were visualized on a 1% TBE-agarose gel and 100 bp ladder was used as a marker. The red arrow indicates the 300 bp line in the marker and the expected product length is 319 bp, which is found almost up to the 300 bp line.*

The PCR analysis identified 10 $CFTR^{WT}$ mice, 18 heterozygous mice, and 14 CFTR mutant homozygous mice. Subsequently, the mice were grouped based on their genotype and the specific molecule or vehicle to be administered.

4.4 Chronic administration for 15 days and evaluation of the CFTR protein expression.

Following the formation of the experimental groups, the subsequent phase of this project involved a 15-day chronic treatment with NV848 molecule to assess its effectiveness in nonsense CFTR $^{G542X/G542X}$ mouse model. The selected dosage of 60 mg/Kg was based on the previous results obtained from biodistribution experiments. The intragastric administration of the specified NV848 dose was carried out in five $CFTR^{G542X/\ G542X}$ (named:

M17, M11, M6, M5, and M3), besides, one $CFTR^{WT}$ mouse and one $CFTR^{G542X/\ G542X}$ mouse were administered only with the vehicle (water), to serve as experimental controls.

Treatments commenced after genotyping and subjects were administered once daily. On the 15th day, the animals were euthanized for organ collection, in preparation for the subsequent analyses.

Specifically, molecular and immunohistochemical analyses were conducted on the lungs, which are the organs most affected by human CF.

To assess the CFTR mRNA expression after the treatment, five $CFTR^{G542X/G542X}$ mice were treated with 60 mg/Kg of NV848, and total mRNAs were analysed by real-time RT PCR (**Figure 45- A**). The mRNA of a $CFTR^{G542X/G542X}$ mouse treated with water was used as a negative control. The figure shows high variability in expression between individual specimens following the treatment with NV848. Notwithstanding, a trend towards higher mRNA levels in the treated mice is observed, with the exception of the M17, compared to the control.

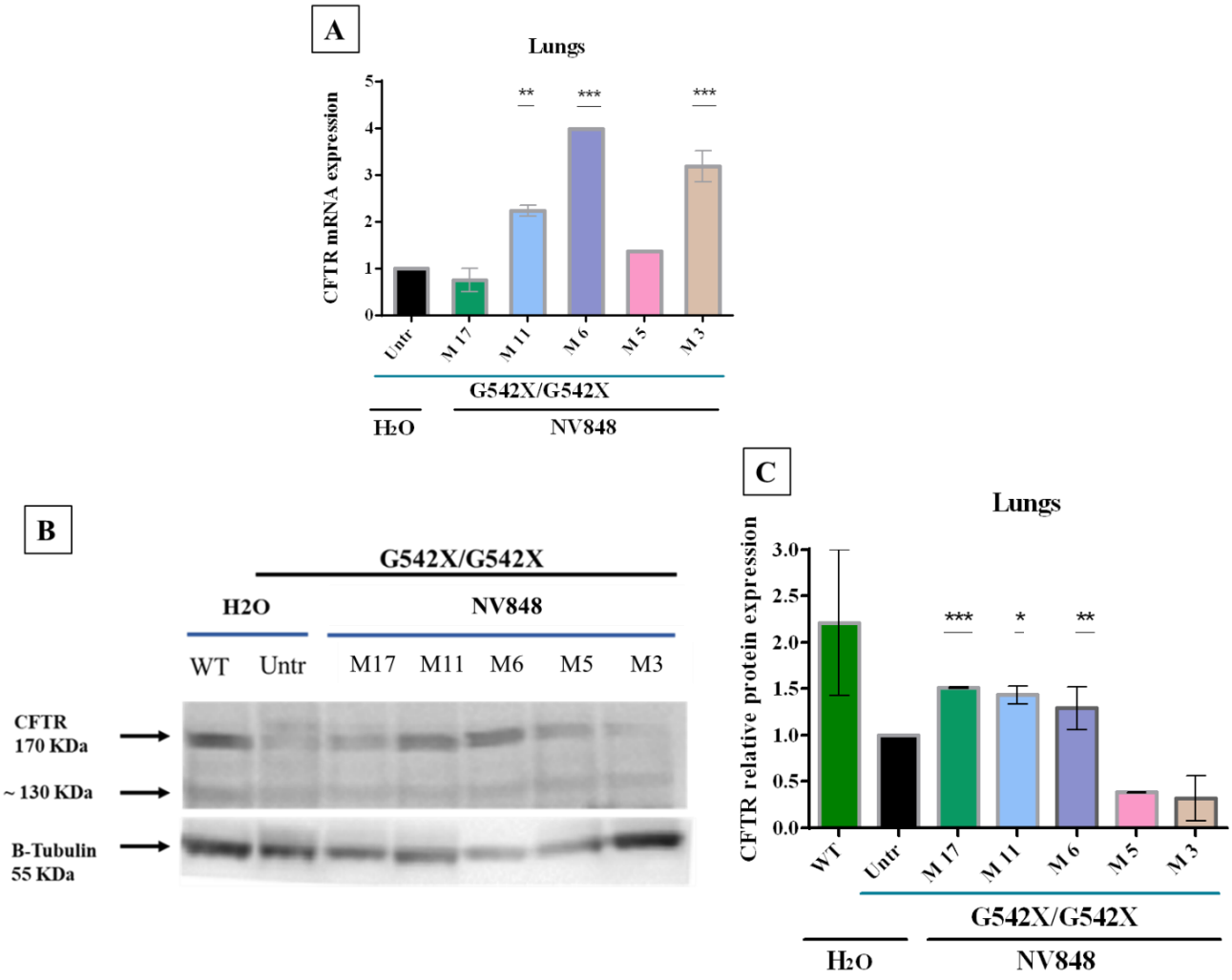

Figure 45. (A) *Real-time RT PCR graph shows CFTR mRNA levels in the lungs of negative control (only water) and tested mice (M 17, 11, 6, 5, 3, NV848 60 mg/Kg). The primers used for this analysis are listed in Table 4.* ***(B)*** *Representative image of one of the two Western blots performed.* ***(C)*** *Graph illustrating the relative*

band density of the CFTR protein presented as the mean of two experiments conducted in duplicate. The p-value was calculated by the one-way ANOVA test.

After the chronic administration of the NV848 molecule, CFTR mRNA levels and protein expression were analysed in $CFTR^{G542X/G542X}$ mice. As controls, the analysis was performed on the total lung mRNA and protein extracts from one $CFTR^{WT}$ mouse and one $CFTR^{G542X/G542X}$ mouse that received only the vehicle (water) used as positive and negative controls, alongside five $CFTR^{G542X/G542X}$ mice treated with 60 mg/Kg of NV848.
The results of the Real-time RT PCR showed a variation among the five $CFTR^{G542X/G542X}$ mice treated with NV848 in CFTR mRNA expression. Specifically, in 4 of 5 mice (M 11, M 6, M 5, and M 3) the mRNA levels were higher than that of the untreated control (water).
Furthermore, the analysis of the bands revealed an increase in protein expression in 3 of 5 treated mice, compared to the control sample. In particular, M17, M11, and M6 reached approximately 1.5-fold higher levels of CFTR protein expression (**Figure 45- C**).

4.4.1 Immunohistochemistry experiments for the evaluation of chronic treatment safety and CFTR protein rescue expression in vivo.

To visualize CFTR localization in the mice lung tissue samples were analysed by immunohistochemistry.
Immunohistochemistry analysis was performed on lung sections of WT and CFTR $^{G542X/G542X}$ mice treated with NV848 at 60 mg/Kg for 15 days or administered with water as control.
Sections were stained with H & E staining to examine the tissue integrity and to evaluate possible deleterious effects of the long-term treatment.
Two antibodies were used in the analysis: a thyroid transcription factor 1 (TTF1) antibody to assess the responsiveness and the reactivity of tissue slides, and an anti-CFTR antibody to detect the protein of interest.
Samples were incubated with the antibody recognizing the TTF1, a protein expressed in nuclei of thyroid and pulmonary cell epithelia (Aversa S., and Bellan, C., 2018). As seen in **Figures 46-A and 46-B**, TTF1 is detected in its correct nuclear localization in all samples, allowing us to confirm that tissues were positive for TTF1 staining (**black arrows**).
CFTR protein detection was performed using a specific primary antibody. In the WT sample CFTR staining (**black arrows, Figure 46-A**) is revealed in the apical membranes of pulmonary ducts, creating a highly intense brown coloration. In contrast, in the negative control (mouse 16), CFTR staining is not bright and clear and is mostly localized in intracellular compartments (**black arrows, Figure 46-A)**, rather than in apical membranes, and it appears non-uniform.
Moreover, the light brown seen in the images of mouse 16, corresponding to CFTR detection, could be due to a kind of background effect in the detection system.
Lastly, in mouse 3 treated with NV848, CFTR expression is highlighted in the apical membranes of epithelial cells of pulmonary ducts, forming a more defined line delimiting this area (**black arrows, Figure 46-B and 46-C**), similar to the WT sample. This allows to conclude that the protein was expressed and reached the

correct localization. However, even in this case, some signals are also evident in intracellular compartments, similar to the negative control (mouse 16).

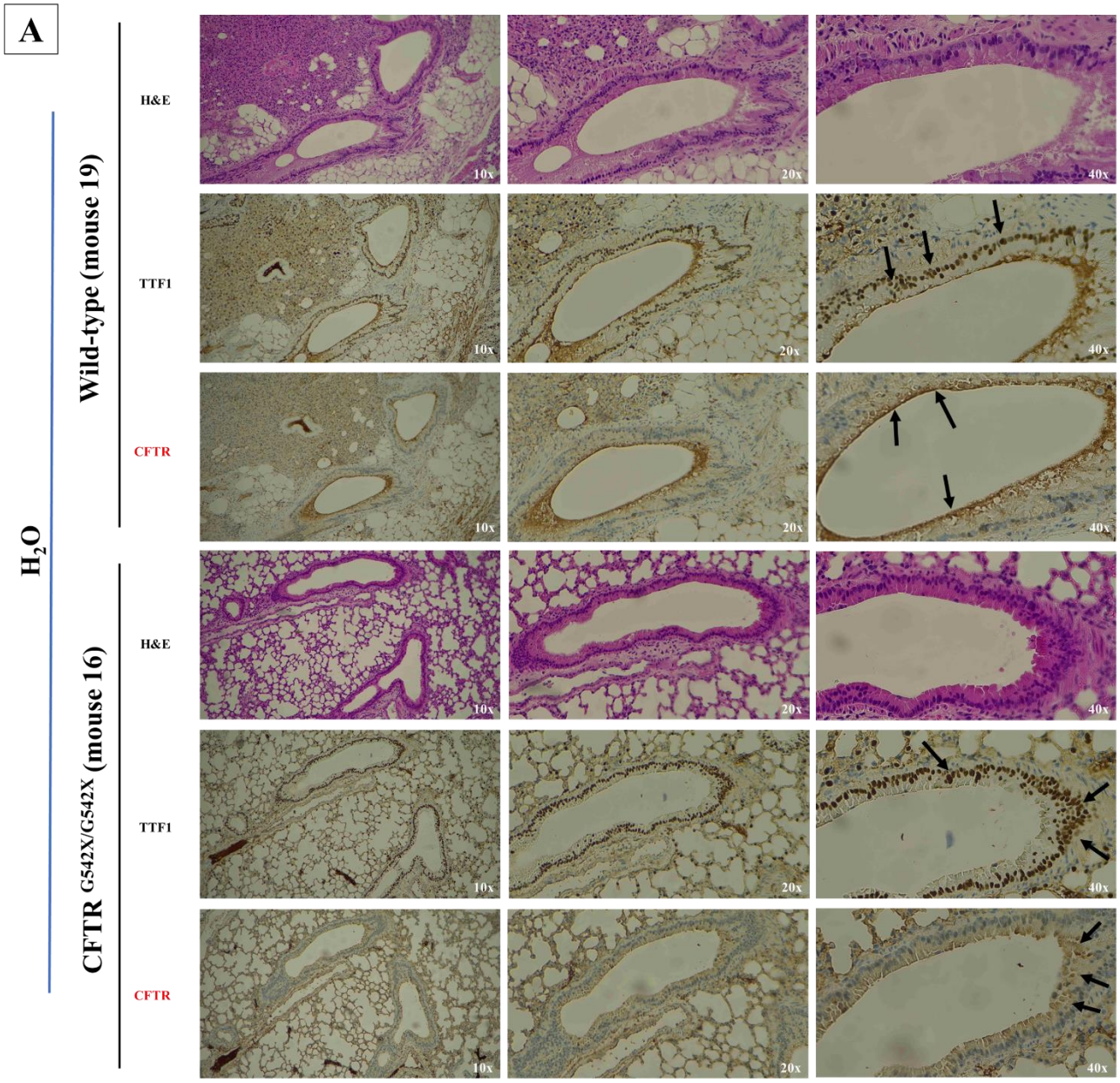

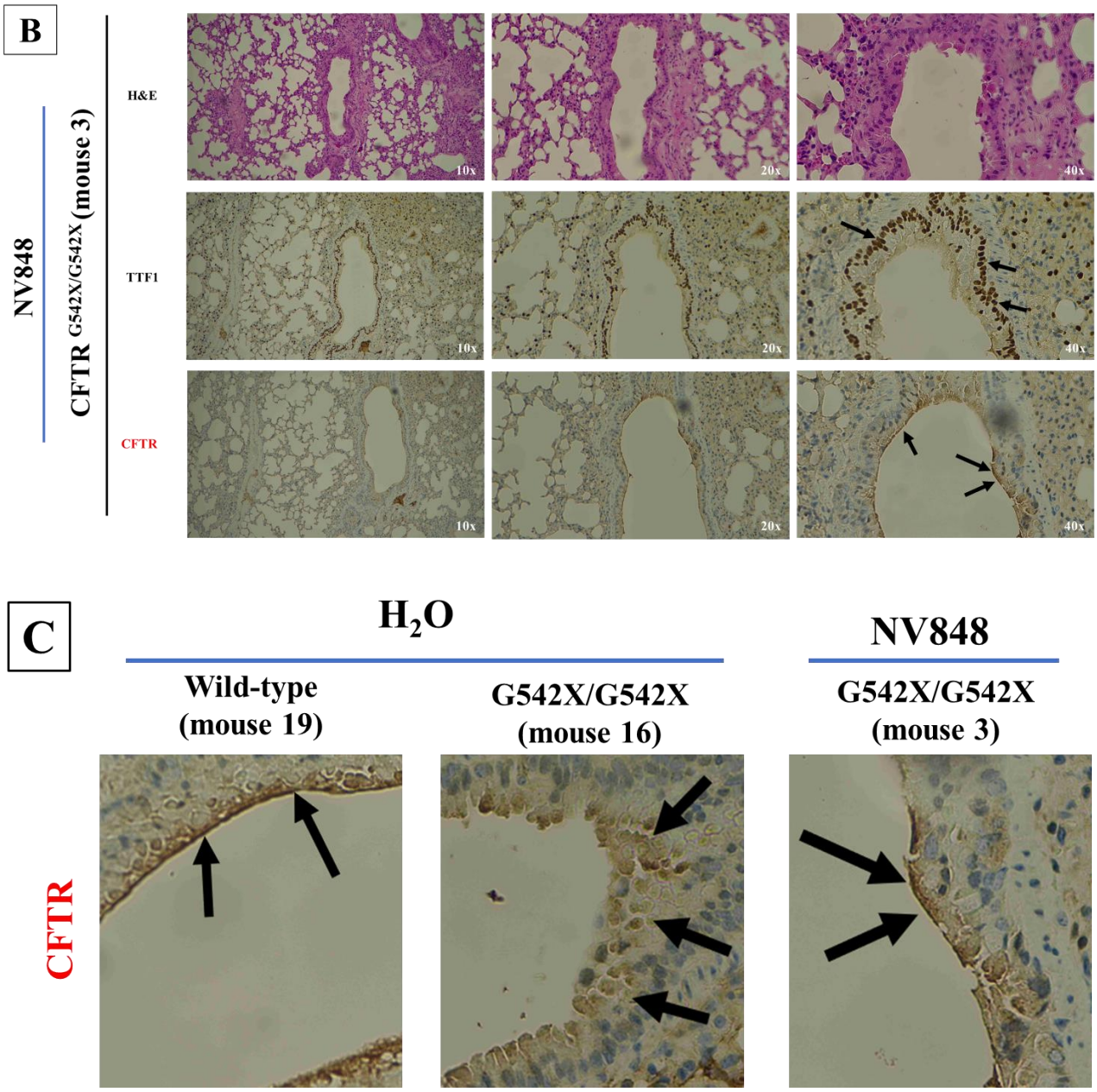

Figure 46. *Images related to immunohistochemistry analyses on (**A**) mouse 19 (Wild-type), 16 (CFTR $^{G542X/G542X}$, only water), and (**B**) mouse 3 (CFTR $^{G542X/G542X}$, treated with NV848 60 mg/Kg). Lung slides were stained with haematoxylin and eosin (H & E) and incubated with anti-TTF1 or with anti-CFTR antibodies. 10X, 20X and 40X magnifications are displayed. (**C**) Close-ups of the areas with CFTR staining in the three samples, with black arrows indicating the localization of CFTR.*

Objective No.3:

a) *In vitro* CFTR protein rescue evaluation by the Ussing Chamber technique in engineered 16HBE cells with the G542X and W1282X nonsense mutations.

4.5 Study of the CFTR functionality in human bronchial epithelial cells through short-circuit current measurements.

In addition to assessing protein expression evaluation by Western blot and immunohistochemistry analyses on the tissue samples, the Ussing chamber technique was employed to better understand whether the rescued protein reached its natural folding, and if its functionality was restored. To achieve this, 16HBEge $CFTR^{G542X}$ and $CFTR^{W1282X}$ cell lines were employed.

This objective was pursued during my period as visiting student, as part of the PhD program, at the Institut Necker Enfants Malades (INEM), under the supervision of Professor, M.D, PhD Isabelle Sermet-Gaudelus.

Each cell line was kept in culture in specific inserts until they differentiated forming an airway epithelium. The cells were then treated chronically for 48 hours with NV848 (1 mM) or Geneticin (G418) (100 µM), with or without the addition of NMD inhibitor SMG1i (referred to as NMDi) and CFTR modulators, such as Trikafta (referred to as TK) (Tezacaftor - VX-661, Elexacaftor - VX-445, and Ivacaftor - VX-770).

a) 16HBEge $CFTR^{G542X}$ cells experiments:

In **Figure 47-A,** the measurement of Isc (Intensity of short current circuit) is shown after the addition of Amiloride, which blocks ENaC channels and allows the selective recording of CFTR protein activity. The results show a consistent pattern in most samples, except for the treatment with NMDi + TK, which resulted in a positive registration of chloride current. Additionally, the treatment with the tested molecule produced consistent results both when administered alone and in combination with NMDi + TK. These findings suggest that all the epithelia analysed were viable and responsive to drugs, both in terms of individual treatments and Ussing chamber analysis.

The graphs in **Figures 47-B and C** report data relative to Isc measurement for the induction or inhibition of CFTR activity. To assess specific CFTR activity, CFTR stimulation is achieved using IBMX/forskolin, while inhibition is accomplished with the specific inhibitor Inh172.

Figures 47-B and C indicate that the NV848 treatment alone and in combination with NMDi + TK does not achieve the same level of CFTR induction as Geneticin (G418) (administered alone or in combination). However, when the specific CFTR inhibitor is added to the solution, NV848 treatment yields nearly the same level of response as Geneticin (G418).

These results suggest that the treatment is safe, as epithelia remain viable; and the current registration is specific to the CFTR protein. However, NV848 may not be sufficient to fully rescue CFTR functioning in this model system carrying the G542X nonsense mutation in the CFTR gene.

A

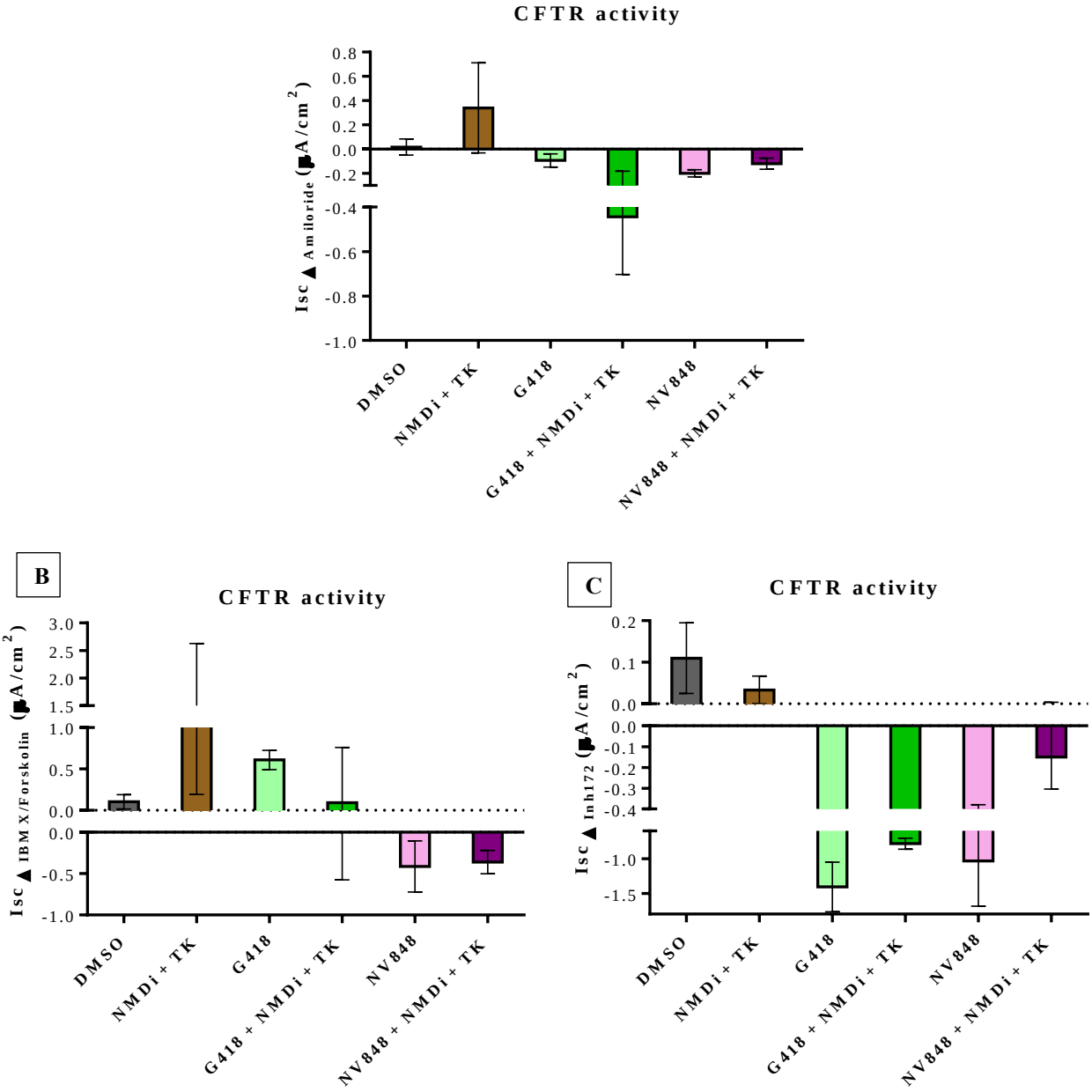

Figure 47*. Graph showing short-current measurement (Isc) following the addition of (**A**) amiloride (100μM), (**B**) IBMX (100μM)/Forskolin (10μM), or (**C**) CFTR inhibitor Inh172 (40μM). Data were analysed using LabChart8 Readers software (ADInstruments).*

b) *<u>16HBEge CFTR^{W1282X} cells experiments:</u>*

The same investigation was conducted on the 16HBEge CFTR^{W1282X} cell lines.

As before, in **Figure 48-A** the effect of amiloride addition is shown, aimed at inhibiting the activity of ENaC channels, in order to selectively register chloride transport only attributable to the CFTR protein. **Figures 48-B and C** report the CFTR activation and the inhibition, respectively.

In these graphs (**Figures 48-B and C**), the CFTR-mediated chloride current registration indicates that NV848 treatment alone did not induce CFTR activity (F**igure 48-B**) in the same manner as the positive control, the Geneticin (G418) treatment, which gave a slight response too.

However, when used in combination with NMDi and TK (combo), NV848 reached more than half of the level achieved by Geneticin (G418) in combo. Regarding CFTR inhibition, the results (**Figure 48-C**) showed that, when alone, NV848 treatment gave almost the same result as G418 alone, but in combination with NMDi+TK, the action of the drug is profoundly boosted, showing the same trend of the Geneticin (G418).

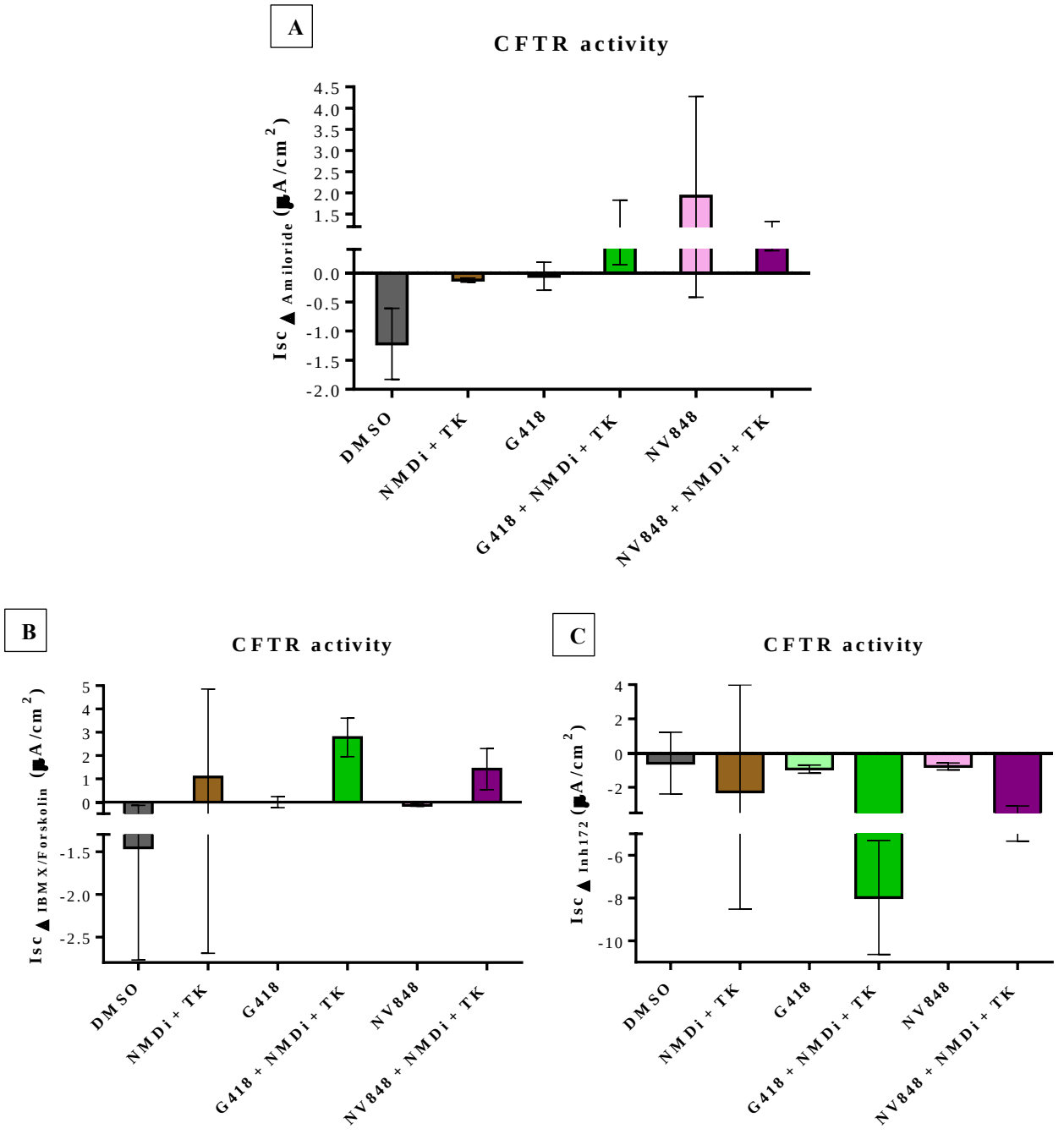

Figure 48. *Graph showing short-current measurement (Isc) after the addition of (**A**) amiloride (100μM), (**B**) IBMX (100μM)/Forskolin (10μM), or (**C**) CFTR inhibitor Inh172 (40μM). Measurements were analysed using LabChart8 Readers software (ADInstruments).*

These results suggest that the NV848 treatment could be a potential molecule able to rescue CFTR protein activity in the CFTR-W1282X nonsense mutation context, but the use of NMD inhibitors and CFTR potentiators and correctors could be needed to maximize CFTR activity, in a synergic action with the readthrough compound NV848.

c) Real-time RT PCR on 16 HBEge CFTR^{G542X} and CFTR^{W1282X}.

Real-time RT PCR was carried out to evaluate CFTR mRNA expression on the same sample examined with Ussing Chamber, and the results are shown below (**Figure 55**).

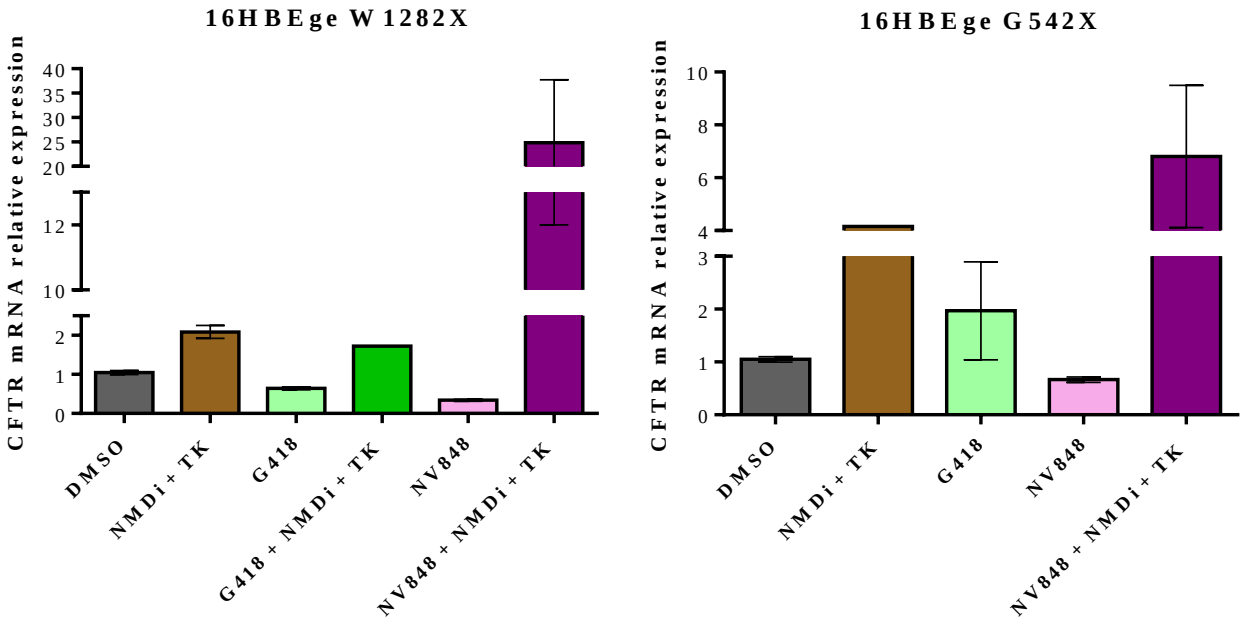

***Figure 49**. qPCR analyses are presented in the graphs, corresponding to 16HBEge G542X (**left**) and W1282X (**right**). qPCR was performed in duplicate.*

These analyses reveal a similar pattern for the genotypes, G542X and W1282X. In fact, the addition of NMDi and TK induces an improvement in the CFTR mRNA expression, which is further enhanced when TRIDs are included in the treatment, as seen with NV848 and Geneticin (G418). However, for CFTR-G542X cell lines, due to some samples with poor quality, only one NMDi + TK was analysed, and, unfortunately, no G418 + NMDi + TK sample was available for the same reason.

Taken together, these results suggest that NV848 TRID holds promise in the context of the nonsense mutation W1282X, but further investigation is needed to determine its potential for inducing the readthrough of the G542X stop codon.

b) Assessing the ability of NV molecules to induce readthrough in a different genetic context *in vitro,* using primary human fibroblasts with the UGA-R1683X mutation in the *LRBA* gene.

4.6 Investigation of the effects and activity of NV848, NV914 and NV930 on primary human fibroblasts with the LRBA^{R1683XR1683X}mutation.

Given that approximately 11% of inherited diseases are caused by nonsense mutations, finding a molecule that can act across various genetic contexts and pathologies, would be extremely beneficial in improving patients' conditions and quality of life. For this reason, the functionality of the three NV compounds was previously explored in CF and SD. Additionally, the current project aims to assess the effectiveness of the three NV TRIDs in promoting readthrough of the R1683X nonsense mutation in the *LRBA* gene, a factor contributing to the onset of Primary Immune Regulatory Disorders (PIRDs).

4.6.1 Evaluation of LRBA$^{R1683X/R1683X}$ primary fibroblasts after 24, 48, and 72 hours of NV compounds treatment.

To assess the effects of TRIDs treatment on LRBA$^{R1683X/R1683X}$ human primary fibroblasts, cells were plated and treated for 0, 24, 48, and 72 hours. (**Figure 50**).

As shown in the graph in F**igure 50**, NV848 treatment (blue) had no impact on cell proliferation. In the case of NV914 (green), and NV930 (pink), a significant decrease in cell proliferation was observed after 48 and 72 hours. The Geneticin (G418) and Ataluren were used as experimental controls. In the case of the Geneticin (G418), cells exhibited a substantial decrease in proliferation at all time points, while Ataluren produced results similar to the NV914 and NV930 treatments.

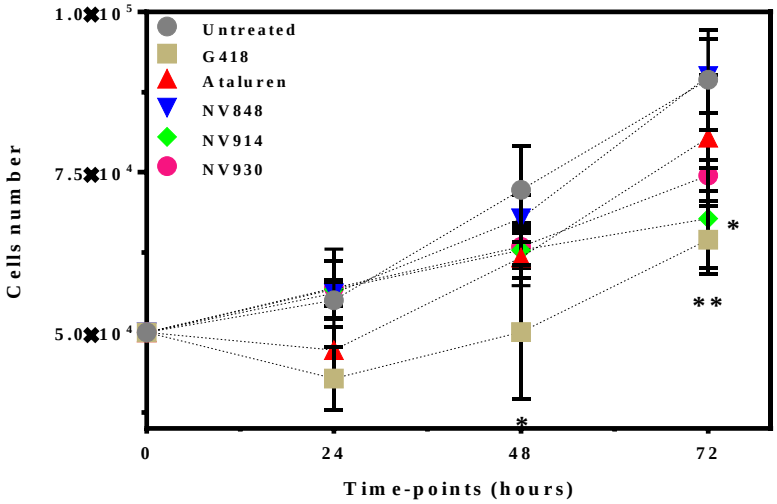

Figure 50. *Graph illustrating fibroblast growth curve after 24, 48, and 72 hours of chronic treatment with the specified molecules (in triplicate). Geneticin (G418) (430µM) and Ataluren (PTC124) (12µM) were used as controls. NV848, NV914, and NV930 (12µM) were compared to Geneticin (G418), Ataluren (PTC124), and untreated samples. A p value summary <0.0001 was calculated by the two-way ANOVA test.*

A subsequent step involved the evaluation of mRNA levels post-treatment, and a Real-time RT PCR analysis was performed. The analysis revealed an increase in the LRBA transcript levels in NV848-treated cells (**Figure 51**).

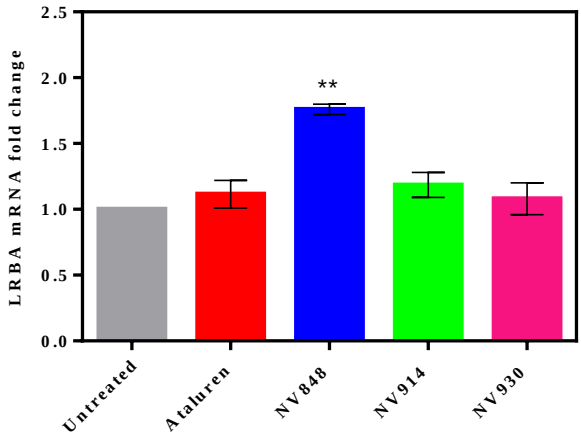

Figure 51. *Real-time RT PCR of LRBA transcript in untreated and NV TRIDs or Ataluren (PTC124) (12µM) treated primary fibroblasts LRBA$^{R1683X/R1683X}$ for 72 hours. The experiments were conducted in triplicate. A p value < 0.0001 was calculated by one-way ANOVA test statistical analysis.*

The presence of a premature stop codon typically affects the mRNA stability through the action of the NMD pathway. To investigate the potential impact of NV848 on the transcript sequence, an NGS analysis was performed on NV848-treated cells.

For this purpose, total RNA was extracted, then, retrotranscribed, and cDNA was amplified using primers designed to anneal in the region containing the mutation (c. 5047 C>T) (**Table 5**).

NGS analysis (conducted by BMR Genomics) revealed that NV848 treatment did not alter nucleotide sequence integrity, as the sequence of the NV848 treated samples remained identical to the untreated ones. Both sequences were also compared to the reference (NM_006726.4) (**Figure S 1, Supplementary section**).

Bioinformatic analysis established that both sequences (NV848 and untreated) retained the same nucleotide in position 5047, which was "T". This indicates that the mutation characteristic of the patient's cells was preserved, and that the treatment did not induce any change in the mRNA sequence.

4.6.2 Evaluation of LRBA protein expression, localization, and functionality rescue after 72 hours of NV molecules treatment.

Finally, to assess the expression of the LRBA protein after readthrough, cells were treated for 72 hours with NV848, NV914, NV930, and Ataluren (PTC124), and the proteins were extracted and analysed by Western blot (**Figure 52**).

Two positive controls were used: Hela and IMR-90 cells.

As shown in **Figure 52**, NV848, NV914, and NV930 treatments induced a significant expression of the LRBA protein, compared to the untreated sample.

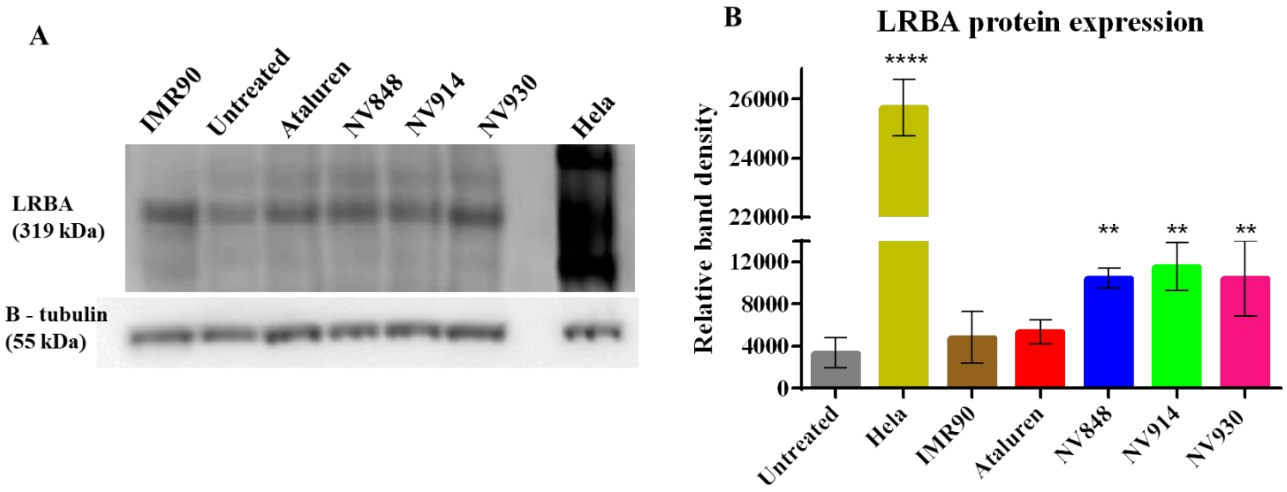

Figure 52. *(**A**) Western blot analysis showing LRBA protein (319 kDa) expression following the indicated treatments in human LRBA$^{R1683X/R1683X}$ fibroblasts. Beta-tubulin (55 kDa) was used as a loading control. Images were analysed using ImageJ software and the band density was reported in graph (**B**). A p value <0.0001 was calculated by one-way ANOVA test statistical analysis.*

The ultimate goal was to investigate the LRBA localization and functionality.

For this purpose, primary LRBA$^{R1683X/R1683X}$ fibroblasts were treated for 72 hours with NV molecules or Ataluren (PTC124), and LRBA protein was detected by immunofluorescence analysis. Hela cells were utilized as a positive control.

The result of this assay indicated that NV848 and NV914 treatments restored protein expression and localization, within intracellular compartments and the perinuclear area. NV930 yielded a weaker signal, similar to Ataluren (PTC124), in comparison to untreated cells (**Figure 53**).

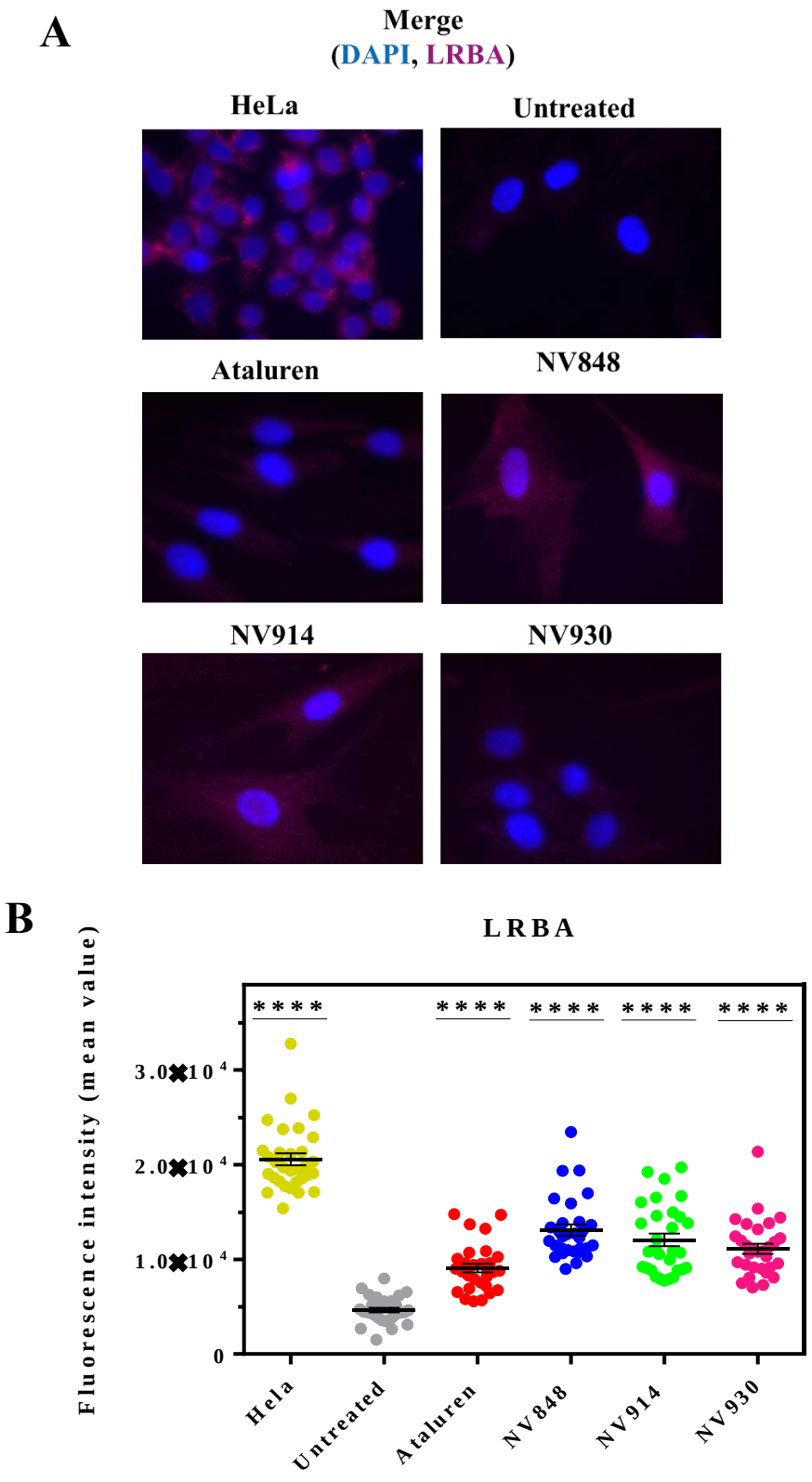

Figure 53. A) *Immunofluorescence images of the Hela and primary LRBA$^{R1683X/R1683X}$ cells, either untreated or treated with the NV compounds or Ataluren (PTC124) (12 µM). The panel displays DAPI staining for nuclei, LRBA positive signals, and merged staining.* ***B)*** *The graph depicts the results of fluorescence intensity analysis. The experiments were replicated in duplicate. A p value <0.0001 was calculated by one-way ANOVA test statistical analysis.*

To assess LRBA functionality, an indirect approach was employed. Specifically, EGFR localization was chosen as an indirect measure of the LRBA functionality.

Indeed, EGFR transport and recycling in the plasma membrane and in the intracellular vesicles have been proposed to be linked to LRBA protein-associated vesicles (Sigismund S., *et al.,* 2008; Sigismund S., *et al.,* 2017; Martinez-Jaramillo, C., and Truijllo-Vargas, C. M., 2018; Murphrey M. B., *et al.,* 2022).

In normal conditions, an equilibrium between EGFR transport to the plasma membrane, and endocytic internalization is expected (Tomas A., *et al.,* 2014).

The hypothesis was that if LRBA was rescued, correct EGFR trafficking and recycling should be observed.

Hela cells were used as a positive control since, in cancer cells, EGFR is mainly localized in the plasma membranes. Primary $LRBA^{R1683X/R1683X}$ fibroblasts were either untreated or treated for 72 hours with NV molecules or Ataluren (PTC124).

In **Figure 54**, EGFR staining (yellow) analyses showed EGFR localization in both plasma membrane and in the cytosol of the treated cells, confirming the hypothesis of LRBA involvement in the EGFR transport.

However, in the case of NVs and Ataluren (PTC124) treatments, the results are promising. NV848 appeared to be the most effective among the NV molecules because EGFR signals (white arrows) are observed not only in plasma membranes but also as spots in the cytosol. This observation suggests that EGFR is correctly expressed in the membranes and properly recycled, maintaining cellular homeostasis.

This result confirms that the rescue of LRBA functionality occurred with NV848 treatment, as indicated by the absence of signals in untreated samples (magnification **Figure 54-A**). NV914, NV930, and Ataluren (PTC124) treatments improved EGFR expression, but did not achieve the same levels of EGFR expression under NV848 treatment (**Figure 54-B**).

Furthermore, since the LRBA-EGFR pathway has not been clearly elucidated, these analyses shed light on potential future investigations to understand this pathway.

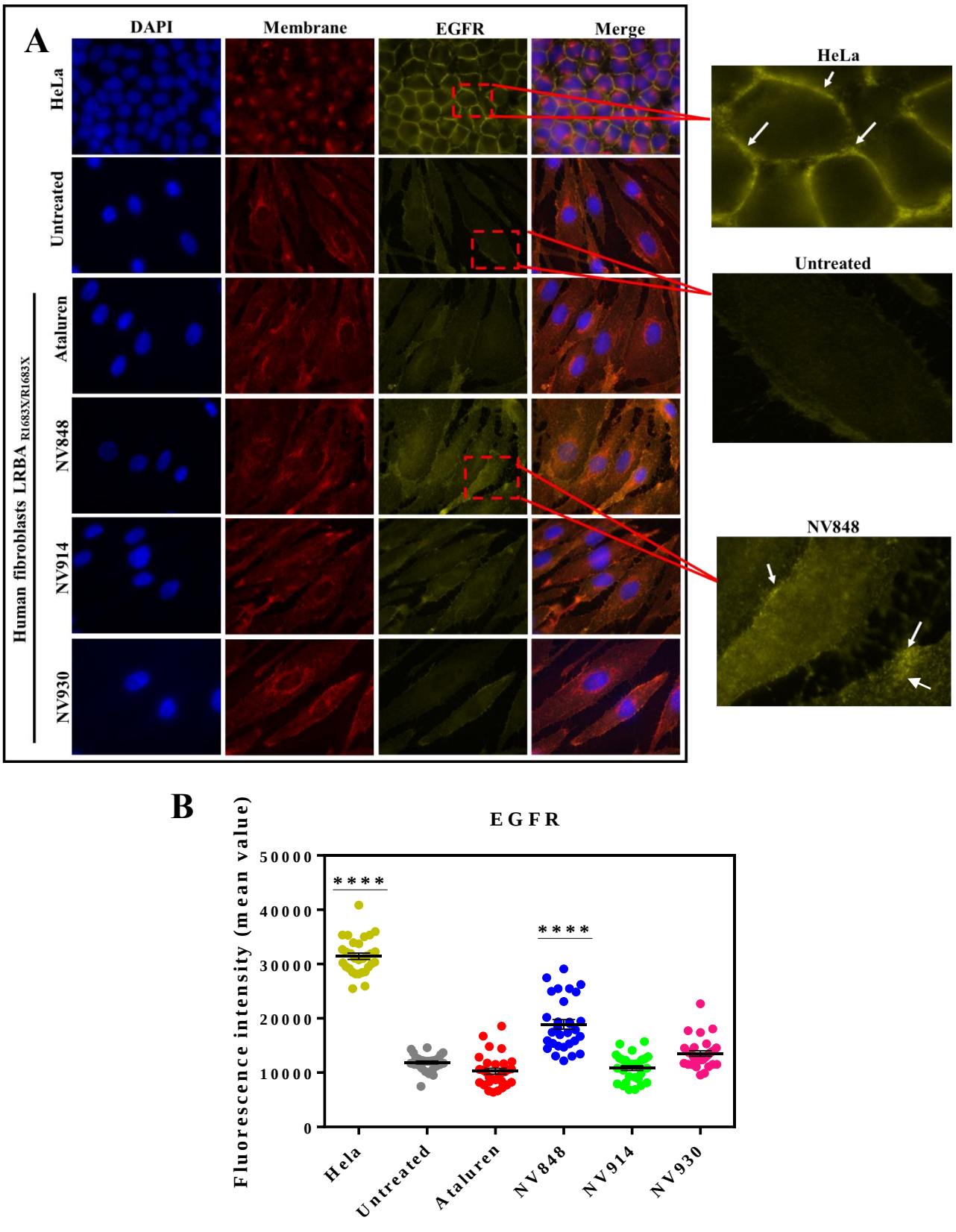

Figure 54. A) *Immunofluorescence analysis to visualize EGFR protein expression in primary LRBA$^{R1683X/R1683X}$ cells treated with NV848, NV914, NV930, and Ataluren (PTC124) (12 µM). Hela cells were utilized as a positive control.* ***B)*** *The graph presents the mean fluorescence intensity. The experiments were conducted in duplicate. A p value <0.0001 was calculated by one-way ANOVA test statistical analysis.*

Collectively, these results confirm that NV molecules, with a primary emphasis on NV848, have the potential to serve as potent TRID for treating NRDs. Furthermore, the data obtained from these recent investigations on $LRBA^{R1683X/R1683X}$ could open the door to further investigations into the role of LRBA in intracellular vesicles and the discovery of other LRBA targets.

Similarly, elucidating the correlation and the pathways influenced by the presence or absence of LRBA may provide a valuable strategy for comprehending and treating LRBA mutations in the context of precision medicine.

5 DISCUSSION

Nonsense mutations are responsible for approximately 11% of life-threatening inherited diseases. These mutations lead to the presence of a premature termination codon (PTC) in the mRNA sequence, resulting in the complete absence of the protein encoded by the aberrant mRNA.

Currently, there are no treatments available for *Nonsense Related Disorders* (NRDs).

However, suppression therapy using *Translational Readthrough-Inducing Drugs* (TRIDs) represents one of the most promising strategies to overcome this defect.

In this scenario, three newly optimized molecules, namely NV848, NV914, and NV930, have recently been tested in cell models of CF and Schwachman-Diamond syndrome. These studies have revealed the specificity, safety, effectiveness, and a possible mechanism of action of these molecules *in vitro* (Pibiri I., *et al.,* 2020; Bezzerri V., *et al.,* 2022; Carollo P. S., *et al.,* 2023; Perriera R., *et al.,* 2023).

Up to this point, the efficacy of NV molecules was demonstrated *in vitro*. In this thesis, the objective was to evaluate the safety, biodistribution, and potential activity also in an *in vivo* model, which is a crucial step in the development of new substances.

To achieve this aim, murine models were utilized in this project. Specifically, two main goals were pursued to assess the tolerability and biodistribution in C57BL/6 mice.

Particularly, a well-established protocol, from OECD guidelines for *in vivo* chemicals testing (OECD No. 420), was chosen to assess the acute toxicity of NV molecules using a fixed dose. The protocol permitted us to use the smallest number of animals required to achieve statistical significance.

A first pilot study, conducted on a single animal, allowed us to determine the potential toxic effects of the maximal dose of 2000 mg/Kg of the tested drugs (NV8484, NV919, or NV930), comparing the results with the control group (Ataluren - PTC124). Two of the NV molecules, specifically NV848 and NV930, proved to be lethal at this dosage, while NV914 did not. Therefore, it was established that the maximum tolerated dose was 2000 mg/Kg for NV914, as well as for the positive control, Ataluren (PTC124), and 300 mg/Kg for NV848 and NV930. Consequently, the main study was conducted using these doses (Corrao F., *et al*., 2022).

The study continued through the administration of the three NV molecules to the specimens. After the administration and during the monitoring of the animals, the effects of the different treatments were recorded and appeared to be very similar to each other and comparable to the positive control, Ataluren (PTC124).

Given that Ataluren (PTC124) is an approved drug for the nonsense Duchene muscular dystrophy treatment (Ryan N. J., 2014; https://www.ema.europa.eu/en/medicines/human/EPAR/translarna#authorisation-details-section), this result appears to be reassuring. In any case, all the symptoms observed following the administration of the three NV molecules were found to be transient and disappeared within approximately four hours.

Confirmation of the safety of the molecules comes from histological examinations performed on the 15th day at the end of the observational period. The results of analyses performed on the brain, heart, lungs, liver, spleen, pancreas, small and large intestines, kidney, bone marrow, testis, and ovaries revealed that no alterations in

morphology or tissue development were present, reinforcing the data that NV molecules, even at the elevated doses administered, are safe and well tolerated *in vivo.*

The assessment of NV molecules' safety allowed us to plan the next step, which involved investigating the biodistribution in the same mouse model used for the toxicity study. We focused our attention on the NV848, and experiments were performed using the dose of 60 mg/Kg corresponding to the dose used in the literature for Ataluren, our positive control (Du M., *et al.,* 2008). Following the protocol adapted by the work of Kayali (Kayali R., *et al.,* 2012), the amount of NV848 was analysed at different time points in target organs relevant in Cystic Fibrosis.

High-Performance Liquid-Chromatography (HPLC) performed on the above-mentioned organs revealed the presence of NV848 in all the analysed organs.

In addition, the molecule does not remain in the organs for an extended period, indicating that it is likely easily metabolized. It is also noteworthy that NV848 becomes undetectable in the kidneys, leading to speculate that it is efficiently excreted, thus preventing any potential toxic effects arising from the accumulation of the molecule.

These data, which suggest the absence of toxicity and the favourable biodistribution profile, allowed us to plan to test the readthrough activity of NV848 in a murine model characterised by the nonsense mutation G542X in the CFTR gene. This mutation is one of the most common among CF patients, and this recent mouse model was produced to present the mutation in the endogenous CFTR gene in all tissue districts (McHugh D. R., *et al*., 2018).

From the heterozygous mice gifted by Professor Hodge, a colony of mutant CFTR mice was established to obtain homozygous $CFTR^{G542X/G542X}$ individuals, which were selected through genotyping of newborns.

Chronic oral treatment in mice was performed for 15 days, and then the organs were collected. The analysis of the CFTR expression was focused on the effects of the NV848 treatment. The analysis results revealed that, following the extended treatment, three out of five homozygous mutant mice showed a rescue in CFTR protein expression, evidenced by Western blot analysis. Furthermore, immunohistochemistry analyses on lung samples from the animal groups revealed the presence of differences in CFTR expression among the control, homozygous untreated, and treated groups. In fact, the analyses indicated that in the $CFTR^{WT}$ mouse (mouse 19) the brown staining, corresponding to the CFTR expression, was homogeneous, precise, and delineated on the apical membranes of the epithelial cells in the pulmonary ducts.

In the case of the negative control (untreated $CFTR^{G542X/G542X}$ homozygous mouse; mouse 16), the CFTR detection was varied and not uniform. This variation may be due to some off-target effect of the antibody. Finally, in the $CFTR^{G542X/G542X}$ homozygous NV848-treated subject (mouse 3), the specific signal on the apical membrane was detected and uniform, as in the WT, but with lower intensity. Additionally, some dots were found on the intracellular side. This precise and correct signal suggests CFTR protein was rescued, not only in terms of the full-length translation but also in its proper localization, and possibly its function.

Additionally, an interesting observation was that the chronic treatment did not alter the integrity, development, and morphology of the tissues, allowing us to assess that the molecule is safe when administered continuously for a two-week period.

These results seem very promising, but they need to be confirmed by increasing the number of animals.

The final part of this study on CFTR protein rescue, involved *in vitro* models, specifically the 16HBEge cell lines harbouring the two most common nonsense mutations: G542X and W1282X.

The Ussing chamber technique, which is the gold standard for investigating CFTR functional rescue, was employed for this purpose.

In this context, a crucial factor influencing the readthrough was considered. Particularly, the NMD pathway, responsible for aberrant mRNAs degradation, as in the case of PTC-mRNAs. Since blocking NMD has been shown to enhance the effects of readthrough drugs, several NMD inhibitors have been studied over the last few decades (Isken O. and Maquat L. E., 2007; Romão L., 2019; McHugh, D. R., *et al.,* 2020).

For the current investigation, cells were treated for 48 hours with the NVs molecules or Geneticin (G418) as a control, either individually or in combination with NMDi and CFTR potentiators and correctors, such as Trikafta (TK) (VX-445, VX-661, VX-770).

The Ussing experiments revealed that, in the 16HBEge $CFTR^{G542X}$ cells, CFTR protein was not activated under the NV TRID, compared to the Geneticin (G418), which is still low.

However, in the 16HBEge $CFTR^{W1282X}$ cells, the response to treatment showed few differences. When CFTR was stimulated by the addition of forskolin/IBMX, NV848 in combination produced a positive activation of CFTR function. This activation was lower than achieved with Geneticin (G418) in combination, but higher than the treatment with NMDi + TK alone. This suggests that CFTR restoration after NV848 treatment, occurs synergistically with NMDi and TK.

Furthermore, the CFTR mRNA levels were investigated under the same treatment conditions as the Ussing analyses. The results indicated that NV848 in combination significantly induced mRNA expression and stabilization in both genetic contexts: the 16HBEge $CFTR^{G542X}$ and the $CFTR^{W1282X}$ cell lines. This effect was more pronounced than that observed with Geneticin (G418) in combination.

These findings may pave the way for future investigations in different genetic contexts and with other NV TRIDs, to gain a better understanding of potential mechanisms of action for improving treatment with NV molecules.

The final objective of this research was to assess the efficacy of NV TRIDs to rescue the effects of a recently discovered nonsense mutation in the *LRBA* gene (Lopez-Herrera G., *et al.,* 2012). This involved, evaluating the effectiveness of these compounds in a different disease influenced by a distinct genetic background.

For this purpose, primary human fibroblasts with the $LRBA^{R1683X/R1683X}$ mutations were treated with the three NV molecules.

The initial question was whether the treatment could affect cell growth, which was assessed after 0, 24, 48, and 72 hours of treatment. The results showed that NV848 did not negatively impact cell growth being similar to the untreated sample. However, NV930 and NV914, as well as the control with Ataluren (PTC124), resulted in a slight decrease in cell growth.

Subsequently, the assessment of LRBA mRNA levels revealed an increase after NV848 treatment, as well as observed in the CFTR study. To rule out the possibility that mRNA stabilization resulted from a change in the

stop codon, the region of interest in the mRNA was sequenced, and it was demonstrated that such changes did not occur.

Then, the LRBA protein expression was analysed after 72 hours of treatment with NVs and Ataluren (PTC124). Initially, the Western blot revealed that protein production was rescued under NVs treatment. Subsequently, the protein localization was examined, which indicated a recovery in the correct LRBA localization, primarily with NV848 and NV914 treatment.

Moreover, an indirect assessment of LRBA protein function rescue was conducted. Specifically, on the basis of the fact that the EGFR protein transport and localization have been shown to be linked to LRBA-associated vesicle-mediated transport, I aimed to determine EGFR localization as an indirect measure of LRBA functionality. Specifically, EGFR should not only be present in the plasma membrane, as this is associated with tumorigenic cell proliferation, but also in intracellular compartments (Tomas A., *et al.,* 2014). Through immunofluorescence analysis, it was observed that, in Hela cells, EGFR was perfectly localized only in the plasma membrane.

In contrast, under the NV848 treatment, EGFR was found in both plasma membranes and in the cytosol.

6 CONCLUSIONS

In conclusion, the *in vivo* safety assessment of NV TRIDs demonstrated their excellent tolerability, even at higher concentrations (2000 mg/Kg for NV914, 300 mg/Kg for NV848 and NV930). Moreover, this study suggests classifying NV molecules as low-risk compounds according to the GHS chemical classification.

The biodistribution analysis, with a specific focus on NV848, revealed the molecule's efficient targeting of key organs relevant to CF, including the lungs, pancreas, intestine, plasma, kidney, and even the brain, when administered at 60 mg/Kg. Furthermore, NV848 was rapidly metabolized, with most organs showing undetectable levels after just 2 hours, except for the kidney, where the compound became undetectable after 45 minutes. The assessment of NV848's efficacy in a murine CF nonsense model yielded significant results. It led to mRNA stabilization and increased protein production in over 50% of the mice treated with NV848 at 60 mg/Kg. While promising, further analyses involving more organs and subjects are required to establish statistical significance.

Following the *in vivo* phase of the project, the focus shifted to two *in vitro* models, one for CF and one for LRBA. In particular, 16HBEge $CFTR^{G542X}$ and $CFTR^{W1282X}$ cell lines were employed to evaluate NV848's potential to promote CFTR protein function rescue, using the Ussing chamber. NV848 treatment, either alone or in combination with NMDi and Trikafta, did not yield significant results for the G542X nonsense mutation. However, for the W1282X mutation, a slight activation and improvement in CFTR functionality were observed with NV848 treatment in combination.

For the LRBA protein investigation, all three NV molecules were used, successfully promoting LRBA protein rescue, with NV848 and NV914 exhibiting more efficient activities. Ultimately, NV848 treatment appeared to be the most effective TRID in restoring LRBA protein functionality, as demonstrated by the evaluation of EGFR as an indirect target of LRBA-associated vesicles.

7 SUPPLEMENTARY

7.1 Histopathological analysis scores in mice undergoing the toxicity study.

In this section, tables relative to the scores of the histopathological analyses are reported. These data report the specific indications and morphological features considered during the analyses of each organ of the mice subjected to the toxicity study (**Objective No.1, Results section**) (**Tables S 1 – 12**).

Tissue	Treatment	ID	Interstitial fibrosis (severity)	Interstitial fibrosis (extension)	Cardiomyocyte changes (severity)	Cardiomyocyte changes (extension)
Heart	NV 930	1	0	0	0	0
		2	0	0	0,13	0
		3	0	0	0	0
		4	0	0	0	0
		5	0	0	0	0
		6	0	0	0	0
	NV 848	7	0	0	0	0
		8	0	0	0	0
		9	0	0	0	0
		15	0	0	0	0,708
		16	0	0	0	0
		18	0	0	0	0
	PTC 124	10	0	0	0	0
		11	0	0	0	0
		12	0	0	0	0
		13	0	0	0	0
		25	0	0	0	0
		26	0	0	0	0
	NV 914	14	0	0	0	0
		17	0	0	0	0
		19	0	0	0	0
		20	0	0	0	0
		21	0	0	0	0
		22	0	0	0	0
	CTRLs	23	0	0	0	0
		24	0	0	0	0
		27	0	0	0	0
		28	0	0	0	0
		29	0	0	0	0
		30	0	0	0	0

Tissue	Treatment	ID	Interstitial cellularity increase (severity)	Interstitial cellularity increase (extension)	Interstitial inflammatory infiltration (severity)	Interstitial inflammatory infiltration (extension)
Lung	NV930	1	0	0	0	0
		2	0	0	0	0
		3	0	0	0	0
		4	0	0	0	0
		5	0	0	0	0
		6	0	0	0	0
	NV 848	7	0	0	0	0
		8	0	0	0	0
		9	0	0	0	0
		15	0	0	0	0
		16	0	0	0	0
		18	0	0	0	0
	PTC 124	10	0	0	0	0
		11	0	0	0	0
		12	0	0	0	0
		13	0	0	0	0
		25	0	0	0	0
		26	0	0	0	0
	NV 914	14	0	0	0	0
		17	0	0	0	0
		19	0	0	0	0
		20	0	0	0	0
		21	0	0	0	0
		22	0	0	0	0
	CTRLs	23	0	0	0	0
		24	0	0	0	0
		27	0	0	0	0
		28	0	0	0	0
		29	0	0	0	0
		30	0	0	0	0

Tissue	Treatment	ID	Lobular architectural disarray (severity)	Lobular architectural disarray (extension)	Periportal inflammatory infiltrate (severity)	Periportal inflammatory infiltrate (extension)	Centrolobular inflammatory infiltrate (severity)	Centrolobular inflammatory infiltrate (extension)	Necrosis (severity)	Necrosis (extension)	Sclerosis (severity)	Sclerosis (extension)
Liver	NV 930	1	0	0	0	0	0	0	0	0	0	0
		2	0	0	0	0	0	0	0	0	0	0
		3	0	0	0	0	0	0	0	0	0	0
		4	0	0	0	0	0	0	0	0	0	0
		5	0	0	0	0	0	0	0	0	0	0
		6	0	0	0	0	0	0	0	0	0	0
	NV 848	7	0	0	0	0	0	0	0	0	0	0
		8	0	0	0	0	0	0	0	0	0	0
		9	0	0	0	0	0	0	0	0	0	0
		15	0	0	0	0	0	0	0	0	0	0
		16	0	0	0	0	0	0	0	0	0	0
		18	0	0	0	0	0	0	0	0	0	0
	PTC 124	10	0	0	0	0	0	0	0	0	0	0
		11	0	0	0	0	0	0	0	0	0	0
		12	0	0	0	0	0	0	0	0	0	0
		1	0	0	0	0	0	0	0	0	0	0
		25	0	0	0	0	0	0	0	0	0	0
		26	0	0	0	0	0	0	0	0	0	0
	NV 914	14	0	0	0	0	0	0	0	0	0	0
		17	0	0	0	0	0	0	0	0	0	0
		19	0	0	0	0	0	0	0	0	0	0
		20	0	0	0	0	0	0	0	0	0	0
		21	0	0	0	0	0	0	0	0	0	0
		22	0	0	0	0	0	0	0	0	0	0
	CTRLs	23	0	0	0	0	0	0	0	0	0	0
		24	0	0	0	0	0	0	0	0	0	0
		27	0	0	0	0	0	0	0	0	0	0
		28	0	0	0	0	0	0	0	0	0	0
		29	0	0	0	0	0	0	0	0	0	0
		30	0	0	0	0	0	0	0	0	0	0

Tissue	Treatment	ID	White pulp effacement (severity)	White pulp effacement (extension)	Red pulp hyperplasia (severity)	Red pulp hyperplasia (extension)	Myeloid/erythroid precursor increase (severity)	Myeloid/erythroid precursor increase (extension)	Megakaryocyte hyperplasia and clustering (severity)	Megakaryocyte hyperplasia and clustering (extension)
Spleen	NV 930	1	0	0	0	0	0	0	0	0
		2	0	0	0	0	0	0	0	0
		3	0	0	0	0	0	0	0	0
		4	0	0	0	0	0	0	0	0
		5	0	0	0	0	0	0	0	0
		6	0	0	0	0	0	0	0	0
	NV 848	7	0	0	0	0	0	0	0	0
		8	0	0	0	0	0	0	0	0
		9	0	0	0	0	0	0	0	0
		15	0	0	0	0	0	0	0	0
		16	0	0	0	0	0	0	0	0
		18	0	0	0	0	0	0	0	0
	PTC 124	10	0	0	0	0	0	0	0	0
		11	0	0	0	0	0	0	0	0
		12	0	0	0	0	0	0	0	0
		13	0	0	0	0	0	0	0	0
		25	0	0	0	0	0	0	0	0
		26	0	0	0	0	0	0	0	0
	NV 914	14	0	0	0	0	0	0	0	0
		17	0	0	0	0	0	0	0	0
		19	0	0	0	0	0	0	0	0
		20	0	0	0	0	0	0	0	0
		21	0	0	0	0	0	0	0	0
		22	0	0	0	0	0	0	0	0
	CTRLs	23	0	0	0	0	0	0	0	0
		24	0	0	0	0	0	0	0	0
		27	0	0	0	0	0	0	0	0
		28	0	0	0	0	0	0	0	0
		29	0	0	0	0	0	0	0	0
		30	0	0	0	0	0	0	0	0

Tissue	Treatment	ID	Loss of acinar tissue (severity)	Loss of acinar tissue (extension)	Duct changes loss of acinar cells (severity)	Duct changes loss of acinar cells (extension)	Periductal inflammatory infiltrate (severity)	Periductal inflammatory infiltrate (extension)	Fibrosis (severity)	Fibrosis (extension)	Preservation of islets (severity)	Preservation of islets (extension)
Pancreas	NV 930	1	0	0	0	0	0	0	0	0	0	0
		2	0	0	0	0	0	0	0	0	0	0
		3	0	0	0	0	0	0	0	0	0	0
		4	0	0	0	0	0	0	0	0	0	0
		5	0	0	0	0	0	0	0	0	0	0
		6	0	0	0	0	0	0	0	0	0	0
	NV 848	7	0	0	0	0	0	0	0	0	0	0
		8	0	0	0	0	0	0	0	0	0	0
		9	0	0	0	0	0	0	0	0	0	0
		15	0	0	0	0	0	0	0	0	0	0
		16	0	0	0	0	0	0	0	0	0	0
		18	0	0	0	0	0	0	0	0	0	0
	PTC 124	10	0	0	0	0	0	0	0	0	0	0
		11	0	0	0	0	0	0	0	0	0	0
		12	0	0	0	0	0	0	0	0	0	0
		13	0	0	0	0	0	0	0	0	0	0
		25	0	0	0	0	0	0	0	0	0	0
		26	0	0	0	0	0	0	0	0	0	0
	NV 914	14	0	0	0	0	0	0	0	0	0	0
		17	0	0	0	0	0	0	0	0	0	0
		19	0	0	0	0	0	0	0	0	0	0
		20	0	0	0	0	0	0	0	0	0	0
		21	0	0	0	0	0	0	0	0	0	0
		22	0	0	0	0	0	0	0	0	0	0
	CTRLs	23	0	0	0	0	0	0	0	0	0	0
		24	0	0	0	0	0	0	0	0	0	0
		27	0	0	0	0	0	0	0	0	0	0
		28	0	0	0	0	0	0	0	0	0	0
		29	0	0	0	0	0	0	0	0	0	0
		30	0	0	0	0	0	0	0	0	0	0

Tissue	Treatment	ID	Tubular damages (severity)	Tubular damages (extension)	Glomerular alterations (severity)	Glomerular alterations (extension)	Vascular congestion (severity)	Vascular congestion (extension)	Glomerulosclerosis (severity)	Glomerulosclerosis (extension)	Interstitial fibrosis (severity)	Interstitial fibrosis (extension)	Arteriolar hyalinosis (severity)	Arteriolar hyalinosis (extension)
Kidney	NV 930	1	0	0	0	0	0	0	0	0	0	0	0	0
		2	0	0	0	0	0	0	0	0	0	0	0	0
		3	0	0	0	0	0	0	0	0	0	0	0	0
		4	0	0	0	0	0	0	0	0	0	0	0	0
		5	0	0	0	0	0	0	0	0	0	0	0	0
		6	0	0	0	0	0	0	0	0	0	0	0	0
	NV 848	7	0	0	0	0	0	0	0	0	0	0	0	0
		8	0	0	0	0	0	0	0	0	0	0	0	0
		9	0	0	0	0	0	0	0	0	0	0	0	0
		15	0	0	0	0	0	0	0	0	0	0	0	0
		16	0	0	0	0	0	0	0	0	0	0	0	0
		18	0	0	0	0	0	0	0	0	0	0	0	0
	PTC 124	10	0	0	0	0	0	0	0	0	0	0	0	0
		11	0	0	0	0	0	0	0	0	0	0	0	0
		12	0	0	0	0	0	0	0	0	0	0	0	0
		13	0	0	0	0	0	0	0	0	0	0	0	0
		25	0	0	0	0	0	0	0	0	0	0	0	0
		26	0	0	0	0	0	0	0	0	0	0	0	0
	NV 914	14	0	0	0	0	0	0	0	0	0	0	0	0
		17	0	0	0	0	0	0	0	0	0	0	0	0
		19	0	0	0	0	0	0	0	0	0	0	0	0
		20	0	0	0	0	0	0	0	0	0	0	0	0
		21	0	0	0	0	0	0	0	0	0	0	0	0
		22	0	0	0	0	0	0	0	0	0	0	0	0
	CTRLs	23	0	0	0	0	0	0	0	0	0	0	0	0
		24	0	0	0	0	0	0	0	0	0	0	0	0
		27	0	0	0	0	0	0	0	0	0	0	0	0
		28	0	0	0	0	0	0	0	0	0	0	0	0
		29	0	0	0	0	0	0	0	0	0	0	0	0
		30	0	0	0	0	0	0	0	0	0	0	0	0

Tissue	Treatment	ID	Cryptitis (severity)	Cryptitis (extension)	Chorion inflammatory infiltration (severity)	Chorion inflammatory infiltration (extension)	Suppression of mucosecretory activity (severity)	Suppression of mucosecretory activity (extension)	Regenerative/displastic alterations (severity)	Regenerative/displastic alterations (extension)	Glandular atrophy (severity)	Glandular atrophy (extension)
Large Intestine	NV 930	1	0	0	0	0	0	0	0	0	0	0
		2	0	0	0	0	0	0	0	0	0	0
		3	0	0	0	0	0	0	0	0	0	0
		4	0	0	0	0	0	0	0	0	0	0
		5	0	0	0	0	0	0	0	0	0	0
		6	0	0	0	0	0	0	0	0	0	0
	NV 848	7	0	0	0	0	0	0	0	0	0	0
		8	0	0	0	0	0	0	0	0	0	0
		9	0	0	0	0	0	0	0	0	0	0
		15	0	0	0	0	0	0	0	0	0	0
		16	0	0	0	0	0	0	0	0	0	0
		18	0	0	0	0	0	0	0	0	0	0
	PTC 124	10	0	0	0	0	0	0	0	0	0	0
		11	0	0	0	0	0	0	0	0	0	0
		12	0	0	0	0	0	0	0	0	0	0
		13	0	0	0	0	0	0	0	0	0	0
		25	0	0	0	0	0	0	0	0	0	0
		26	0	0	0	0	0	0	0	0	0	0
	NV 914	14	0	0	0	0	0	0	0	0	0	0
		17	0	0	0	0	0	0	0	0	0	0
		19	0	0	0	0	0	0	0	0	0	0
		20	0	0	0	0	0	0	0	0	0	0
		21	0	0	0	0	0	0	0	0	0	0
		22	0	0	0	0	0	0	0	0	0	0
	CTRLs	23	0	0	0	0	0	0	0	0	0	0
		24	0	0	0	0	0	0	0	0	0	0
		27	0	0	0	0	0	0	0	0	0	0
		28	0	0	0	0	0	0	0	0	0	0
		29	0	0	0	0	0	0	0	0	0	0
		30	0	0	0	0	0	0	0	0	0	0

Tissue	Treatment	ID	Villi atrophy (severity)	Villi atrophy (extension)	Crypts hyperplasia (severity)	Crypts hyperplasia (extension)	Regenerative/displastic alterations (severity)	Regenerative/displastic alterations (extension)	Inflammatory infiltration (severity)	Inflammatory infiltration (extension)	Cryptitis (severity)	Cryptitis (extension)
Small Intestine	NV 930	1	0	0	0	0	0	0	0	0	0	0
		2	0	0	0	0	0	0	0	0	0	0
		3	0	0	0	0	0	0	0	0	0	0
		4	0	0	0	0	0	0	0	0	0	0
		5	0	0	0	0	0	0	0	0	0	0
		6	0	0	0	0	0	0	0	0	0	0
	NV 848	7	0	0	0	0	0	0	0	0	0	0
		8	0	0	0	0	0	0	0	0	0	0
		9	0	0	0	0	0	0	0	0	0	0
		15	0	0	0	0	0	0	0	0	0	0
		16	0	0	0	0	0	0	0	0	0	0
		18	0	0	0	0	0	0	0	0	0	0
	PTC 124	10	0	0	0	0	0	0	0	0	0	0
		11	0	0	0	0	0	0	0	0	0	0
		12	0	0	0	0	0	0	0	0	0	0
		13	0	0	0	0	0	0	0	0	0	0
		25	0	0	0	0	0	0	0	0	0	0
		26	0	0	0	0	0	0	0	0	0	0
	NV 914	14	0	0	0	0	0	0	0	0	0	0
		17	0	0	0	0	0	0	0	0	0	0
		19	0	0	0	0	0	0	0	0	0	0
		20	0	0	0	0	0	0	0	0	0	0
		21	0	0	0	0	0	0	0	0	0	0
		22	0	0	0	0	0	0	0	0	0	0
	CTRL	23	0	0	0	0	0	0	0	0	0	0
		24	0	0	0	0	0	0	0	0	0	0
		27	0	0	0	0	0	0	0	0	0	0
		28	0	0	0	0	0	0	0	0	0	0
		29	0	0	0	0	0	0	0	0	0	0
		30	0	0	0	0	0	0	0	0	0	0

Tissue	Treatment	ID	Erythroid colonies expansion (severity)	Erythroid colonies expansion (extension)	Myeloid cells expansion (segmented) (severity)	Myeloid cells expansion (segmented) (extension)	Myeloid cells expansion (immature) (severity)	Myeloid cells expansion (immature) (extension)	Megakaryocyte clustering (severity)	Megakaryocyte clustering (extension)	Megakaryocyte pleiomorphism (severity)	Megakaryocyte clustering (extension)	Erythro/Hemophagocytosis (severity)	Erythro/Hemophagocytosis (extension)
Bone Marrow	NV930	1	0	0	0	0	0	0	0	0	0	0	0	0
		2	0	0	0	0	0	0	0	0	0	0	0	0
		3	0	0	0	0	0	0	0	0	0	0	0	0
		4	0	0	0	0	0	0	0	0	0	0	0	0
		5	0	0	0	0	0	0	0	0	0	0	0	0
		6	0	0	0	0	0	0	0	0	0	0	0	0
	NV848	7	0	0	0	0	0	0	0	0	0	0	0	0
		8	0	0	0	0	0	0	0	0	0	0	0	0
		9	0	0	0	0	0	0	0	0	0	0	0	0
		15	0	0	0	0	0	0	0	0	0	0	0	0
		16	0	0	0	0	0	0	0	0	0	0	0	0
		18	0	0	0	0	0	0	0	0	0	0	0	0
	PTC 124	10	1	2	0	0	1	2	0	0	0	0	0	0
		11	1	2	0	0	1	2	0	0	0	0	0	0
		12	0	0	0	0	0	0	0	0	0	0	0	0
		13	0	0	0	0	0	0	0	0	0	0	0	0
		25	0	0	0	0	0	0	0	0	0	0	0	0
		26	0	0	0	0	0	0	0	0	0	0	0	0
	NV914	14	0	0	0	0	0	0	0	0	0	0	0	0
		17	0	0	0	0	0	0	0	0	0	0	0	0
		19	0	0	0	0	0	0	0	0	0	0	0	0
		20	0	0	0	0	0	0	0	0	0	0	0	0
		21	1	2	0	0	1	2	0	0	0	0	0	0
		22	1	2	0	0	1	2	0	0	0	0	0	0
	CTRL	23	0	0	0	0	0	0	0	0	0	0	0	0
		24	0	0	0	0	0	0	0	0	0	0	0	0
		27	0	0	0	0	0	0	0	0	0	0	0	0
		28	0	0	0	0	0	0	0	0	0	0	0	0
		29	0	0	0	0	0	0	0	0	0	0	0	0
		30	0	0	0	0	0	0	0	0	0	0	0	0

Tissue	Treatment	ID	Cortical necrosis (severity)	Cortical necrosis (extension)	Intracerebral hemorrhage (severity)	Intracerebral hemorrhage (extension)	Neuronal degeneration edema (severity)	Neuronal degeneration edema (extension)	Inflammatory response (severity)	Inflammatory response (extension)
Brain	NV 930	1	0	0	0	0	0	0	0	0
		2	0	0	0	0	0	0	0	0
		3	0	0	0	0	0	0	0	0
		4	0	0	0	0	0	0	0	0
		5	0	0	0	0	0	0	0	0
		6	0	0	0	0	0	0	0	0
	NV 848	7	0	0	0	0	0	0	0	0
		8	0	0	0	0	0	0	0	0
		9	0	0	0	0	0	0	0	0
		15	0	0	0	0	0	0	0	0
		16	0	0	0	0	0	0	0	0
		18	0	0	0	0	0	0	0	0
	PTC 124	10	0	0	0	0	0	0	0	0
		11	0	0	0	0	0	0	0	0
		12	0	0	0	0	0	0	0	0
		13	0	0	0	0	0	0	0	0
		25	0	0	0	0	0	0	0	0
		26	0	0	0	0	0	0	0	0
	NV 914	14	0	0	0	0	0	0	0	0
		17	0	0	0	0	0	0	0	0
		19	0	0	0	0	0	0	0	0
		20	0	0	0	0	0	0	0	0
		21	0	0	0	0	0	0	0	0
		22	0	0	0	0	0	0	0	0
	CTRL	23	0	0	0	0	0	0	0	0
		24	0	0	0	0	0	0	0	0
		27	0	0	0	0	0	0	0	0
		28	0	0	0	0	0	0	0	0
		29	0	0	0	0	0	0	0	0
		30	0	0	0	0	0	0	0	0

Tissue	Treatment	ID	Maturation defects (severity)	Maturation defects (extension)	Inflammatory infiltrate (severity)	Inflammatory infiltrate (extension)	Fibrosis (severity)	Fibrosis (extension)	Necrosis (severity)	Necrosis (extension)
Ovary	NV 930	1	0	0	0	0	0	0	0	0
		2	0	0	0	0	0	0	0	0
		3	0	0	0	0	0	0	0	0
	NV 848	7	0	0	0	0	0	0	0	0
		8	0	0	0	0	0	0	0	0
		16	0	0	0	0	0	0	0	0
	PTC 124	10	0	0	0	0	0	0	0	0
		11	0	0	0	0	0	0	0	0
		26	0	0	0	0	0	0	0	0
	NV 914	17	0	0	0	0	0	0	0	0
		21	0	0	0	0	0	0	0	0
		22	0	0	0	0	0	0	0	0
	CTRL	24	0	0	0	0	0	0	0	0
		28	0	0	0	0	0	0	0	0
		30	0	0	0	0	0	0	0	0

Tissue	Treatment	ID	Maturation defects (severity)	Maturation defects (extension)	Apoptosis figures (severity)	Apoptosis figures (extension)	Sertoli cells alterations (severity)	Sertoli cells alterations (extension)	Necrosis (severity)	Necrosis (extension)
Testis	NV 930	4	0	0	0	0	0	0	0	0
		5	0	0	0	0	0	0	0	0
		6	0	0	0	0	0	0	0	0
	NV 848	9	0	0	0	0	0	0	0	0
		15	0	0	0	0	0	0	0	0
		18	0	0	0	0	0	0	0	0
	PTC 124	12	0	0	0	0	0	0	0	0
		13	0	0	0	0	0	0	0	0
		25	0	0	0	0	0	0	0	0
	NV 914	14	0	0	0	0	0	0	0	0
		19	0	0	0	0	0	0	0	0
		20	0	0	0	0	0	0	0	0
	CTRL	23	0	0	0	0	0	0	0	0
		27	0	0	0	0	0	0	0	0
		29	0	0	0	0	0	0	0	0

Figures S1 – 12. *In these tables are reported the detailed scores individuated and registered during histopathological analyses on tissues derived from the toxicity study. The organs analysed were the heart, lung, liver, spleen, pancreas, kidney, large intestine, small intestine, bone marrow, brain, ovary, and testis (Corrao F., et al., 2022).*

7.2 NGS analyses for the evaluation of NV848 treatment safety towards the integrity of the mRNA sequence.

The following panel illustrates the results obtained by the NGS analyses of the cDNA sequences.

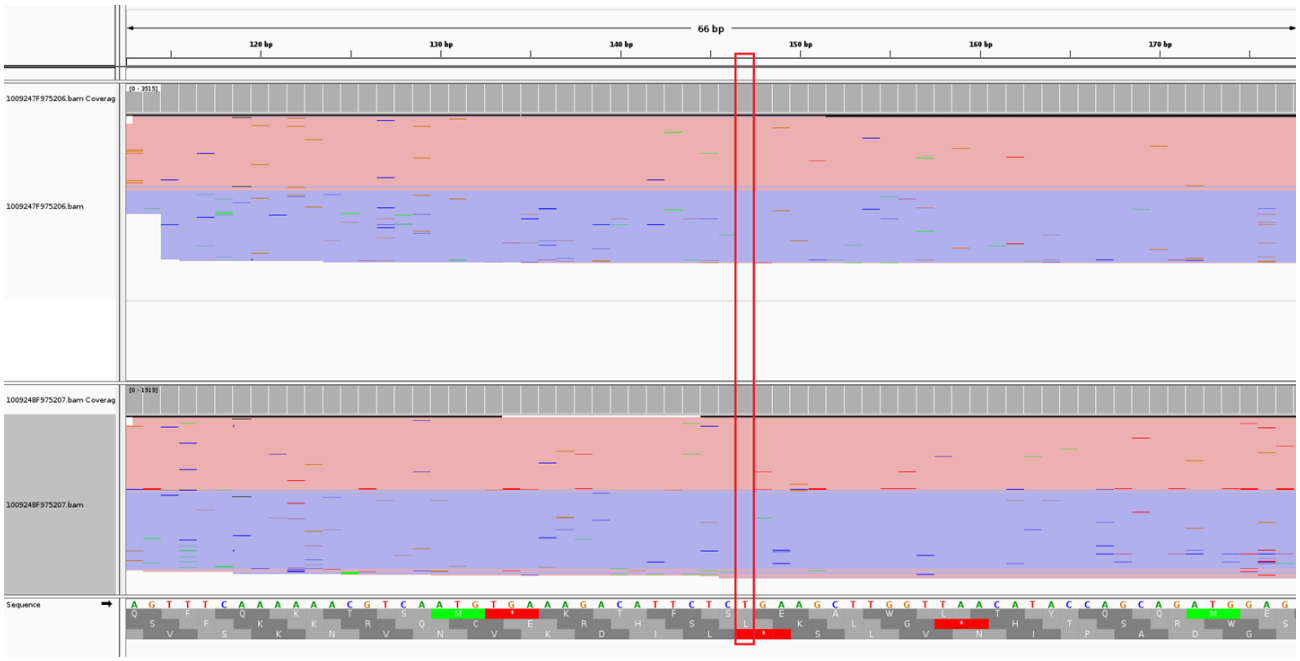

Figure S 1. *This figure shows the comparison between the reads obtained by NGS sequencing in the untreated (up) and NV848-treated (down) samples. In the red rectangle is evidenced the position (5047) of the nucleotide to check, which is a T in the reference sequence.*

7.3 Ussing chamber curves on 16HBE CFTR^{G542X} and CFTR^{W1282X} cell lines.

Following are reported all the registrations of the triplicates (16HBEge CFTR^{G542X}) and of the duplicates (16HBEge CFTR^{W1282X}) made by Ussing chamber experiments for the evaluation of CFTR functionality activity after NV848 TRID and Geneticin (G418) treatment.

7.3.1 Curves of the 16HBEge CFTR$^{G542X.}$

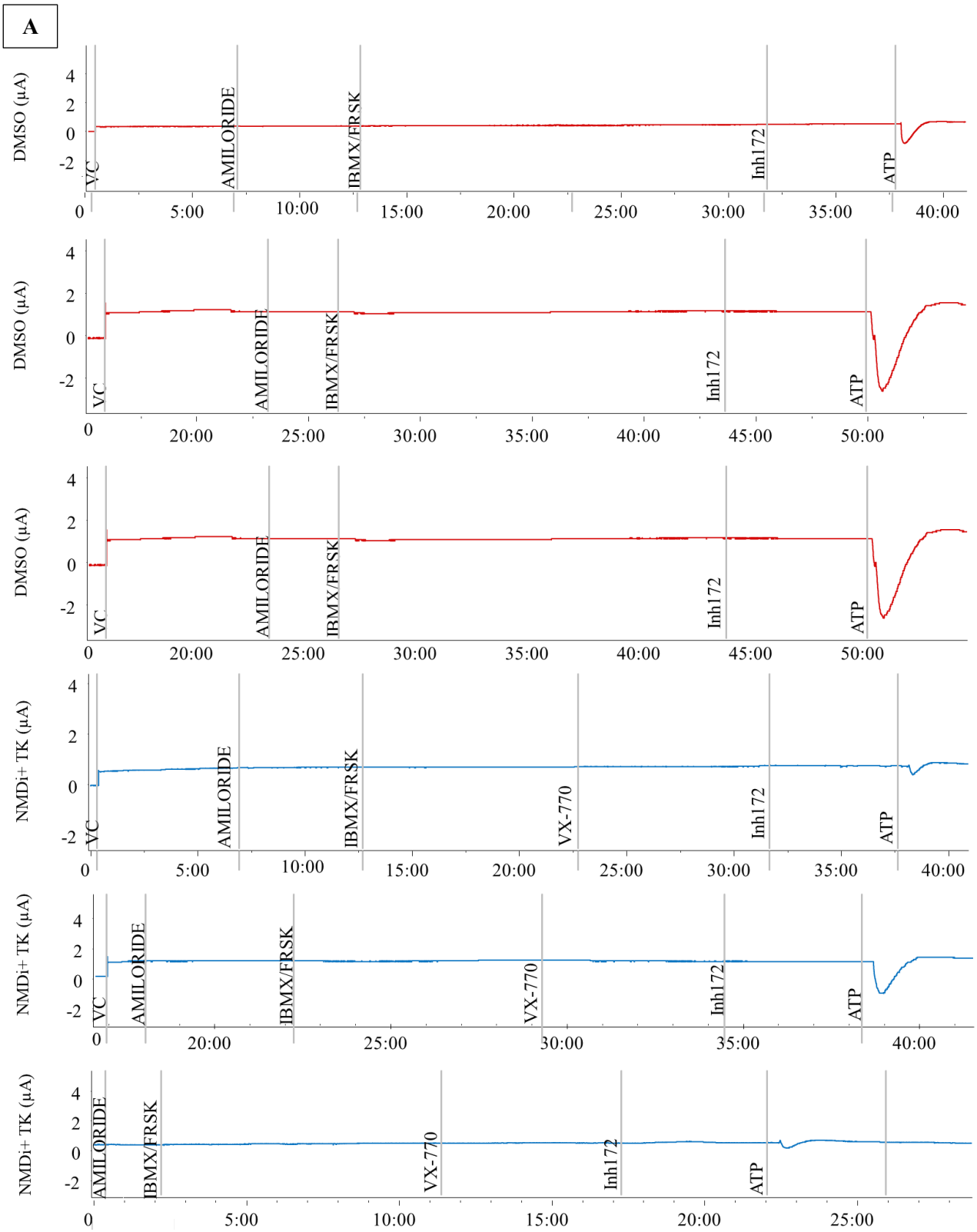

B

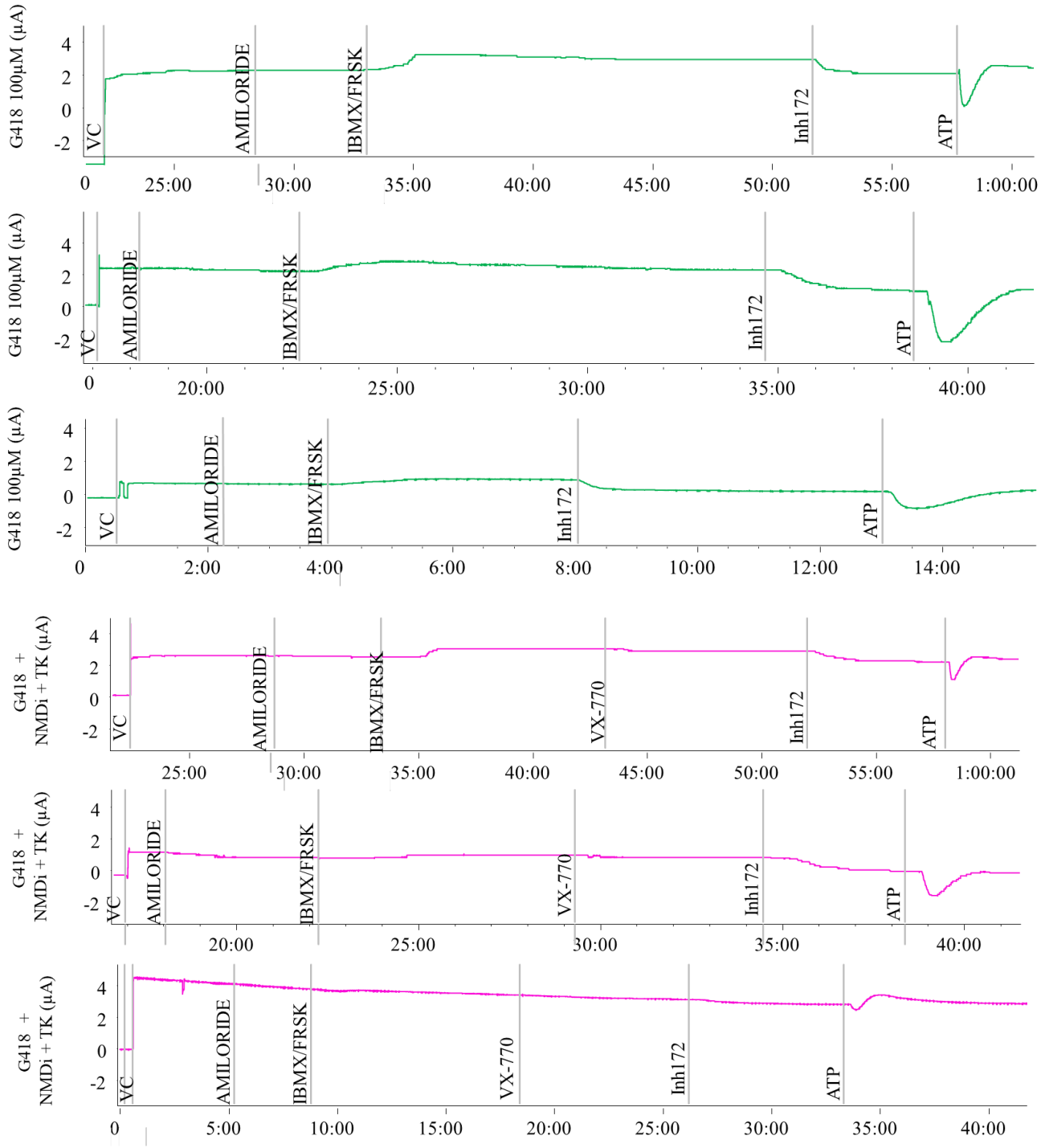
G418 100µM (µA)
VC
AMILORIDE
IBMX/FRSK
Inh172
ATP
G418 + NMDi + TK (µA)
VX-770

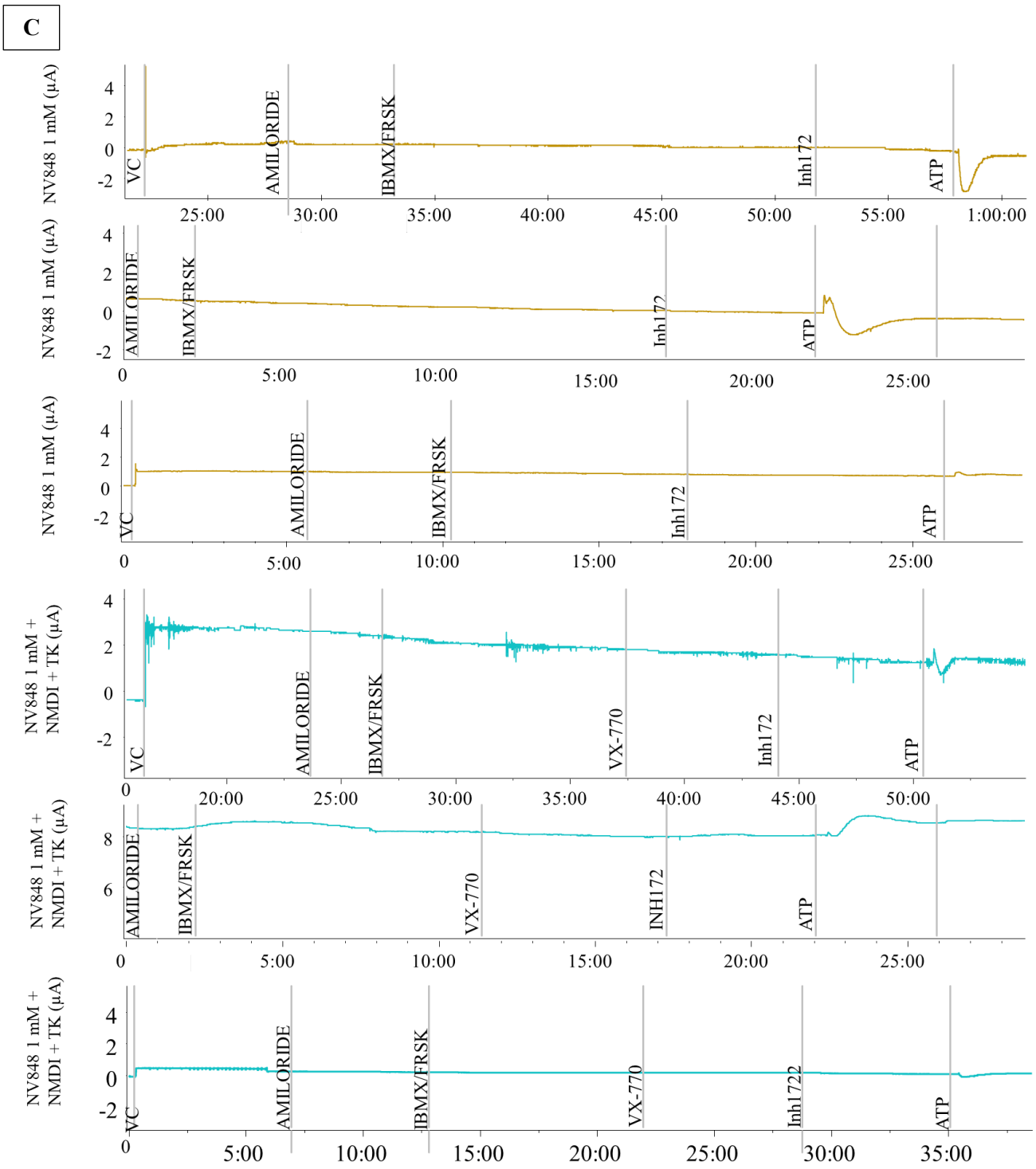

Figure S 2. *These images show the measurements of the Isc relative to the chloride current after different treatments. Precisely, in* ***A)*** *the curves of DMSO, and NMDi + TK; in* ***B)*** *Geneticin (G418), and Geneticin (G418) + NMDi + TK; in* ***C)*** *NV848 + NMDi + TK. Registrations were made using LabChart8 Readers software (ADInstruments).*

7.3.2 *Curves of the 16HBEge CFTR$^{W1282X.}$*

A

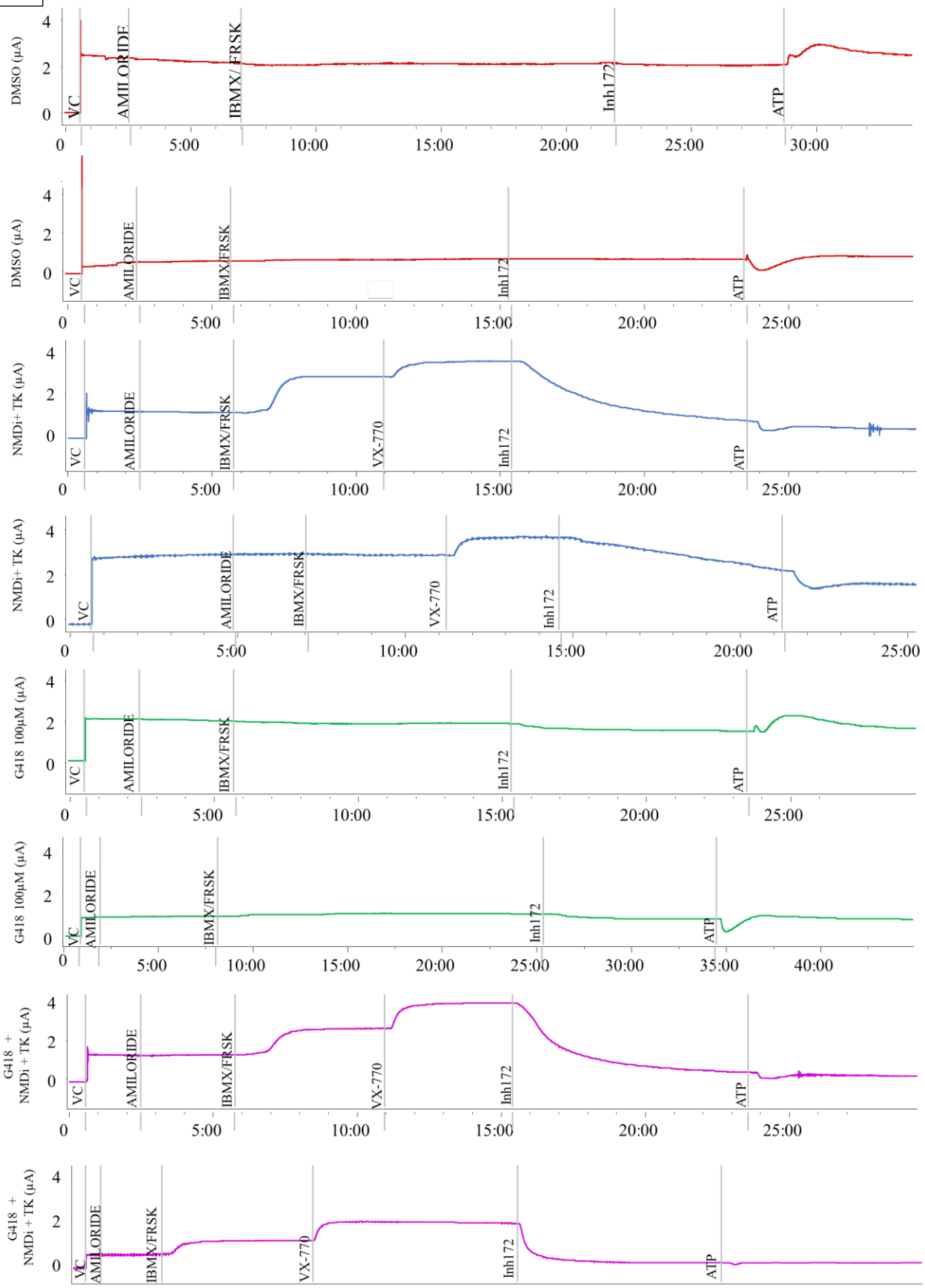

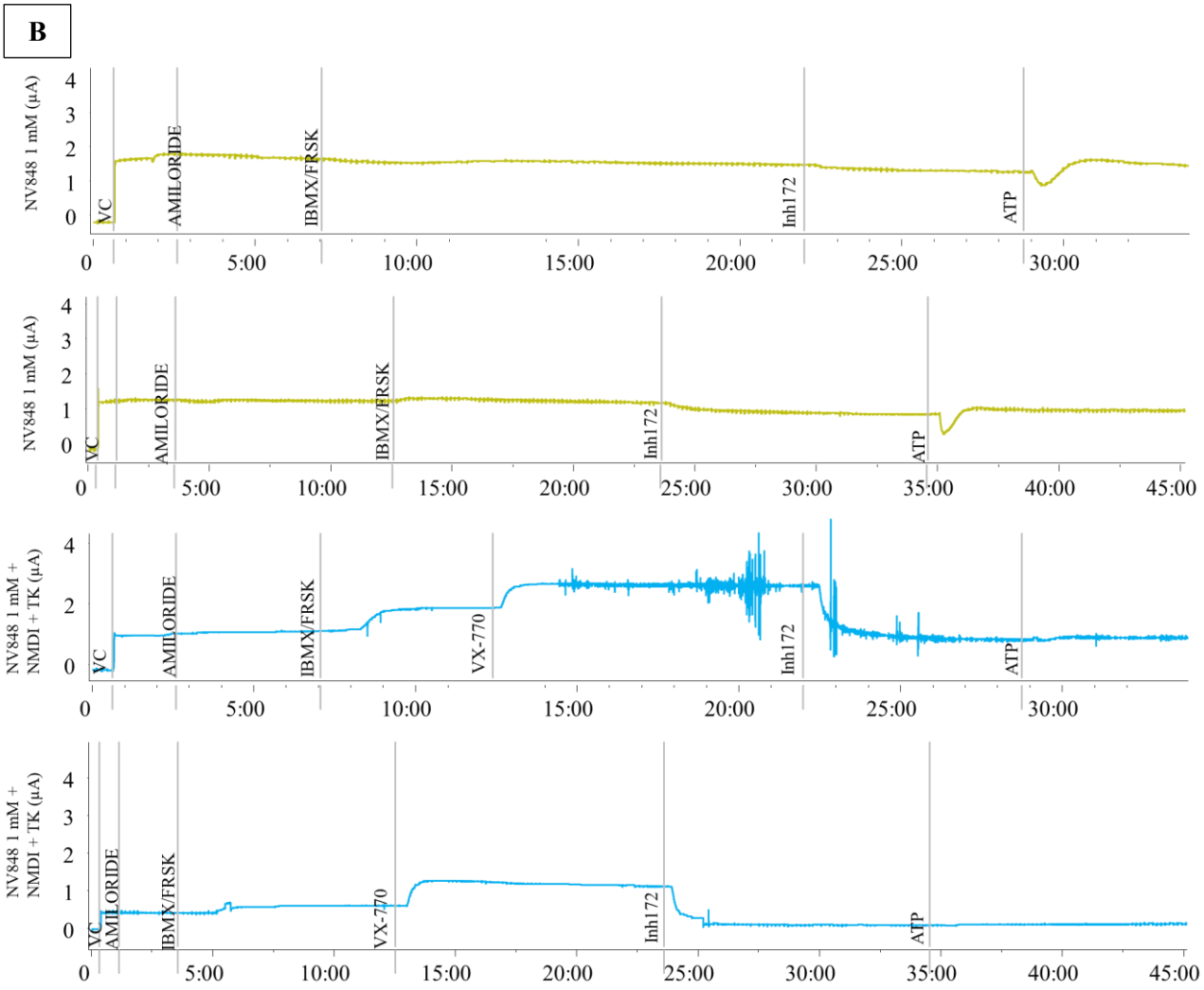

Figure S 3. *These images show the registration of the Isc relative to the chloride current after different treatments. Precisely, in* ***A)*** *the curves of DMSO, and NMDi + TK, Geneticin (G418), and Geneticin (G418) + NMDi + TK; in* ***B)*** *NV848 + NMDi + TK. Registrations were made using LabChart8 Readers software (ADInstruments).*

8 ACKNOWLEDGMENTS

I would like to express my gratitude to my tutor, Professor Laura Lentini, and my co-tutor, Professor Maria Grazia Zizzo, for having supervised, supported, and guided me during the development of this project. Moreover, they have had an important role as professional and personal mentors, giving me the possibility to growth and learn more than I could have imagined or thought.

I would also thank Professors Raffaella Melfi and Ivana Pibiri, for believing in me and making my problems easier with their help and advice. In addition, they have relieved my days with their smiles and their positive attitude.

These four amazing women are my "Scientific Mums", as I name them.

My heartfelt thank goes to Dr. Fabrizio Di Pietra and Dr. Gaetano Felice Caldara, who have trained me with patience during procedure development and the experimentations. Their kind behaviour impressed me, and I will never forget the moments spent with them.

I would also thank Professor Claudio Tripodo and his research group (PROMISE, Unipa) for their collaboration and help with the histological analyses. In the same manner, MSc, PhD Francesco Genovese (ASP Palermo) was an important resource and help for immunohistochemistry analyses.

I wish to acknowledge all the PhD students, researcher, and Professors of the laboratory staff, because I cannot imagine other people with whom I would share my days, my ups and downs.

Every day is a good day for celebrating and being happy with them: Professor Aldo Di Leonardo, who was a guide also during my bachelor's and master's degrees; Professor Viviana Barra and Dr. Pier Salvo Carollo, who share with me the love for Paris and for France, but they represent for me a victory in this life and in this path, with their kindness, happiness and positive way of facing life; Simona Titoli and Serena Gargano, the twins of the lab, who are also good and special companies during lunch and celebrations; Salvatore Martino, always gentle, educated, and ready to help, no matter what.

A very special thank goes to three very important colleagues and friends: Emanuele Vitale, a respectful student, which is like a "scientific son for me" and a special colleague and help, like a little brother; Davide Ricci, who is fuel for this team, with his ideas, energy, and a little bit of craziness, he seems to be me if I was a man; Ignazio Fiduccia, we are so different but sometimes also so similar, knowing that we can trust each other, which is a fundamental feature.

I would like to warmly thank the guys in "the other side of the moon", Cesare D'amico, Fabiola Vaglica, Emanuela Peri, and Sefora Marino, for supporting each other and always finding a reason to smile and make me smile. Nevertheless, Adele Cicio was always available, no matter what, or why, or when, and I sincerely thank her for helping me every time I needed.

Last but not least, the University gave me the opportunity to meet special people in the Chemistry Department: Laura and Natale, who were able to "read" me, without saying a word, just a hug.

And now, we move to my personal side.

I would like to show my gratitude to my parents, who have believed in my choices, every day, and supported me even when I was the worst daughter on Earth. They have spent their life educating me and my brother and they sacrificed themself for us, which is not expected, nowadays.
I would like to recognize the importance of a person whom I don't mention often: my brother. We are like two faces of the same medal, so different, but still the same. I would like to say sorry if I have been unkind to you, because you are the best brother everyone could have.
I would also thank two amazing women with are like sisters to me: Maria, my cousin, and Giusy, one of my best friends. Every word I could spend for you would not be enough, so I just say, "thank you, with all of my heart".
I wish to recognize the relevance of my best friends, THE GIRLS, everyone with a special characteristic, but altogether we are like magic: Fede, J, Ire, Guendi, Ambra e Gogi.
In the end, I was not so sure of writing about him. These last months were the most difficult of my life, and I learned that you were always there for me, even if I could not see you. You know me, you will still learn to know me, and the same I will do with you. We are growing together, appreciating each other, and you support me with no limits, and also with my craziness. Thank you for being with me, at my side in these three and half years, pushing me to never give up.
All these people, together, were the light when I was in darkness.

9 BIBLIOGRAPHY

1. Goetz, L. H., & Schork, N. J. (2018). Personalized medicine: motivation, challenges, and progress. Fertility and sterility, 109(6), 952–963. https://doi.org/10.1016/j.fertnstert.2018.05.006.
2. König, I. R., Fuchs, O., Hansen, G., von Mutius, E., & Kopp, M. V. (2017). What is precision medicine?. The European respiratory journal, 50(4), 1700391. https://doi.org/10.1183/13993003.00391-2017.
3. Barry, P. J., Mall, M. A., Polineni, D., & VX18-445-104 Study Group (2021). Triple Therapy for Cystic Fibrosis Phe508del-Gating and -Residual Function Genotypes. Reply. The New England journal of medicine, 385(23), 2208. https://doi.org/10.1056/NEJMc2115966.
4. Mort, M., Ivanov, D., Cooper, D. N., & Chuzhanova, N. A. (2008). A meta-analysis of nonsense mutations causing human genetic disease. Human mutation, 29(8), 1037–1047. https://doi.org/10.1002/humu.20763.
5. Ghelfi, M. D., Bhat, S. Y., Li, H., & Cooperman, B. S. (2023). A High-Throughput Assay for In Vitro Determination of Release Factor-Dependent Peptide Release from a Pretermination Complex by Fluorescence Anisotropy-Application to Nonsense Suppressor Screening and Mechanistic Studies. Biomolecules, 13(2), 242. https://doi.org/10.3390/biom13020242.
6. Schaefer, E., Mehta, A., & Gal, A. (2005). Genotype and phenotype in Fabry disease: analysis of the Fabry Outcome Survey. Acta paediatrica (Oslo, Norway : 1992). Supplement, 94(447), 87–79. https://doi.org/10.1111/j.1651-2227.2005.tb02119.x.
7. Wilschanski M. (2012). Class 1 CF Mutations. Frontiers in pharmacology, 3, 117. https://doi.org/10.3389/fphar.2012.00117.
8. Lopez-Herrera, G., Tampella, G., Pan-Hammarström, Q., Herholz, P., Trujillo-Vargas, C. M., Phadwal, K., Simon, A. K., Moutschen, M., Etzioni, A., Mory, A., Srugo, I., Melamed, D., Hultenby, K., Liu, C., Baronio, M., Vitali, M., Philippet, P., Dideberg, V., Aghamohammadi, A., Rezaei, N., … Grimbacher, B. (2012). Deleterious mutations in LRBA are associated with a syndrome of immune deficiency and autoimmunity. American journal of human genetics, 90(6), 986–1001. https://doi.org/10.1016/j.ajhg.2012.04.015.
9. Bladen, C. L., Salgado, D., Monges, S., Foncuberta, M. E., Kekou, K., Kosma, K., Dawkins, H., Lamont, L., Roy, A. J., Chamova, T., Guergueltcheva, V., Chan, S., Korngut, L., Campbell, C., Dai, Y., Wang, J., Barišić, N., Brabec, P., Lahdetie, J., Walter, M. C., … Lochmüller, H. (2015). The TREAT-NMD DMD Global Database: analysis of more than 7,000 Duchenne muscular dystrophy mutations. Human mutation, 36(4), 395–402. https://doi.org/10.1002/humu.22758.
10. Imani, S., Ijaz, I., Shasaltaneh, M. D., Fu, S., Cheng, J., & Fu, J. (2018). Molecular genetics characterization and homology modeling of the CHM gene mutation: A study on its association with choroideremia. Mutation research. Reviews in mutation research, 775, 39–50. https://doi.org/10.1016/j.mrrev.2018.02.001.

11. Neri, M., Rossi, R., Trabanelli, C., Mauro, A., Selvatici, R., Falzarano, M. S., Spedicato, N., Margutti, A., Rimessi, P., Fortunato, F., Fabris, M., Gualandi, F., Comi, G., Tedeschi, S., Seia, M., Fiorillo, C., Traverso, M., Bruno, C., Giardina, E., Piemontese, M. R., … Ferlini, A. (2020). The Genetic Landscape of Dystrophin Mutations in Italy: A Nationwide Study. Frontiers in genetics, 11, 131. https://doi.org/10.3389/fgene.2020.00131.
12. Zhang, M., Yang, D., & Gold, B. (2021). Origins of nonsense mutations in human tumor suppressor genes. Mutation research, 823, 111761. https://doi.org/10.1016/j.mrfmmm.2021.111761.
13. de Valles-Ibáñez, G., Esteve-Solé, A., Piquer, M., González-Navarro, E. A., Hernandez-Rodriguez, J., Laayouni, H., González-Roca, E., Plaza-Martin, A. M., Deyà-Martínez, Á., Martín-Nalda, A., Martínez-Gallo, M., García-Prat, M., Del Pino-Molina, L., Cuscó, I., Codina-Solà, M., Batlle-Masó, L., Solís-Moruno, M., Marquès-Bonet, T., Bosch, E., López-Granados, E., … Casals, F. (2018). Evaluating the Genetics of Common Variable Immunodeficiency: Monogenetic Model and Beyond. Frontiers in immunology, 9, 636. https://doi.org/10.3389/fimmu.2018.00636.
14. Elborn J. S. (2016). Cystic fibrosis. Lancet (London, England), 388(10059), 2519–2531. https://doi.org/10.1016/S0140-6736(16)00576-6.
15. Campagna, G., Amato, A., Majo, F., Ferrari, G., Quattrucci, S., Padoan, R., Floridia, G., Salvatore, D., Carnovale, V., Puppo Fornaro, G., Taruscio, D., Salvatore, M., & Gruppo di lavoro RIFC (2022). Registro italiano Fibrosi Cistica (RIFC). Rapporto 2019-2020 [Italian Cystic Fibrosis Registry (ICFR). Report 2019-2020]. Epidemiologia e prevenzione, 46(4 Suppl 2), 1–38. https://doi.org/10.19191/EP22.4S2.060.
16. Clarke, L. A., Awatade, N. T., Felício, V. M., Silva, I. A., Calucho, M., Pereira, L., Azevedo, P., Cavaco, J., Barreto, C., Bertuzzo, C., Gartner, S., Beekman, J., & Amaral, M. D. (2019). The effect of premature termination codon mutations on CFTR mRNA abundance in human nasal epithelium and intestinal organoids: a basis for read-through therapies in cystic fibrosis. Human mutation, 40(3), 326–334. https://doi.org/10.1002/humu.23692.
17. Potapova N. A. (2022). Nonsense Mutations in Eukaryotes. Biochemistry. Biokhimiia, 87(5), 400–412. https://doi.org/10.1134/S0006297922050029.
18. Dabrowski, M., Bukowy-Bieryllo, Z., & Zietkiewicz, E. (2018). Advances in therapeutic use of a drug-stimulated translational readthrough of premature termination codons. Molecular medicine (Cambridge, Mass.), 24(1), 25. https://doi.org/10.1186/s10020-018-0024-7.
19. Benhabiles, H., Jia, J., and Lejeune, F. Nonsense Mutation Correction in Human Diseases, An Approach for Targeted Medicine. ISBN 978-0-12-804468-1. DOI https://doi.org/10.1016/C2014-0-04358-4. 2016 Elsevier Inc.
20. Keeling, K. M., Xue, X., Gunn, G., & Bedwell, D. M. (2014). Therapeutics based on stop codon readthrough. Annual review of genomics and human genetics, 15, 371–394. https://doi.org/10.1146/annurev-genom-091212-153527.

21. Palma, M., & Lejeune, F. (2021). Deciphering the molecular mechanism of stop codon readthrough. Biological reviews of the Cambridge Philosophical Society, 96(1), 310–329. https://doi.org/10.1111/brv.12657.
22. Brown, A., Shao, S., Murray, J., Hegde, R. S., & Ramakrishnan, V. (2015). Structural basis for stop codon recognition in eukaryotes. Nature, 524(7566), 493–496. https://doi.org/10.1038/nature14896.
23. Hellen C. U. T. (2018). Translation Termination and Ribosome Recycling in Eukaryotes. Cold Spring Harbor perspectives in biology, 10(10), a032656. https://doi.org/10.1101/cshperspect.a032656.
24. Lombardi, S., Testa, M. F., Pinotti, M., & Branchini, A. (2020). Molecular Insights into Determinants of Translational Readthrough and Implications for Nonsense Suppression Approaches. International journal of molecular sciences, 21(24), 9449. https://doi.org/10.3390/ijms21249449.
25. Isken, O., & Maquat, L. E. (2007). Quality control of eukaryotic mRNA: safeguarding cells from abnormal mRNA function. Genes & development, 21(15), 1833–1856. https://doi.org/10.1101/gad.1566807.
26. Romão, L. Advances in Experimental Medicine and Biology. The mRNA metabolism in human disease https://doi.org/10.1007/978-3-030-19966-. © Springer Nature Switzerland AG 2019. ISSN 0065-2598 ISSN 2214-8019.
27. Le Hir, H., Gatfield, D., Izaurralde, E., & Moore, M. J. (2001). The exon-exon junction complex provides a binding platform for factors involved in mRNA export and nonsense-mediated mRNA decay. The EMBO journal, 20(17), 4987–4997. https://doi.org/10.1093/emboj/20.17.4987.
28. Bongiorno, R., Colombo, M. P., & Lecis, D. (2021). Deciphering the nonsense-mediated mRNA decay pathway to identify cancer cell vulnerabilities for effective cancer therapy. Journal of experimental & clinical cancer research: CR, 40(1), 376. https://doi.org/10.1186/s13046-021-02192-2.
29. Popp, M. W., & Maquat, L. E. (2013). Organizing principles of mammalian nonsense-mediated mRNA decay. Annual review of genetics, 47, 139–165. https://doi.org/10.1146/annurev-genet-111212-133424.
30. Kurosaki, T., Popp, M. W., & Maquat, L. E. (2019). Quality and quantity control of gene expression by nonsense-mediated mRNA decay. Nature reviews. Molecular cell biology, 20(7), 406–420. https://doi.org/10.1038/s41580-019-0126-2.
31. Andjus, S., Morillon, A., & Wery, M. (2021). From Yeast to Mammals, the Nonsense-Mediated mRNA Decay as a Master Regulator of Long Non-Coding RNAs Functional Trajectory. Non-coding RNA, 7(3), 44. https://doi.org/10.3390/ncrna7030044.
32. Kervestin, S., Li, C., Buckingham, R., & Jacobson, A. (2012). Testing the faux-UTR model for NMD: analysis of Upf1p and Pab1p competition for binding to eRF3/Sup35p. Biochimie, 94(7), 1560–1571. https://doi.org/10.1016/j.biochi.2011.12.021.
33. Silva, A. L., Ribeiro, P., Inácio, A., Liebhaber, S. A., & Romão, L. (2008). Proximity of the poly(A)-binding protein to a premature termination codon inhibits mammalian nonsense-mediated mRNA decay. RNA (New York, N.Y.), 14(3), 563–576. https://doi.org/10.1261/rna.815108.

34. Lindeboom, R. G., Supek, F., & Lehner, B. (2016). The rules and impact of nonsense-mediated mRNA decay in human cancers. Nature genetics, 48(10), 1112–1118. https://doi.org/10.1038/ng.3664.
35. Bühler, M., Steiner, S., Mohn, F., Paillusson, A., & Mühlemann, O. (2006). EJC-independent degradation of nonsense immunoglobulin-mu mRNA depends on 3' UTR length. Nature structural & molecular biology, 13(5), 462–464. https://doi.org/10.1038/nsmb1081.
36. Metze, S., Herzog, V. A., Ruepp, M. D., & Mühlemann, O. (2013). Comparison of EJC-enhanced and EJC-independent NMD in human cells reveals two partially redundant degradation pathways. RNA (New York, N.Y.), 19(10), 1432–1448. https://doi.org/10.1261/rna.038893.113.
37. Karousis, E. D., & Mühlemann, O. (2019). Nonsense-Mediated mRNA Decay Begins Where Translation Ends. Cold Spring Harbor perspectives in biology, 11(2), a032862. https://doi.org/10.1101/cshperspect.a032862.
38. Spelier, S., van Doorn, E. P. M., van der Ent, C. K., Beekman, J. M., & Koppens, M. A. J. (2023). Readthrough compounds for nonsense mutations: bridging the translational gap. Trends in molecular medicine, 29(4), 297–314. https://doi.org/10.1016/j.molmed.2023.01.004.
39. Usuki, F., Yamashita, A., Higuchi, I., Ohnishi, T., Shiraishi, T., Osame, M., & Ohno, S. (2004). Inhibition of nonsense-mediated mRNA decay rescues the phenotype in Ullrich's disease. Annals of neurology, 55(5), 740–744. https://doi.org/10.1002/ana.20107.
40. Lentini, L., Melfi, R., Cancemi, P., Pibiri, I., & Di Leonardo, A. (2019). Caffeine boosts Ataluren's readthrough activity. Heliyon, 5(6), e01963. https://doi.org/10.1016/j.heliyon.2019.e01963.
41. Gopalsamy, A., Bennett, E. M., Shi, M., Zhang, W. G., Bard, J., & Yu, K. (2012). Identification of pyrimidine derivatives as hSMG-1 inhibitors. Bioorganic & medicinal chemistry letters, 22(21), 6636–6641. https://doi.org/10.1016/j.bmcl.2012.08.107.
42. Martin, L., Grigoryan, A., Wang, D., Wang, J., Breda, L., Rivella, S., Cardozo, T., & Gardner, L. B. (2014). Identification and characterization of small molecules that inhibit nonsense-mediated RNA decay and suppress nonsense p53 mutations. Cancer research, 74(11), 3104–3113. https://doi.org/10.1158/0008-5472.CAN-13-2235).
43. Wang, D., Wengrod, J., & Gardner, L. B. (2011). Overexpression of the c-myc oncogene inhibits nonsense-mediated RNA decay in B lymphocytes. The Journal of biological chemistry, 286(46), 40038–40043. https://doi.org/10.1074/jbc.M111.266361.
44. Bhuvanagiri, M., Lewis, J., Putzker, K., Becker, J. P., Leicht, S., Krijgsveld, J., Batra, R., Turnwald, B., Jovanovic, B., Hauer, C., Sieber, J., Hentze, M. W., & Kulozik, A. E. (2014). 5-azacytidine inhibits nonsense-mediated decay in a MYC-dependent fashion. EMBO molecular medicine, 6(12), 1593–1609. https://doi.org/10.15252/emmm.201404461.
45. Pawlicka, K., Kalathiya, U., & Alfaro, J. (2020). Nonsense-Mediated mRNA Decay: Pathologies and the Potential for Novel Therapeutics. Cancers, 12(3), 765. https://doi.org/10.3390/cancers12030765.

46. Wang, X., Shan, X., Gregory-Evans, K., & Gregory-Evans, C. Y. (2020). RNA-based therapies in animal models of Leber congenital amaurosis causing blindness. Precision clinical medicine, 3(2), 113–126. https://doi.org/10.1093/pcmedi/pbaa009.
47. Sahoo, S., Singh, D., Singh, A., Pandit, M., Vasu, K., Som, S., Pullagurla, N. J., Laha, D., & Eswarappa, S. M. (2022). Identification and functional characterization of mRNAs that exhibit stop codon readthrough in Arabidopsis thaliana. The Journal of biological chemistry, 298(8), 102173. https://doi.org/10.1016/j.jbc.2022.102173.
48. Bidou, L., Allamand, V., Rousset, J. P., & Namy, O. (2012). Sense from nonsense: therapies for premature stop codon diseases. Trends in molecular medicine, 18(11), 679–688. https://doi.org/10.1016/j.molmed.2012.09.008.
49. Roy, B., Friesen, W. J., Tomizawa, Y., Leszyk, J. D., Zhuo, J., Johnson, B., Dakka, J., Trotta, C. R., Xue, X., Mutyam, V., Keeling, K. M., Mobley, J. A., Rowe, S. M., Bedwell, D. M., Welch, E. M., & Jacobson, A. (2016). Ataluren stimulates ribosomal selection of near-cognate tRNAs to promote nonsense suppression. Proceedings of the National Academy of Sciences of the United States of America, 113(44), 12508–12513. https://doi.org/10.1073/pnas.1605336113.
50. Floquet, C., Hatin, I., Rousset, J. P., & Bidou, L. (2012). Statistical analysis of readthrough levels for nonsense mutations in mammalian cells reveals a major determinant of response to gentamicin. PLoS genetics, 8(3), e1002608. https://doi.org/10.1371/journal.pgen.1002608.
51. Tork, S., Hatin, I., Rousset, J. P., & Fabret, C. (2004). The major 5' determinant in stop codon read-through involves two adjacent adenines. Nucleic acids research, 32(2), 415–421. https://doi.org/10.1093/nar/gkh201.
52. Dabrowski, M., Bukowy-Bieryllo, Z., & Zietkiewicz, E. (2015). Translational readthrough potential of natural termination codons in eucaryotes--The impact of RNA sequence. RNA biology, 12(9), 950–958. https://doi.org/10.1080/15476286.2015.1068497.
53. Wangen, J. R., & Green, R. (2020). Stop codon context influences genome-wide stimulation of termination codon readthrough by aminoglycosides. eLife, 9, e52611. https://doi.org/10.7554/eLife.52611.
54. Beryozkin, A., Nagel-Wolfum, K., Banin, E., & Sharon, D. (2023). Factors Affecting Readthrough of Natural Versus Premature Termination Codons. Advances in experimental medicine and biology, 1415, 149–155. https://doi.org/10.1007/978-3-031-27681-1_23.
55. Pibiri, I., Lentini, L., Melfi, R., Gallucci, G., Pace, A., Spinello, A., Barone, G., & Di Leonardo, A. (2015). Enhancement of premature stop codon readthrough in the CFTR gene by Ataluren (PTC124) derivatives. European journal of medicinal chemistry, 101, 236–244. https://doi.org/10.1016/j.ejmech.2015.06.038.
56. Pibiri, I., Melfi, R., Tutone, M., Di Leonardo, A., Pace, A., & Lentini, L. (2020). Targeting Nonsense: Optimization of 1,2,4-Oxadiazole TRIDs to Rescue CFTR Expression and Functionality in Cystic Fibrosis Cell Model Systems. International journal of molecular sciences, 21(17), 6420. https://doi.org/10.3390/ijms21176420.

57. Cystic Fibrosis Foundation Patient Registry. 2017. 2016 Annual Data Report. Bethesda, MD: Cystic Fibrosis Found.
58. Dorothy H. Andersen, M.D. Cystic fibrosis of the pancreas and its relation to celiac disease clinical and pathologic study. Am J Dis Child. August 19381938;56(2):344-399. doi:10.1001/archpedi.1938.01980140114013).
59. Clague S. (2014). Dorothy Hansine Andersen. The Lancet. Respiratory medicine, 2(3), 184–185. https://doi.org/10.1016/S2213-2600(14)70057-8.
60. Riordan, J. R., Rommens, J. M., Kerem, B., Alon, N., Rozmahel, R., Grzelczak, Z., Zielenski, J., Lok, S., Plavsic, N., & Chou, J. L. (1989). Identification of the cystic fibrosis gene: cloning and characterization of complementary DNA. Science (New York, N.Y.), 245(4922), 1066–1073. https://doi.org/10.1126/science.2475911.
61. Lopes-Pacheco M. (2020). CFTR Modulators: The Changing Face of Cystic Fibrosis in the Era of Precision Medicine. Frontiers in pharmacology, 10, 1662. https://doi.org/10.3389/fphar.2019.01662.
62. Dawson, R., Locher, K. Structure of a bacterial multidrug ABC transporter. Nature 443, 180–185 (2006). https://doi.org/10.1038/nature05155.
63. Liu, F., Zhang, Z., Csanády, L., Gadsby, D. C., & Chen, J. (2017). Molecular Structure of the Human CFTR Ion Channel. Cell, 169(1), 85–95.e8. https://doi.org/10.1016/j.cell.2017.02.024.
64. Vergani, P., Lockless, S. W., Nairn, A. C., & Gadsby, D. C. (2005). CFTR channel opening by ATP-driven tight dimerization of its nucleotide-binding domains. Nature, 433(7028), 876–880. https://doi.org/10.1038/nature03313.
65. Della Sala, A., Prono, G., Hirsch, E., & Ghigo, A. (2021). Role of Protein Kinase A-Mediated Phosphorylation in CFTR Channel Activity Regulation. Frontiers in physiology, 12, 690247. https://doi.org/10.3389/fphys.2021.690247.
66. Denning, G. M., Ostedgaard, L. S., Cheng, S. H., Smith, A. E., & Welsh, M. J. (1992). Localization of cystic fibrosis transmembrane conductance regulator in chloride secretory epithelia. The Journal of clinical investigation, 89(1), 339–349. https://doi.org/10.1172/JCI115582.
67. Wang, Y., Wrennall, J. A., Cai, Z., Li, H., & Sheppard, D. N. (2014). Understanding how cystic fibrosis mutations disrupt CFTR function: from single molecules to animal models. The international journal of biochemistry & cell biology, 52, 47–57. https://doi.org/10.1016/j.biocel.2014.04.001.
68. Lukasiak, A., & Zajac, M. (2021). The Distribution and Role of the CFTR Protein in the Intracellular Compartments. Membranes, 11(11), 804. https://doi.org/10.3390/membranes11110804.
69. De Boeck, K., & Amaral, M. D. (2016). Progress in therapies for cystic fibrosis. The Lancet. Respiratory medicine, 4(8), 662–674. https://doi.org/10.1016/S2213-2600(16)00023-0.
70. De Boeck K. (2020). Cystic fibrosis in the year 2020: A disease with a new face. Acta paediatrica (Oslo, Norway : 1992), 109(5), 893–899. https://doi.org/10.1111/apa.15155.
71. Marson FAL, Bertuzzo CS, Ribeiro JD. Classification of CFTR mutation classes. Lancet Respir Med. 2016;4(8):e37-e38. doi:10.1016/S2213-2600(16)30188-6.

72. Pranke, I., Golec, A., Hinzpeter, A., Edelman, A., & Sermet-Gaudelus, I. (2019). Emerging Therapeutic Approaches for Cystic Fibrosis. From Gene Editing to Personalized Medicine. Frontiers in pharmacology, 10, 121. https://doi.org/10.3389/fphar.2019.00121.
73. Dechecchi, M. C., Tamanini, A., & Cabrini, G. (2018). Molecular basis of cystic fibrosis: from bench to bedside. Annals of translational medicine, 6(17), 334. https://doi.org/10.21037/atm.2018.06.48.
74. Fanen, P., Wohlhuter-Haddad, A., & Hinzpeter, A. (2014). Genetics of cystic fibrosis: CFTR mutation classifications toward genotype-based CF therapies. The international journal of biochemistry & cell biology, 52, 94–102. https://doi.org/10.1016/j.biocel.2014.02.023.
75. Chu, C. S., Trapnell, B. C., Curristin, S., Cutting, G. R., & Crystal, R. G. (1993). Genetic basis of variable exon 9 skipping in cystic fibrosis transmembrane conductance regulator mRNA. Nature genetics, 3(2), 151–156. https://doi.org/10.1038/ng0293-151.
76. Ramalho, A. S., Lewandowska, M. A., Farinha, C. M., Mendes, F., Gonçalves, J., Barreto, C., Harris, A., & Amaral, M. D. (2009). Deletion of CFTR translation start site reveals functional isoforms of the protein in CF patients. Cellular physiology and biochemistry : international journal of experimental cellular physiology, biochemistry, and pharmacology, 24(5-6), 335–346. https://doi.org/10.1159/000257426.
77. Derichs N. (2013). Targeting a genetic defect: cystic fibrosis transmembrane conductance regulator modulators in cystic fibrosis. European respiratory review : an official journal of the European Respiratory Society, 22(127), 58–65. https://doi.org/10.1183/09059180.00008412.
78. Bobadilla, J. L., Macek, M., Jr, Fine, J. P., & Farrell, P. M. (2002). Cystic fibrosis: a worldwide analysis of CFTR mutations--correlation with incidence data and application to screening. Human mutation, 19(6), 575–606. https://doi.org/10.1002/humu.10041.
79. Tsui, L. C., & Dorfman, R. (2013). The cystic fibrosis gene: a molecular genetic perspective. Cold Spring Harbor perspectives in medicine, 3(2), a009472. https://doi.org/10.1101/cshperspect.a009472.
80. Shteinberg, M., Haq, I. J., Polineni, D., & Davies, J. C. (2021). Cystic fibrosis. Lancet (London, England), 397(10290), 2195–2211. https://doi.org/10.1016/S0140-6736(20)32542-3.
81. Elborn J. S. (2013). Personalised medicine for cystic fibrosis: treating the basic defect. European respiratory review: an official journal of the European Respiratory Society, 22(127), 3–5. https://doi.org/10.1183/09059180.00008112.
82. Bradbury N.A. (2020). CFTR and Cystic Fibrosis: A Need for Personalized Medicine. In: Hamilton, K.L., Devor, D.C. (eds) Studies of Epithelial Transporters and Ion Channels. Physiology in Health and Disease. Springer, Cham. https://doi.org/10.1007/978-3-030-55454-5_15.
83. Yu, H., Burton, B., Huang, C. J., Worley, J., Cao, D., Johnson, J. P., Jr, Urrutia, A., Joubran, J., Seepersaud, S., Sussky, K., Hoffman, B. J., & Van Goor, F. (2012). Ivacaftor potentiation of multiple CFTR channels with gating mutations. Journal of cystic fibrosis : official journal of the European Cystic Fibrosis Society, 11(3), 237–245. https://doi.org/10.1016/j.jcf.2011.12.005.

84. King, J. A., Nichols, A. L., Bentley, S., Carr, S. B., & Davies, J. C. (2022). An Update on CFTR Modulators as New Therapies for Cystic Fibrosis. Paediatric drugs, 24(4), 321–333. https://doi.org/10.1007/s40272-022-00509-y.
85. Jia, S., & Taylor-Cousar, J. L. (2023). Cystic Fibrosis Modulator Therapies. Annual review of medicine, 74, 413–426. https://doi.org/10.1146/annurev-med-042921-021447.
86. Ledford, H., & Callaway, E. (2020). Pioneers of revolutionary CRISPR gene editing win chemistry Nobel. Nature, 586(7829), 346–347. https://doi.org/10.1038/d41586-020-02765-9.
87. Melfi, R., Cancemi, P., Chiavetta, R., Barra, V., Lentini, L., & Di Leonardo, A. (2020). Investigating REPAIRv2 as a Tool to Edit CFTR mRNA with Premature Stop Codons. International journal of molecular sciences, 21(13), 4781. https://doi.org/10.3390/ijms21134781
88. Albers, S., Allen, E. C., Bharti, N., Davyt, M., Joshi, D., Perez-Garcia, C. G., Santos, L., Mukthavaram, R., Delgado-Toscano, M. A., Molina, B., Kuakini, K., Alayyoubi, M., Park, K. J., Acharya, G., Gonzalez, J. A., Sagi, A., Birket, S. E., Tearney, G. J., Rowe, S. M., Manfredi, C., … Ignatova, Z. (2023). Engineered tRNAs suppress nonsense mutations in cells and in vivo. Nature, 618(7966), 842–848. https://doi.org/10.1038/s41586-023-06133-1
89. Nagel-Wolfrum, K., Möller, F., Penner, I., Baasov, T., & Wolfrum, U. (2016). Targeting Nonsense Mutations in Diseases with Translational Read-Through-Inducing Drugs (TRIDs). BioDrugs : clinical immunotherapeutics, biopharmaceuticals and gene therapy, 30(2), 49–74. https://doi.org/10.1007/s40259-016-0157-6.
90. Krause, K. M., Serio, A. W., Kane, T. R., & Connolly, L. E. (2016). Aminoglycosides: An Overview. Cold Spring Harbor perspectives in medicine, 6(6), a027029. https://doi.org/10.1101/cshperspect.a027029.
91. Jospe-Kaufman, M., Siomin, L., & Fridman, M. (2020). The relationship between the structure and toxicity of aminoglycoside antibiotics. Bioorganic & medicinal chemistry letters, 30(13), 127218. https://doi.org/10.1016/j.bmcl.2020.127218.
92. Martins-Dias, P., & Romão, L. (2021). Nonsense suppression therapies in human genetic diseases. Cellular and molecular life sciences: CMLS, 78(10), 4677–4701. https://doi.org/10.1007/s00018-021-03809-7.
93. Manuvakhova, M., Keeling, K., & Bedwell, D. M. (2000). Aminoglycoside antibiotics mediate context-dependent suppression of termination codons in a mammalian translation system. RNA (New York, N.Y.), 6(7), 1044–1055. https://doi.org/10.1017/s1355838200000716.
94. Wohlgemuth, I., Garofalo, R., Samatova, E., Günenç, A. N., Lenz, C., Urlaub, H., & Rodnina, M. V. (2021). Translation error clusters induced by aminoglycoside antibiotics. Nature communications, 12(1), 1830. https://doi.org/10.1038/s41467-021-21942-6.
95. Le, T. A., Hiba, T., Chaudhari, D., Preston, A. N., Palowsky, Z. R., Ahmadzadeh, S., Shekoohi, S., Cornett, E. M., & Kaye, A. D. (2023). Aminoglycoside-Related Nephrotoxicity and Ototoxicity in

Clinical Practice: A Review of Pathophysiological Mechanism and Treatment Options. Advances in therapy, 40(4), 1357–1365. https://doi.org/10.1007/s12325-023-02436-x.

96. Li, S., Li, J., Shi, W., Nie, Z., Zhang, S., Ma, F., Hu, J., Chen, J., Li, P., & Xie, X. (2023). Pharmaceuticals Promoting Premature Termination Codon Readthrough: Progress in Development. Biomolecules, 13(6), 988. https://doi.org/10.3390/biom13060988.
97. Welch, E. M., Barton, E. R., Zhuo, J., Tomizawa, Y., Friesen, W. J., Trifillis, P., Paushkin, S., Patel, M., Trotta, C. R., Hwang, S., Wilde, R. G., Karp, G., Takasugi, J., Chen, G., Jones, S., Ren, H., Moon, Y. C., Corson, D., Turpoff, A. A., Campbell, J. A., … Sweeney, H. L. (2007). PTC124 targets genetic disorders caused by nonsense mutations. Nature, 447(7140), 87–91. https://doi.org/10.1038/nature05756.
98. Du, M., Liu, X., Welch, E. M., Hirawat, S., Peltz, S. W., & Bedwell, D. M. (2008). PTC124 is an orally bioavailable compound that promotes suppression of the human CFTR-G542X nonsense allele in a CF mouse model. Proceedings of the National Academy of Sciences of the United States of America, 105(6), 2064–2069. https://doi.org/10.1073/pnas.0711795105.
99. Kayali, R., Ku, J. M., Khitrov, G., Jung, M. E., Prikhodko, O., & Bertoni, C. (2012). Read-through compound 13 restores dystrophin expression and improves muscle function in the mdx mouse model for Duchenne muscular dystrophy. Human molecular genetics, 21(18), 4007–4020. https://doi.org/10.1093/hmg/dds223.
100. Torriano, S., Erkilic, N., Baux, D., Cereso, N., De Luca, V., Meunier, I., Moosajee, M., Roux, A. F., Hamel, C. P., & Kalatzis, V. (2018). The effect of PTC124 on choroideremia fibroblasts and iPSC-derived RPE raises considerations for therapy. Scientific reports, 8(1), 8234. https://doi.org/10.1038/s41598-018-26481-7.
101. Wang, D., Xue, X., Gunn, G., Du, M., Siddiqui, A., Weetall, M., & Keeling, K. M. (2022). Ataluren suppresses a premature termination codon in an MPS I-H mouse. Journal of molecular medicine (Berlin, Germany), 100(8), 1223–1235. https://doi.org/10.1007/s00109-022-02232-0.
102. Campofelice, A., Lentini, L., Di Leonardo, A., Melfi, R., Tutone, M., Pace, A., & Pibiri, I. (2019). Strategies against Nonsense: Oxadiazoles as Translational Readthrough-Inducing Drugs (TRIDs). International journal of molecular sciences, 20(13), 3329. https://doi.org/10.3390/ijms20133329.
103. Kerem, E., Konstan, M. W., De Boeck, K., Accurso, F. J., Sermet-Gaudelus, I., Wilschanski, M., Elborn, J. S., Melotti, P., Bronsveld, I., Fajac, I., Malfroot, A., Rosenbluth, D. B., Walker, P. A., McColley, S. A., Knoop, C., Quattrucci, S., Rietschel, E., Zeitlin, P. L., Barth, J., Elfring, G. L., … Cystic Fibrosis Ataluren Study Group (2014). Ataluren for the treatment of nonsense-mutation cystic fibrosis: a randomised, double-blind, placebo-controlled phase 3 trial. The Lancet. Respiratory medicine, 2(7), 539–547. https://doi.org/10.1016/S2213-2600(14)70100-6.
104. Zainal Abidin, N., Haq, I. J., Gardner, A. I., & Brodlie, M. (2017). Ataluren in cystic fibrosis: development, clinical studies and where are we now?. Expert opinion on pharmacotherapy, 18(13), 1363–1371. https://doi.org/10.1080/14656566.2017.1359255.

105. Konstan, M. W., VanDevanter, D. R., Rowe, S. M., Wilschanski, M., Kerem, E., Sermet-Gaudelus, I., DiMango, E., Melotti, P., McIntosh, J., De Boeck, K., & ACT CF Study Group (2020). Efficacy and safety of ataluren in patients with nonsense-mutation cystic fibrosis not receiving chronic inhaled aminoglycosides: The international, randomized, double-blind, placebo-controlled Ataluren Confirmatory Trial in Cystic Fibrosis (ACT CF). Journal of cystic fibrosis : official journal of the European Cystic Fibrosis Society, 19(4), 595–601. https://doi.org/10.1016/j.jcf.2020.01.007.
106. Ryan N. J. (2014). Ataluren: first global approval. Drugs, 74(14), 1709–1714. https://doi.org/10.1007/s40265-014-0287-4.
107. Brasell, E. J., Chu, L. L., Akpa, M. M., Eshkar-Oren, I., Alroy, I., Corsini, R., Gilfix, B. M., Yamanaka, Y., Huertas, P., & Goodyer, P. (2019). The novel aminoglycoside, ELX-02, permits CTNSW138X translational read-through and restores lysosomal cystine efflux in cystinosis. PloS one, 14(12), e0223954. https://doi.org/10.1371/journal.pone.0223954.
108. Crawford, D. K., Alroy, I., Sharpe, N., Goddeeris, M. M., & Williams, G. (2020). ELX-02 Generates Protein via Premature Stop Codon Read-Through without Inducing Native Stop Codon Read-Through Proteins. The Journal of pharmacology and experimental therapeutics, 374(2), 264–272. https://doi.org/10.1124/jpet.120.265595.
109. Crawford, D. K., Mullenders, J., Pott, J., Boj, S. F., Landskroner-Eiger, S., & Goddeeris, M. M. (2021). Targeting G542X CFTR nonsense alleles with ELX-02 restores CFTR function in human-derived intestinal organoids. Journal of cystic fibrosis : official journal of the European Cystic Fibrosis Society, 20(3), 436–442. https://doi.org/10.1016/j.jcf.2021.01.009.
110. Chen, J., Thrasher, K., Fu, L., Wang, W., Aghamohammadzadeh, S., Wen, H., Tang, L., Keeling, K. M., Falk Libby, E., Bedwell, D. M., & Rowe, S. M. (2023). The synthetic aminoglycoside ELX-02 induces readthrough of G550X-CFTR producing superfunctional protein that can be further enhanced by CFTR modulators. American journal of physiology. Lung cellular and molecular physiology, 324(6), L756–L770. https://doi.org/10.1152/ajplung.00038.2023.
111. Pranke, I. M., Varilh, J., Hatton, A., Faucon, C., Girodon, E., Dreano, E., Chevalier, B., Karri, S., Reix, P., Durieu, I., Bidou, L., Namy, O., Taulan, M., Hinzpeter, A., & Sermet-Gaudelus, I. (2023). The U UGA C sequence provides a favorable context to ELX-02 induced CFTR readthrough. Journal of cystic fibrosis: official journal of the European Cystic Fibrosis Society, 22(3), 560–563. https://doi.org/10.1016/j.jcf.2022.10.010.
112. Trzaska, C., Amand, S., Bailly, C., Leroy, C., Marchand, V., Duvernois-Berthet, E., Saliou, J. M., Benhabiles, H., Werkmeister, E., Chassat, T., Guilbert, R., Hannebique, D., Mouray, A., Copin, M. C., Moreau, P. A., Adriaenssens, E., Kulozik, A., Westhof, E., Tulasne, D., Motorin, Y., … Lejeune, F. (2020). 2,6-Diaminopurine as a highly potent corrector of UGA nonsense mutations. Nature communications, 11(1), 1509. https://doi.org/10.1038/s41467-020-15140-z.
113. Leroy, C., Spelier, S., Essonghe, N. C., Poix, V., Kong, R., Gizzi, P., Bourban, C., Amand, S., Bailly, C., Guilbert, R., Hannebique, D., Persoons, P., Arhant, G., Prévotat, A., Reix, P., Hubert, D., Gérardin, M.,

Chamaillard, M., Prevarskaya, N., Rebuffat, S., … Lejeune, F. (2023). Use of 2,6-diaminopurine as a potent suppressor of UGA premature stop codons in cystic fibrosis. Molecular therapy : the journal of the American Society of Gene Therapy, 31(4), 970–985. https://doi.org/10.1016/j.ymthe.2023.01.014

114. Tutone, M., Pibiri, I., Perriera, R., Campofelice, A., Culletta, G., Melfi, R., Pace, A., Almerico, A. M., & Lentini, L. (2020). Pharmacophore-Based Design of New Chemical Scaffolds as Translational Readthrough-Inducing Drugs (TRIDs). ACS medicinal chemistry letters, 11(5), 747–753. https://doi.org/10.1021/acsmedchemlett.9b00609.
115. Bezzerri, V., Lentini, L., Api, M., Busilacchi, E. M., Cavalieri, V., Pomilio, A., Diomede, F., Pegoraro, A., Cesaro, S., Poloni, A., Pace, A., Trubiani, O., Lippi, G., Pibiri, I., & Cipolli, M. (2022). Novel Translational Read-through-Inducing Drugs as a Therapeutic Option for Shwachman-Diamond Syndrome. Biomedicines, 10(4), 886. https://doi.org/10.3390/biomedicines10040886.
116. Carollo, P. S., Tutone, M., Culletta, G., Fiduccia, I., Corrao, F., Pibiri, I., Di Leonardo, A., Zizzo, M. G., Melfi, R., Pace, A., Almerico, A. M., & Lentini, L. (2023). Investigating the Inhibition of FTSJ1, a Tryptophan tRNA-Specific 2'-O-Methyltransferase by NV TRIDs, as a Mechanism of Readthrough in Nonsense Mutated CFTR. International journal of molecular sciences, 24(11), 9609. https://doi.org/10.3390/ijms24119609.
117. Corrao, F., Zizzo, M. G., Tutone, M., Melfi, R., Fiduccia, I., Carollo, P. S., Leonardo, A. D., Caldara, G., Perriera, R., Pace, A., Belmonte, B., Sammataro, S., Pibiri, I., & Lentini, L. (2022). Nonsense codons suppression. An acute toxicity study of three optimized TRIDs in murine model, safety and tolerability evaluation. Biomedicine & pharmacotherapy = Biomedecine & pharmacotherapie, 156, 113886. https://doi.org/10.1016/j.biopha.2022.113886.
118. Osum, S. H., Oribamise, E. I., Corbière, S. M. A. S., Taisto, M., Jubenville, T., Coutts, A., Kirstein, M. N., Fisher, J., Moertel, C., Du, M., Bedwell, D., Largaespada, D. A., & Watson, A. L. (2023). Combining nonsense mutation suppression therapy with nonsense-mediated decay inhibition in neurofibromatosis type 1. Molecular therapy. Nucleic acids, 33, 227–239. https://doi.org/10.1016/j.omtn.2023.06.018.
119. Wagner, R. N., Wießner, M., Friedrich, A., Zandanell, J., Breitenbach-Koller, H., & Bauer, J. W. (2023). Emerging Personalized Opportunities for Enhancing Translational Readthrough in Rare Genetic Diseases and Beyond. International journal of molecular sciences, 24(7), 6101. https://doi.org/10.3390/ijms24076101.
120. Sharma J, Keeling KM, Rowe SM. Pharmacological approaches for targeting cystic fibrosis nonsense mutations. Eur J Med Chem. 2020 Aug 15;200:112436. doi: 10.1016/j.ejmech.2020.112436. Epub 2020 May 21. PMID: 32512483; PMCID: PMC7384597.
121. De Jonge, H. R., Ballmann, M., Veeze, H., Bronsveld, I., Stanke, F., Tümmler, B., & Sinaasappel, M. (2004). Ex vivo CF diagnosis by intestinal current measurements (ICM) in small aperture, circulating Ussing chambers. Journal of cystic fibrosis : official journal of the European Cystic Fibrosis Society, 3 Suppl 2, 159–163. https://doi.org/10.1016/j.jcf.2004.05.034.

122. Ramalho, A. S., Boon, M., Proesmans, M., Vermeulen, F., Carlon, M. S., & Boeck, K. (2022). Assays of CFTR Function In Vitro, Ex Vivo and In Vivo. International journal of molecular sciences, 23(3), 1437. https://doi.org/10.3390/ijms23031437.
123. Li, H., Sheppard, D. N., & Hug, M. J. (2004). Transepithelial electrical measurements with the Ussing chamber. Journal of cystic fibrosis : official journal of the European Cystic Fibrosis Society, 3 Suppl 2, 123–126. https://doi.org/10.1016/j.jcf.2004.05.026.
124. Thomson, A., Smart, K., Somerville, M. S., Lauder, S. N., Appanna, G., Horwood, J., Sunder Raj, L., Srivastava, B., Durai, D., Scurr, M. J., Keita, Å. V., Gallimore, A. M., & Godkin, A. (2019). The Ussing chamber system for measuring intestinal permeability in health and disease. BMC gastroenterology, 19(1), 98. https://doi.org/10.1186/s12876-019-1002-4.
125. Golec, A., Pranke, I., Scudieri, P., Hayes, K., Dreano, E., Dunlevy, F., Hatton, A., Downey, D. G., Galietta, L., & Sermet, I. (2022). Isolation, cultivation, and application of primary respiratory epithelial cells obtained by nasal brushing, polyp samples, or lung explants. STAR protocols, 3(2), 101419. https://doi.org/10.1016/j.xpro.2022.101419.
126. Crystal, R. G., Randell, S. H., Engelhardt, J. F., Voynow, J., & Sunday, M. E. (2008). Airway epithelial cells: current concepts and challenges. Proceedings of the American Thoracic Society, 5(7), 772–777. https://doi.org/10.1513/pats.200805-041HR.
127. Yaghi, A., & Dolovich, M. B. (2016). Airway Epithelial Cell Cilia and Obstructive Lung Disease. Cells, 5(4), 40. https://doi.org/10.3390/cells5040040.
128. Montoro, D. T., Haber, A. L., Biton, M., Vinarsky, V., Lin, B., Birket, S. E., Yuan, F., Chen, S., Leung, H. M., Villoria, J., Rogel, N., Burgin, G., Tsankov, A. M., Waghray, A., Slyper, M., Waldman, J., Nguyen, L., Dionne, D., Rozenblatt-Rosen, O., Tata, P. R., … Rajagopal, J. (2018). A revised airway epithelial hierarchy includes CFTR-expressing ionocytes. Nature, 560(7718), 319–324. https://doi.org/10.1038/s41586-018-0393-7.
129. Davis, J. D., & Wypych, T. P. (2021). Cellular and functional heterogeneity of the airway epithelium. Mucosal immunology, 14(5), 978–990. https://doi.org/10.1038/s41385-020-00370-7.
130. Okuda, K., Dang, H., Kobayashi, Y., Carraro, G., Nakano, S., Chen, G., Kato, T., Asakura, T., Gilmore, R. C., Morton, L. C., Lee, R. E., Mascenik, T., Yin, W. N., Barbosa Cardenas, S. M., O'Neal, Y. K., Minnick, C. E., Chua, M., Quinney, N. L., Gentzsch, M., Anderson, C. W., … Boucher, R. C. (2021). Secretory Cells Dominate Airway CFTR Expression and Function in Human Airway Superficial Epithelia. American journal of respiratory and critical care medicine, 203(10), 1275–1289. https://doi.org/10.1164/rccm.202008-3198OC.
131. Park, J. K., Shrivastava, A., Zhang, C., Pollok, B. A., Finkbeiner, W. E., Gibb, E. R., Ly, N. P., & Illek, B. (2020). Functional Profiling of CFTR-Directed Therapeutics Using Pediatric Patient-Derived Nasal Epithelial Cell Models. Frontiers in pediatrics, 8, 536. https://doi.org/10.3389/fped.2020.00536.
132. Ericsson, A. C., Crim, M. J., & Franklin, C. L. (2013). A brief history of animal modeling. Missouri medicine, 110(3), 201–205.

133. Freires, I. A., Morelo, D. F. C., Soares, L. F. F., Costa, I. S., de Araújo, L. P., Breseghello, I., Abdalla, H. B., Lazarini, J. G., Rosalen, P. L., Pigossi, S. C., & Franchin, M. (2023). Progress and promise of alternative animal and non-animal methods in biomedical research. Archives of toxicology, 97(9), 2329–2342. https://doi.org/10.1007/s00204-023-03532-1.
134. Garattini, S., & Grignaschi, G. (2017). Animal testing is still the best way to find new treatments for patients. European journal of internal medicine, 39, 32–35. https://doi.org/10.1016/j.ejim.2016.11.013.
135. Russell W, Burch R. The principles of humane experimental technique. Hertfordshire: UFAW Publications; 1959.
136. Hubrecht, R. C., & Carter, E. (2019). The 3Rs and Humane Experimental Technique: Implementing Change. Animals : an open access journal from MDPI, 9(10), 754. https://doi.org/10.3390/ani9100754.ù
137. Percie du Sert, N., Hurst, V., Ahluwalia, A., Alam, S., Avey, M. T., Baker, M., Browne, W. J., Clark, A., Cuthill, I. C., Dirnagl, U., Emerson, M., Garner, P., Holgate, S. T., Howells, D. W., Karp, N. A., Lazic, S. E., Lidster, K., MacCallum, C. J., Macleod, M., Pearl, E. J., … Würbel, H. (2020). The ARRIVE guidelines 2.0: Updated guidelines for reporting animal research. PLoS biology, 18(7), e3000410. https://doi.org/10.1371/journal.pbio.3000410
138. Robinson, N. B., Krieger, K., Khan, F. M., Huffman, W., Chang, M., Naik, A., Yongle, R., Hameed, I., Krieger, K., Girardi, L. N., & Gaudino, M. (2019). The current state of animal models in research: A review. International journal of surgery (London, England), 72, 9–13. https://doi.org/10.1016/j.ijsu.2019.10.015).
139. OECD (1992). OECD Guidelines for the Testing of Chemicals No. 420: Acute Oral Toxicity Fixed Dose Method, 7pp. Paris, France: OECD.
140. United Nations Economic Commission for Europe. Globally Harmonized System for the Classification and Labeling of Chemicals (GHS). Part 3. Health Hazards. Geneva: United Nations; 2013. [July 9, 2014]. http://www.unece.org/fileadmin/DAM/trans/danger/publi/ghs/ghs_rev05/English/03e_part3.pdf .
141. McCarron, A., Parsons, D., & Donnelley, M. (2021). Animal and Cell Culture Models for Cystic Fibrosis: Which Model Is Right for Your Application?. The American journal of pathology, 191(2), 228–242. https://doi.org/10.1016/j.ajpath.2020.10.017.
142. Colledge, W. H., Ratcliff, R., Foster, D., Williamson, R., & Evans, M. J. (1992). Cystic fibrosis mouse with intestinal obstruction. Lancet (London, England), 340(8820), 680. https://doi.org/10.1016/0140-6736(92)92223-3.
143. Borowitz, D., & Gelfond, D. (2013). Intestinal complications of cystic fibrosis. Current opinion in pulmonary medicine, 19(6), 676–680. https://doi.org/10.1097/MCP.0b013e3283659ef2.
144. Tobias, J., Tillotson, M., Maloney, L., & Fialkowski, E. (2022). Meconium Ileus, Distal Intestinal Obstruction Syndrome, and Other Gastrointestinal Pathology in the Cystic Fibrosis Patient. The Surgical clinics of North America, 102(5), 873–882. https://doi.org/10.1016/j.suc.2022.07.016.

145. Hodges, C. A., Cotton, C. U., Palmert, M. R., & Drumm, M. L. (2008). Generation of a conditional null allele for Cftr in mice. Genesis (New York, N.Y. : 2000), 46(10), 546–552. https://doi.org/10.1002/dvg.20433.
146. Wilke, M., Buijs-Offerman, R. M., Aarbiou, J., Colledge, W. H., Sheppard, D. N., Touqui, L., Bot, A., Jorna, H., de Jonge, H. R., & Scholte, B. J. (2011). Mouse models of cystic fibrosis: phenotypic analysis and research applications. Journal of cystic fibrosis : official journal of the European Cystic Fibrosis Society, 10 Suppl 2, S152–S171. https://doi.org/10.1016/S1569-1993(11)60020-9.
147. McHugh, D. R., Steele, M. S., Valerio, D. M., Miron, A., Mann, R. J., LePage, D. F., Conlon, R. A., Cotton, C. U., Drumm, M. L., & Hodges, C. A. (2018). A G542X cystic fibrosis mouse model for examining nonsense mutation directed therapies. PloS one, 13(6), e0199573. https://doi.org/10.1371/journal.pone.0199573.
148. Tangye, S. G., Al-Herz, W., Bousfiha, A., Chatila, T., Cunningham-Rundles, C., Etzioni, A., Franco, J. L., Holland, S. M., Klein, C., Morio, T., Ochs, H. D., Oksenhendler, E., Picard, C., Puck, J., Torgerson, T. R., Casanova, J. L., & Sullivan, K. E. (2020). Human Inborn Errors of Immunity: 2019 Update on the Classification from the International Union of Immunological Societies Expert Committee. Journal of clinical immunology, 40(1), 24–64. https://doi.org/10.1007/s10875-019-00737-x.
149. Bogaert, D. J., Dullaers, M., Lambrecht, B. N., Vermaelen, K. Y., De Baere, E., & Haerynck, F. (2016). Genes associated with common variable immunodeficiency: one diagnosis to rule them all?. Journal of medical genetics, 53(9), 575–590. https://doi.org/10.1136/jmedgenet-2015-103690.
150. Kolukısa, B., & Barış, S. (2021). Primary Immune Regulatory Disorders and Targeted Therapies. Turkish journal of haematology : official journal of Turkish Society of Haematology, 38(1), 1–14. https://doi.org/10.4274/tjh.galenos.2021.2020.0724.
151. Picard, C., Al-Herz, W., Bousfiha, A., Casanova, J. L., Chatila, T., Conley, M. E., Cunningham-Rundles, C., Etzioni, A., Holland, S. M., Klein, C., Nonoyama, S., Ochs, H. D., Oksenhendler, E., Puck, J. M., Sullivan, K. E., Tang, M. L., Franco, J. L., & Gaspar, H. B. (2015). Primary Immunodeficiency Diseases: an Update on the Classification from the International Union of Immunological Societies Expert Committee for Primary Immunodeficiency 2015. Journal of clinical immunology, 35(8), 696–726. https://doi.org/10.1007/s10875-015-0201-1.
152. Gámez-Díaz, L., August, D., Stepensky, P., Revel-Vilk, S., Seidel, M. G., Noriko, M., Morio, T., Worth, A. J. J., Blessing, J., Van de Veerdonk, F., Feuchtinger, T., Kanariou, M., Schmitt-Graeff, A., Jung, S., Seneviratne, S., Burns, S., Belohradsky, B. H., Rezaei, N., Bakhtiar, S., Speckmann, C., … Grimbacher, B. (2016). The extended phenotype of LPS-responsive beige-like anchor protein (LRBA) deficiency. The Journal of allergy and clinical immunology, 137(1), 223–230. https://doi.org/10.1016/j.jaci.2015.09.025.
153. Martínez-Jaramillo, C., Gutierrez-Hincapie, S., Arango, J. C. O., Vásquez-Duque, G. M., Erazo-Garnica, R. M., Franco, J. L., & Trujillo-Vargas, C. M. (2019). Clinical, immunological and genetic characteristic of patients with clinical phenotype associated to LRBA-deficiency in Colombia. Colombia medica (Cali, Colombia), 50(3), 176–191. https://doi.org/10.25100/cm.v50i3.3969.

154. Meyts I, Bousfiha A, Duff C, et al. Primary Immunodeficiencies: A Decade of Progress and a Promising Future. Front Immunol. 2021;11:625753. Published 2021 Feb 18. doi:10.3389/fimmu.2020.625753.
155. Wang, J. W., Howson, J., Haller, E., & Kerr, W. G. (2001). Identification of a novel lipopolysaccharide-inducible gene with key features of both A kinase anchor proteins and chs1/beige proteins. Journal of immunology (Baltimore, Md.: 1950), 166(7), 4586–4595. https://doi.org/10.4049/jimmunol.166.7.4586.
156. Wang, J. W., Gamsby, J. J., Highfill, S. L., Mora, L. B., Bloom, G. C., Yeatman, T. J., Pan, T. C., Ramne, A. L., Chodosh, L. A., Cress, W. D., Chen, J., & Kerr, W. G. (2004). Deregulated expression of LRBA facilitates cancer cell growth. Oncogene, 23(23), 4089–4097. https://doi.org/10.1038/sj.onc.1207567.
157. Martínez Jaramillo, C., & Trujillo-Vargas, C. M. (2018). LRBA in the endomembrane system. Colombia medica (Cali, Colombia), 49(3), 236–243. https://doi.org/10.25100/cm.v49i2.3802.
158. Cullinane, A. R., Schäffer, A. A., & Huizing, M. (2013). The BEACH is hot: a LYST of emerging roles for BEACH-domain containing proteins in human disease. Traffic (Copenhagen, Denmark), 14(7), 749–766. https://doi.org/10.1111/tra.12069.
159. Alkhairy, O. K., Abolhassani, H., Rezaei, N., Fang, M., Andersen, K. K., Chavoshzadeh, Z., Mohammadzadeh, I., El-Rajab, M. A., Massaad, M., Chou, J., Aghamohammadi, A., Geha, R. S., & Hammarström, L. (2016). Spectrum of Phenotypes Associated with Mutations in LRBA. Journal of clinical immunology, 36(1), 33–45. https://doi.org/10.1007/s10875-015-0224-7.
160. Moreno-Corona, N. C., Lopez-Ortega, O., Flores Hermenegildo, J. M., Berron-Ruiz, L., Rodriguez-Alba, J. C., Santos-Argumedo, L., & Lopez-Herrera, G. (2020). Lipopolysaccharide-responsive beige-like anchor acts as a cAMP-dependent protein kinase anchoring protein in B cells. Scandinavian journal of immunology, 92(3), e12922. https://doi.org/10.1111/sji.12922.
161. Pérez-Pérez, D., Santos-Argumedo, L., Rodríguez-Alba, J. C., & López-Herrera, G. (2023). Role of Protein Kinase A Activation in the Immune System with an Emphasis on Lipopolysaccharide-Responsive and Beige-like Anchor Protein in B Cells. International journal of molecular sciences, 24(4), 3098. https://doi.org/10.3390/ijms24043098.
162. Avraham, R., & Yarden, Y. (2011). Feedback regulation of EGFR signalling: decision making by early and delayed loops. Nature reviews. Molecular cell biology, 12(2), 104–117. https://doi.org/10.1038/nrm3048.
163. Sobhani N, Tardiel-Cyril DR, Davtyan A, Generali D, Roudi R, Li Y. CTLA-4 in Regulatory T Cells for Cancer Immunotherapy. Cancers (Basel). 2021;13(6):1440. Published 2021 Mar 22. doi:10.3390/cancers13061440.
164. Janman, D., Hinze, C., Kennedy, A., Halliday, N., Waters, E., Williams, C., Rowshanravan, B., Hou, T. Z., Minogue, S., Qureshi, O. S., & Sansom, D. M. (2021). Regulation of CTLA-4 recycling by LRBA and Rab11. Immunology, 164(1), 106–119. https://doi.org/10.1111/imm.13343.
165. Gámez-Díaz, L., & Seidel, M. G. (2021). Different Apples, Same Tree: Visualizing Current Biological and Clinical Insights into CTLA-4 Insufficiency and LRBA and DEF6 Deficiencies. Frontiers in pediatrics, 9, 662645. https://doi.org/10.3389/fped.2021.662645.

166. Ceresa B. P. (2006). Regulation of EGFR endocytic trafficking by rab proteins. Histology and histopathology, 21(9), 987–993. https://doi.org/10.14670/HH-21.987.
167. Tomas, A., Futter, C. E., & Eden, E. R. (2014). EGF receptor trafficking: consequences for signaling and cancer. Trends in cell biology, 24(1), 26–34. https://doi.org/10.1016/j.tcb.2013.11.002.
168. Sigismund, S., Argenzio, E., Tosoni, D., Cavallaro, E., Polo, S., & Di Fiore, P. P. (2008). Clathrin-mediated internalization is essential for sustained EGFR signaling but dispensable for degradation. Developmental cell, 15(2), 209–219. https://doi.org/10.1016/j.devcel.2008.06.012.
169. Sigismund, S., Avanzato, D., & Lanzetti, L. (2018). Emerging functions of the EGFR in cancer. Molecular oncology, 12(1), 3–20. https://doi.org/10.1002/1878-0261.12155
170. Murphrey, M. B., Quaim , L., & Varacallo, M. (2022). Biochemistry, Epidermal Growth Factor Receptor. In StatPearls. StatPearls Publishing.
171. Turner, P. V., Brabb, T., Pekow, C., & Vasbinder, M. A. (2011). Administration of substances to laboratory animals: routes of administration and factors to consider. Journal of the American Association for Laboratory Animal Science : JAALAS, 50(5), 600–613.
172. Charan, J., & Kantharia, N. D. (2013). How to calculate sample size in animal studies?. Journal of pharmacology & pharmacotherapeutics, 4(4), 303–306. https://doi.org/10.4103/0976-500X.119726.
173. Divangahi, M., Balghi, H., Danialou, G., Comtois, A. S., Demoule, A., Ernest, S., Haston, C., Robert, R., Hanrahan, J. W., Radzioch, D., & Petrof, B. J. (2009). Lack of CFTR in skeletal muscle predisposes to muscle wasting and diaphragm muscle pump failure in cystic fibrosis mice. PLoS genetics, 5(7), e1000586. https://doi.org/10.1371/journal.pgen.1000586.
174. van Meegen, M. A., Terheggen-Lagro, S. W., van der Ent, C. K., & Beekman, J. M. (2011). CFTR expression analysis in human nasal epithelial cells by flow cytometry. PloS one, 6(12), e27658. https://doi.org/10.1371/journal.pone.0027658.
175. Ma, B., Cheng, H., Mu, C., Geng, G., Zhao, T., Luo, Q., Ma, K., Chang, R., Liu, Q., Gao, R., Nie, J., Xie, J., Han, J., Chen, L., Ma, G., Zhu, Y., & Chen, Q. (2019). The SIAH2-NRF1 axis spatially regulates tumor microenvironment remodeling for tumor progression. Nature communications, 10(1), 1034. https://doi.org/10.1038/s41467-019-08618-y.
176. Perriera, R., Vitale, E., Pibiri, I., Carollo, P. S., Ricci, D., Corrao, F., Fiduccia, I., Melfi, R., Zizzo, M. G., Tutone, M., Pace, A., & Lentini, L. (2023). Readthrough Approach Using NV Translational Readthrough-Inducing Drugs (TRIDs): A Study of the Possible Off-Target Effects on Natural Termination Codons (NTCs) on TP53 and Housekeeping Gene Expression. International Journal of Molecular Sciences, 24(20), 15084. https://doi.org/10.3390/ijms242015084.
177. Aversa, S., & Bellan, C. (2018). TTF1 Expression in Pulmonary Metastatic Rectal Adenocarcinoma. Case reports in gastrointestinal medicine, 2018, 6405125. https://doi.org/10.1155/2018/6405125.